

# Accessing Bioactive Hydrazones by the Hydrohydrazination of Terminal Alkynes Catalyzed by Gold(I) Acyclic Aminoxy Carbene Complexes and Their Gold(I) Arylthiolato and Gold(III) Tribromo Derivatives: A Combined Experimental and Computational Study

Jyoti Singh,<sup>€</sup> Sunita Sharma,<sup>€</sup> A. P. Prakasham, Gopalan Rajaraman,<sup>\*</sup> and Prasenjit Ghosh<sup>\*</sup>Cite This: *ACS Omega* 2023, 8, 21042–21073

Read Online

ACCESS |



Metrics &amp; More

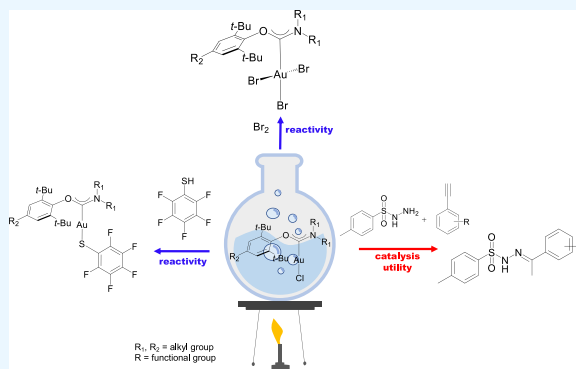


Article Recommendations



Supporting Information

**ABSTRACT:** Hydrohydrazination of terminal alkynes with hydrazides yielding hydrazones **5–14** were successfully catalyzed by a series of gold(I) acyclic aminoxy carbene complexes of the type  $[\{(4-R^2-2,6-t-Bu_2-C_6H_2O)(N(R^1)_2)\}methylidene]AuCl$ , where  $R^2 = H$ ,  $R^1 = Me$  (**1b**);  $R^2 = H$ ,  $R^1 = Cy$  (**2b**);  $R^2 = t-Bu$ ,  $R^1 = Me$  (**3b**);  $R^2 = t-Bu$ ,  $R^1 = Cy$  (**4b**). The mass spectrometric evidence corroborated the existence of the catalytically active solvent-coordinated  $[(AAOC)Au(CH_3CN)]SbF_6$  (**1–4A**) species and the acetylene-bound  $[(AAOC)Au(HC\equiv CPhMe)]SbF_6$  (**3B**) species of the proposed catalysis cycle. The hydrohydrazination reaction was successfully employed in synthesizing several bioactive hydrazone compounds (**15–18**) with anticonvulsant properties using a representative precatalyst (**2b**). The DFT studies favored the 4-ethynyltoluene ( $HC\equiv CPhMe$ ) coordination pathway over the *p*-toluenesulfonyl hydrazide ( $NH_2NHSO_2C_6H_4CH_3$ ) coordination pathway, and that proceeded by a crucial intermolecular hydrazide-assisted proton transfer step. The gold(I) complexes (**1–4b**) were synthesized from the  $[\{(4-R^2-2,6-t-Bu_2-C_6H_2O)(N(R^1)_2)\}CH]^+OTf^-$  (**1–4a**) by treatment with  $(Me_2S)AuCl$  in the presence of NaH as a base. The reactivity studies of (**1–4b**) yielded the gold(III)  $[\{(4-R^2-2,6-t-Bu_2-C_6H_2O)(N(R^1)_2)\}methylidene]AuBr_3$  (**1–4c**) complexes upon reaction with molecular bromine and the gold(I) perfluorophenylthiolato derivatives,  $[\{(4-R^2-2,6-t-Bu_2-C_6H_2O)(N(R^1)_2)\}methylidene]AuSC_6F_5$  (**1–4d**), upon treatment with  $C_6F_5SH$ .



## HIGHLIGHTS

- The acyclic aminoxy carbene (AAOC) ligand stabilizes a variety of  $(AAOC)AuCl$ ,  $(AAOC)AuBr_3$ , and  $(AAOC)Au(SC_6F_5)$ -type complexes.
- $(AAOC)AuBr_3$  and  $(AAOC)Au(SC_6F_5)$  represent the first structurally characterized examples of an acyclic aminoxy carbene ligand.
- The gold(I)  $(AAOC)AuCl$ -type complexes efficiently catalyzed hydrohydrazination of the terminal alkynes with hydrazides giving hydrazones.
- Several bioactive acetohydrazide compounds important for their anticonvulsant properties were synthesized by the hydrohydrazination reaction catalyzed by a gold(I)  $(AAOC)AuCl$ -type complex.
- Various mechanistic pathways were explored using DFT, suggesting that hydrohydrazination catalysis proceeds via alkyne-coordination followed by a crucial intermolecular hydrazide-assisted proton relay step.

## INTRODUCTION

Hydrohydrazination reactions are receiving increasing attention as part of the recent interest in utilizing the industrially important hydrazine and hydrazide reagents.<sup>1–3</sup> Hydrazine has significant footprints in important industrial applications like in the production of polymerization initiators, blowing agents for foamed plastics, fine chemicals, pesticides, and pharmaceuticals, and as rocket fuel and propellant for satellites and aircraft in its anhydrous form.<sup>4</sup> It is currently manufactured in large-scale industrial processes.<sup>5</sup> In addition, various hydrazine derivatives, including alkyl hydrazines and hydrazides, constitute many an important chemical blowing agents, pesticides, fungicides, and pharmaceuticals.<sup>6,7</sup> The challenges associated with using hydrazine stem from its various hazardous properties like its

Received: March 22, 2023

Accepted: May 5, 2023

Published: May 30, 2023



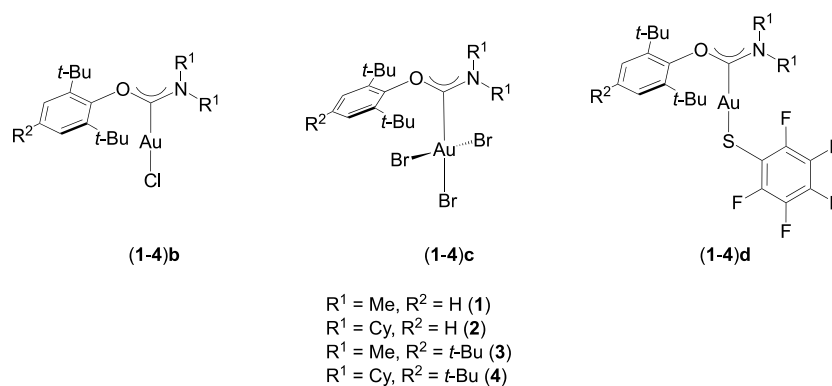


**Figure 1.** Acyclic aminoxy carbene (AAOC)-stabilized gold(I) chloro derivatives (1–4)b, gold(III) tribromo derivatives (1–4)c, and gold(I) perfluorophenylthiolato derivatives (1–4)d.

high energy content, wide flammability range, the potential to support combustion in the absence of air, and high toxicity.<sup>6</sup> In the chemical reactivity space, the highly reducing nature of hydrazine often reduces catalytically active but easily reducible noble metals to their inactive metal(0) state or reduces organic substrates and even deactivates the metal catalysts by complexation reactions.<sup>5,8</sup> The allure of accessing structurally diverse nitrogen-containing compounds, playing pivotal roles as pharmaceuticals, agrochemicals, organic materials, and catalysts, calls for employing effective strategies offering direct access to these target molecules *via* cheap, atom economical, and environmentally friendly approaches like the hydroamination, diamination, aziridination, or oxidative amination reactions.<sup>1,7</sup> The organometallic homogeneous catalysis approach, involving transition-metal-mediated catalysis, provides an alternative solution to overcoming the challenges associated with the inherently high activation energy barriers for the reactions involving electron-rich  $\pi$ -bonds of unsaturated substrates with nitrogen-based reagents.<sup>1</sup>

It is noteworthy that the hydrohydrazination reactions, primarily because of the challenges mentioned above, are comparatively less explored compared to the related hydroamination reactions.<sup>3,9</sup> Quite significantly, the 2008 reports on the hydrohydrazination of terminal alkynes with hydrazine derivatives under metal-free<sup>10</sup> and zinc-mediated catalysis conditions paved the way for the gold-catalyzed one.<sup>11,12,13</sup> The 2008 reports<sup>10,11</sup> further triggered a flurry of activities on other variants of the hydrohydrazination reaction like that of the hydrazide derivatives with alkenes,<sup>14</sup> the hydrohydrazination reaction with hydrazines,<sup>5,15–17</sup> etc.<sup>2</sup> Computational studies indicated that both alkyl hydrazines and hydrazides react *via* a concerted (Cope-type) hydroamination pathway.<sup>1,10</sup>

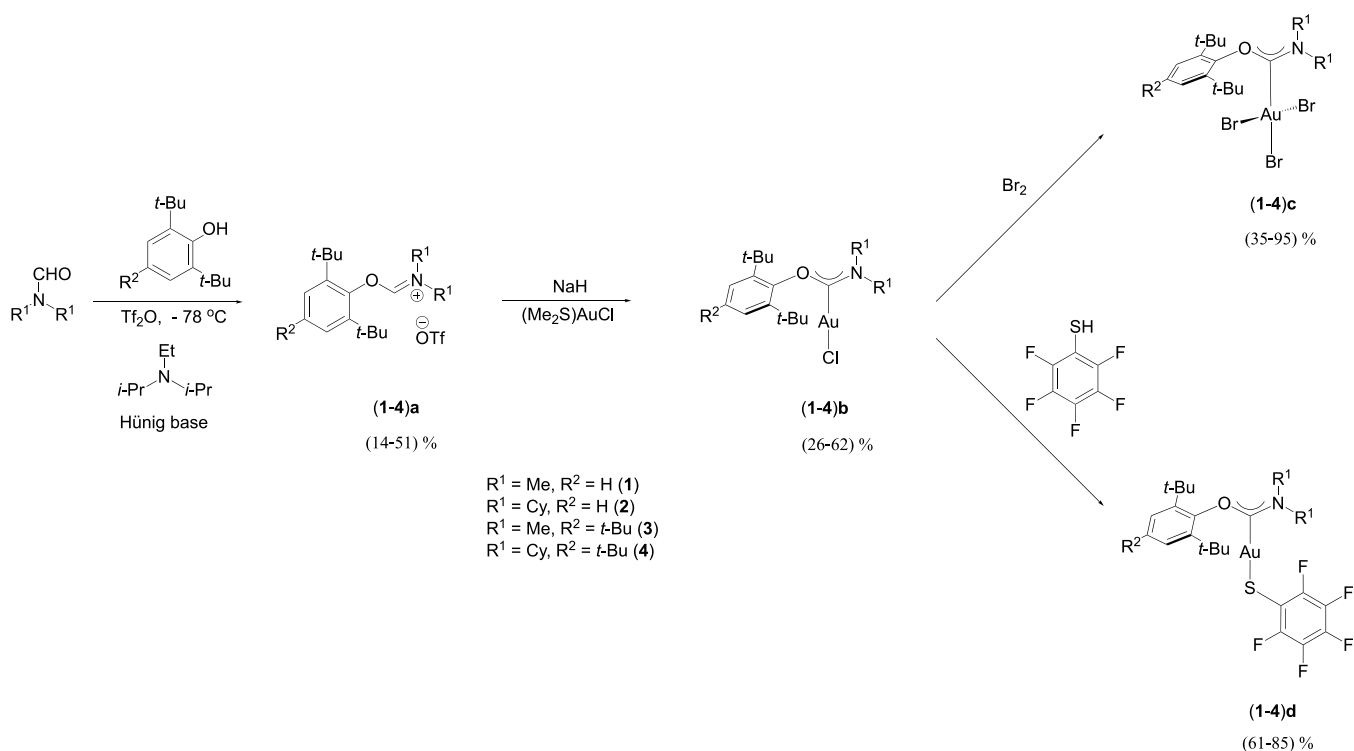
Since the advent of *N*-heterocyclic carbenes in 1991,<sup>18</sup> the families of the stable singlet carbene ligands have continued to grow and expand in scope and diversity by extending the boundaries of the homogeneous catalysis.<sup>19</sup> Several emerging variants of the heteroatom stabilized singlet carbenes like acyclic diamino carbene (ADC),<sup>20</sup> *anti*-Bredt *N*-heterocyclic carbene (NHC),<sup>16,21</sup> cyclic alkyl amino carbene (CAAC),<sup>15,22,23</sup> acyclic aminoxy carbene (AAOC),<sup>24</sup> and abnormal-NHCs like the aza-CAACs<sup>25</sup> have been receiving attention lately among their other contemporaries mainly for the promises they hold. The ease of tunability and the flexibility in the disposition of the heteroatom substituents around the carbene center make these ligands attractive for catalysis.

Because of our dual interests in exploring the potential of transition metal complexes of stable singlet carbenes in homogeneous catalysis<sup>26</sup> and biomedical applications<sup>27</sup> and also in unraveling gold catalysis,<sup>28,29</sup> we chose to employ acyclic aminoxy carbene (AAOC) complexes of gold in the hydrohydrazination reaction of hydrazides with terminal alkynes. Activation of N–H bonds by earth-abundant transition metals has always been very challenging.<sup>30</sup> As theoretical investigations are required to understand the nature of N–H bond activation reactions, we decided to obtain mechanistic insights computationally for the hydrohydrazination catalysis between 4-ethynyltoluene ( $\text{HC}\equiv\text{CPhMe}$ ) and *p*-toluenesulfonyl hydrazide ( $\text{NH}_2\text{NH}\text{SO}_2\text{C}_6\text{H}_4\text{CH}_3$ ) by cationic gold(I) acyclic aminoxy carbene species of the type  $[(\text{AAOC})\text{Au}(\text{CH}_3\text{CN})]^+$ . A detailed theoretical study of the catalytic pathway was performed with the aid of DFT and ORCA calculations.

Here in this manuscript, we report the hydrohydrazination reaction of hydrazides with terminal alkynes giving hydrazones (5–14) as catalyzed by gold(I) complexes (1–4)b of a new variant of acyclic aminoxy carbene (AAOC) ligands (Figure 1). We further demonstrate the hydrohydrazination reaction's utility in preparing the bioactive hydrazone derivatives (15–18) with anticonvulsant properties. We also report the first examples of the gold(I) perfluorophenylthiolato derivatives (1–4)d supported over any class of acyclic heteroatom-stabilized singlet carbene ligands and the gold(III) tribromo complexes (1–4)c obtained from the gold(I) complexes (1–4)b.

## RESULTS AND DISCUSSION

Four new acyclic aminoxy carbene ligands, namely,  $\{(4\text{-}R^2\text{-}2,6\text{-}t\text{-Bu}_2\text{-C}_6\text{H}_2\text{O})(\text{N}(R^1)_2)\}$  methylenide (where  $R^2 = \text{H}, R^1 = \text{Me}$ ;  $R^2 = \text{H}, R^1 = \text{Cy}$ ;  $R^2 = t\text{-Bu}, R^1 = \text{Me}$ ;  $R^2 = t\text{-Bu}, R^1 = \text{Cy}$ ), were synthesized with the intent of stabilizing its gold(I/III) complexes for catalytic application studies. In particular, the ligand precursors,  $\{[(4\text{-}R^2\text{-}2,6\text{-}t\text{-Bu}_2\text{-C}_6\text{H}_2\text{O})(\text{N}(R^1)_2)\text{-CH}]^+\text{OTf}^-$  [where  $R^2 = \text{H}, R^1 = \text{Me}$  (1a);  $R^2 = \text{H}, R^1 = \text{Cy}$  (2a);  $R^2 = t\text{-Bu}, R^1 = \text{Me}$  (3a);  $R^2 = t\text{-Bu}, R^1 = \text{Cy}$  (4a)], were directly synthesized from the corresponding reaction of secondary formamide, namely, *N,N*-dimethylformamide ( $\text{Me}_2\text{NCHO}$ ) and *N,N*-dicyclohexylformamide ( $\text{Cy}_2\text{NCHO}$ ), with a phenol derivative, namely, 2,6-*t*-Bu<sub>2</sub>-C<sub>6</sub>H<sub>3</sub>OH and 2,4,6-*t*-Bu<sub>3</sub>-C<sub>6</sub>H<sub>2</sub>OH, in the presence of the Hünig base and triflic anhydride similar to that reported for a related analog.<sup>31</sup> The diagnostic NCHO peak appeared at  $\delta$  ca. 8.93–9.25 ppm in <sup>1</sup>H NMR (Supporting Information, Figures S1, S2, S35, S36, S68, S69, S99, and S100) and at  $\delta$  ca. 168.1–169.0 ppm in <sup>13</sup>C{<sup>1</sup>H}

**Scheme 1. Synthesis Route to the Acyclic Aminoxy Carbene (AAOC)Stabilized Gold(I) Chloro Derivatives (1–4)b, Gold(III) Tribromo Derivatives (1–4)c, and Gold(I) Perfluorophenylthiolato Derivatives (1–4)d**


NMR (Supporting Information, Figures S3, S4, S37, S38, S70, S71, S101, and S102). The triflate anion displayed a quartet at  $\delta$  ca. 120.4–120.5 ppm, exhibiting  $^1J_{\text{CF}}$  coupling of ca. 318–319 Hz in the  $^{13}\text{C}\{^1\text{H}\}$  NMR and at  $\delta$  ca. –78.38 to –78.70 ppm in the  $^{19}\text{F}\{^1\text{H}\}$  NMR (Supporting Information, Figures S5, S39, S72, and S103).

The molecular structure of the acyclic aminoxy carbene precursors, **1a** and **3a**, as determined by X-ray diffraction studies, revealed the C(1)–O(1) bond length of 1.311(3) Å (**1a**) and 1.325(6) Å (**3a**) and the C(1)–N(1) bond length of 1.277(3) Å (**1a**) and 1.282(6) Å (**3a**) are comparable to the only other structurally characterized example,  $[(2,6\text{-}t\text{-Bu}_2\text{-C}_6\text{H}_3\text{O})(\text{N-}i\text{-Pr}_2)]\text{CH}^+\text{OTf}^-$ , displaying a C(1)–O(1) bond length of 1.321(4) Å and C(1)–N(2) bond length of 1.283(5) Å, respectively<sup>31</sup> (Supporting Information, Figures S9 and S76 and Table S5). Comparison of the C(1)–O(1) and C(1)–N(1) bond distances of **1a** and **3a** with the respective sum of the individual covalent radii [ $d/C_{\text{sp}^2}\text{-O} = 1.39$  Å and  $d/C_{\text{sp}^2}\text{-N} = 1.44$  Å]<sup>32</sup> showed significant shortening of the C(1)–N(1) bond arising from a greater  $\pi$ -bond character. In agreement with the delocalized  $\pi$ -character of the  $\text{C}_{\text{carbene}}\text{-N}$  [C(1)–N(1)] bond in **1a** and **3a**, the angle at the carbene carbon [ $\angle\text{N}(1)\text{-C}(1)\text{-O}(1)$ ] was indeed ca. 120° as observed for **1a** [120.97(19)°] and **3a** [119.9(5)°] and also closely matched that of  $[(2,6\text{-}t\text{-Bu}_2\text{-C}_6\text{H}_3\text{O})(\text{N-}i\text{-Pr}_2)]\text{CH}^+\text{OTf}^-$  [118.8(3)°]<sup>31</sup> (Supporting Information, Figures S9 and S76).

The gold(I) acyclic aminoxy carbene complexes of the type (AAOC)AuCl are primarily prepared by (i) *in situ* deprotonation of the corresponding methanaminium salt with LiHMDS followed by the treatment with  $(\text{Me}_2\text{S})\text{AuCl}$ <sup>33</sup> and (ii) by the direct reaction of ionic gold(I) isocyanide complexes with alcohols derivatives.<sup>34,35</sup> In this regard, all of the gold(I) (AAOC)AuCl-type complexes, (1–4)b, were conveniently obtained by the *in situ* deprotonation method from  $[(4\text{-}R^2\text{-}2,6\text{-}t\text{-Bu}_2\text{-C}_6\text{H}_2\text{O})(\text{N}(\text{R}^1)_2)]\text{CH}^+\text{OTf}^-$  (**1–4**)a in ca. 26–62% yield.

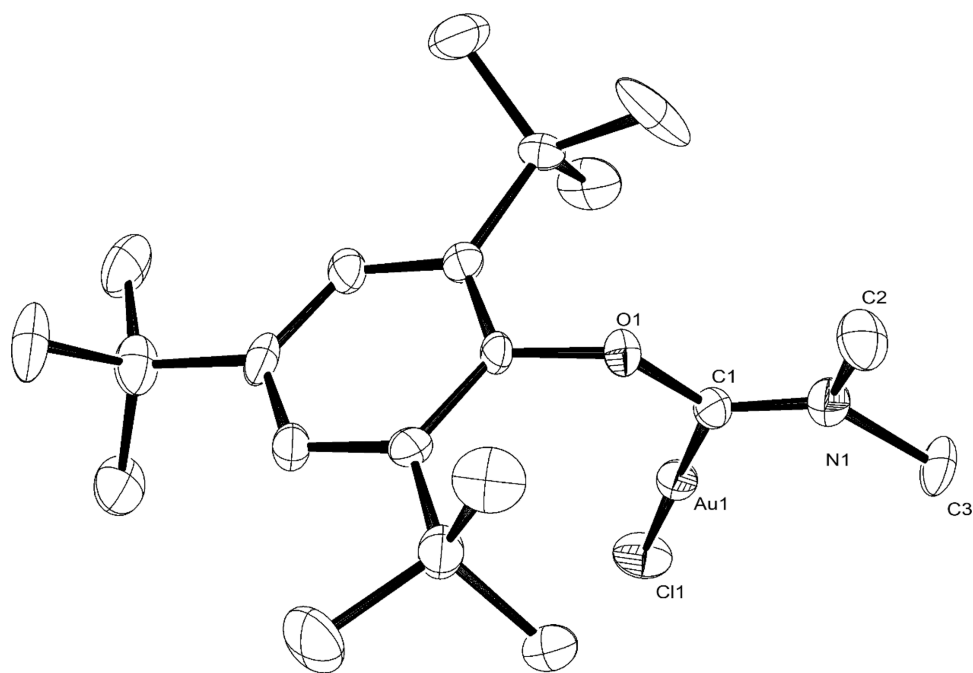
Specifically, the deprotonation of (1–4)a by NaH in dry THF at ca. –78 °C with gradual warming to room temperature gave the air and moisture-stable (AAOC)AuCl-type (1–4)b complexes (Scheme 1).

The methanaminium (NCHO) resonance, seen in the respective carbene precursor (1–4)a, was conspicuously absent in the  $^1\text{H}$  NMR spectrum of the (1–4)b complexes, (Supporting Information, Figures S10, S11, S43, S44, S77, S78, S107, and S108), thereby indicating their formation. Consequently, the distinct gold(I) bound carbene (Au–NCO) resonance at  $\delta$  ca. 210.3 ppm (**1b**), 211.6 ppm (**2b**), 210.5 ppm (**3b**), and 211.8 ppm (**4b**) are in concurrence with related  $[(\text{O-1-Ad})(\text{N-1-Ad})(\text{N-C}_6\text{H}_5)]\text{methylidene}] \text{AuCl}$  (207.8 ppm),<sup>33</sup>  $[(\text{O-1-Ad})(\text{N-2,6-}i\text{-Pr}_2\text{C}_6\text{H}_3)(\text{N-}i\text{-Pr})\text{methylidene}] \text{AuCl}$  (207.3 ppm),<sup>33</sup> and  $[(\text{O-Et})(\text{N-4-MeC}_6\text{H}_4)(\text{NH})\text{methylidene}] \text{AuCl}$  (205.8 ppm)<sup>34</sup> complexes (Table 1). The neutral monomeric nature of the (1–4)b complexes was established by the determination of their molecular structure (Figure 2 and Supporting Information, Figures S17, S50, and S114 and Table S2), which showed that the methylidene and the chloride ligands are bound opposite to each other in a linear geometry at the metal center.

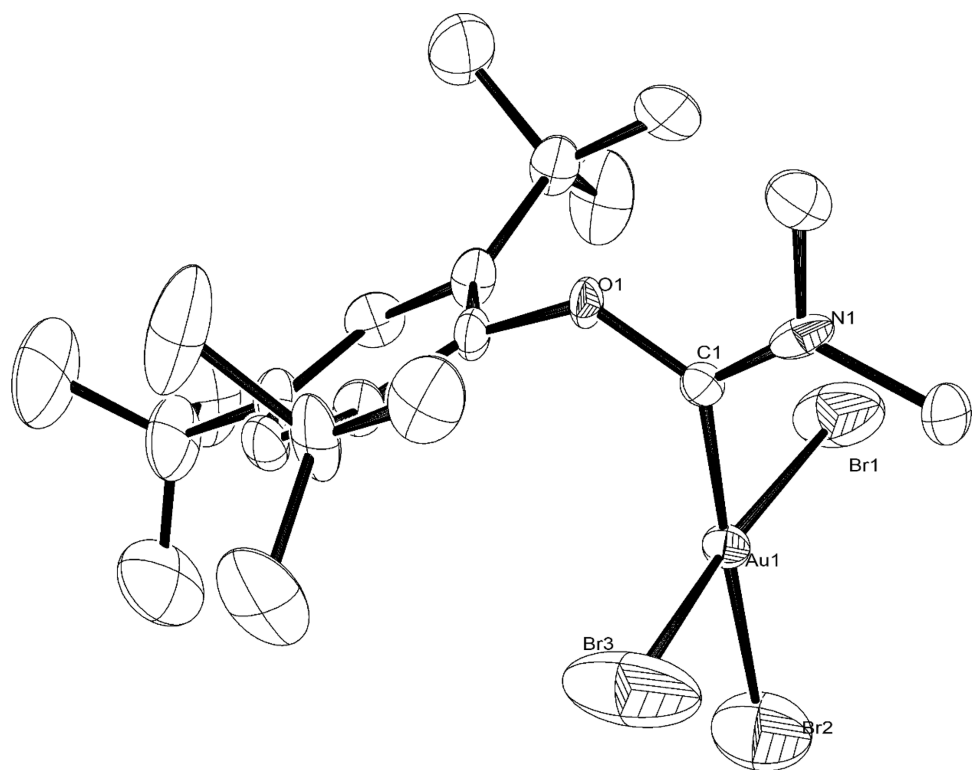
The Au– $\text{C}_{\text{carbene}}$  bond distances of 1.984(6) Å (**1b**), 1.993(3) Å (**2b**), 1.977(6) Å (**3b**), and 1.996(4) Å (**4b**) are slightly shorter than the sum of their individual covalent radii [ $d(\text{C}_{\text{sp}^2}\text{-Au}) = 2.09$  Å]<sup>32</sup> and agree well with structurally characterized analogues,  $[(\text{O-1-Ad})(\text{N-1-Ad})(\text{N-C}_6\text{H}_5)]\text{methylidene}] \text{AuCl}$  [1.996(2) Å],<sup>33</sup>  $[(\text{O-1-Ad})(\text{N-2,6-}i\text{-Pr}_2\text{C}_6\text{H}_3)(\text{N-}i\text{-Pr})\text{methylidene}] \text{AuCl}$  [2.005(4) Å],<sup>33</sup> and  $[(\text{O-Et})(\text{N-4-MeC}_6\text{H}_4)(\text{NH})\text{methylidene}] \text{AuCl}$  [1.98 (3), 2.04 (4) Å]<sup>34</sup> (Figure 2 and Table 1 and Supporting Information, Figures S17, S50, and S114). The Au– $\text{C}_{\text{carbene}}$  bond distances in (1–4)b also agree well with the related imidazole-derived NHC Au

**Table 1.** Comparison of the  $^{13}\text{C}\{^1\text{H}\}$  NMR and the Metrical Data Showing the  $\text{C}_{\text{carbene}}\text{-Au}$  and  $\text{Au-Cl}$  Bond Distances for the Chloro Derivative of Au(I) Acyclic Aminoxy Carbene (AAOC) (1–4)b Complexes with That Known in the Literature.

entry	complexes	$d(\text{C}_{\text{carbene}}\text{-Au})/$ (Å)	$d(\text{Au-Cl})/$ (Å)	$^{13}\text{C}\{^1\text{H}\}$ NMR ( $\text{C}_{\text{carbene}}\text{-Au})/$ ( $\delta$ , ppm)	reference
1.		2.007(2)	2.2910(5)	203.2	[33]
2.		1.996(2)	2.2834(6)	207.8	[33]
3.		2.005(4)	2.287(1)	207.3	[33]
4.		1.983(2), 1.990(2)	2.2883(6), 2.2768(4)	214.5	[33]
5.		1.996(1)	2.2820(4)	214.7	[33]
6.		1.98 (3), 2.04 (4)	2.315 (9), 2.283 (10)	205.8	[34]
7.		1.984(6)	2.2810(16)	210.3	present work
8.		1.993(3)	2.2789(9)	211.6	present work
9.		1.977(6)	2.2787(18)	210.5	present work
10.		1.996(4)	2.2807(11)	211.8	present work



**Figure 2.** ORTEP of **3b** with thermal ellipsoids drawn at the 50% probability level. Hydrogen atoms are omitted for clarity. Selected bond lengths (Å) and angles (°): Au(1)–Cl(1) 2.2787(18), Au(1)–C(1) 1.977(6), O(1)–C(1) 1.343(7), N(1)–C(1) 1.319(8), O(1)–C(1)–Au(1) 123.7(4), N(1)–C(1)–Au(1) 125.2(5), C(1)–Au(1)–Cl(1) 179.15(18), N(1)–C(1)–O(1) 111.1(5).

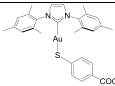
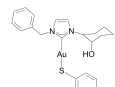
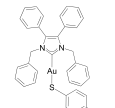
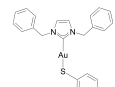
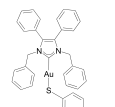
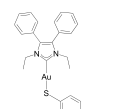
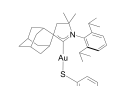
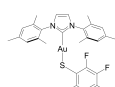
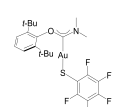
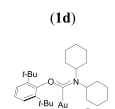
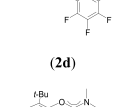
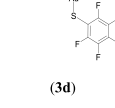


**Figure 3.** ORTEP of **3c** with thermal ellipsoids drawn at the 50% probability level. Hydrogen atoms and solvent ( $\text{CH}_3\text{CN}$ ) molecules are omitted for clarity. Selected bond lengths (Å) and angles (°): O(1)–C(1) 1.351(15), N(1)–C(1) 1.261(18), Au(1)–C(1) 1.986(13), Au(1)–Br(1) 2.383(2), Au(1)–Br(2) 2.369(3), Au(1)–Br(3) 2.347(2), N(1)–C(1)–O(1) 111.3(12), C(1)–Au(1)–Br(1) 90.8(4), C(1)–Au(1)–Br(3) 86.8(4), C(1)–Au(1)–Br(2) 176.2(4).

complexes, namely, [1-(*i*-propyl)-3-(benzyl)imidazol-2-ylidene]AuCl [1.974(4) Å] and [1-(*i*-propyl)-3-(3,3-dimethyl-2-oxobutyl)imidazol-2-ylidene]AuCl [1.975(4) Å].<sup>29</sup>

More lengthening of the  $\text{C}_{\text{carbene}}\text{--N}$  bond in **1b** [1.311(6) Å], **2b** [1.321(4) Å], **3b** [1.319(8) Å], and **4b** [1.311(6) Å] than the  $\text{C}_{\text{carbene}}\text{--O}$  bond in **1b** [1.356(7) Å], **2b** [1.352(4) Å], **3b** [1.343(7) Å], and **4b** [1.356(5) Å] (Figure 2 and Supporting

**Table 2.** Comparison of the  $^{13}\text{C}\{^1\text{H}\}$  NMR and the Metrical Data Showing the  $\text{C}_{\text{carbene}}-\text{Au}$  and  $\text{Au}-\text{S}$  Bond Distances for the Arylthiolato Derivatives of Au(I) Complexes Supported Over Various Heteroatom-Stabilized Singlet Carbene Ligands Known in the Literature with the (1–4)d Complexes

entry	complexes	$d(\text{C}_{\text{carbene}}-\text{Au})/$ (Å)	$d(\text{Au}-\text{S})/$ (Å)	$^{13}\text{C}\{^1\text{H}\}$ NMR ( $\text{C}_{\text{carbene}}-\text{Au})/$ ( $\delta$ , ppm)	reference
1.		1.995(6)	2.2790(17)	184.6	[39]
2.		2.013(4)	2.302(1)	181.0	[43]
3.		2.0133(14)	2.2899(4)	156.3	[40]
4.		1.99(2)	2.297(4)	-	[41]
5.		2.0129(19)	2.3017(7)	182.4	[42]
6.		2.010(3)	2.3050(8)	179.8	[42]
7.		2.006(4)	2.281(1)	249.5	[44]
8.		2.001(2)	2.2931(5)	182.0	[38]
9.	 <b>(1d)</b>	2.002(3)	2.2874(8)	217.0	present work
10.	 <b>(2d)</b>	2.028(2)	2.2920(7)	218.7	present work
11.	 <b>(3d)</b>	2.015(4)	2.2927(12)	218.0	present work
12.	 <b>(4d)</b>	2.027(4)	2.2785(11)	219.6	present work



Information, Figures S17, S50, and S114 and Table S2) was observed with respect to the methanaminium salts, **1a** { $d[\text{C}(1)-\text{N}(1)] = 1.277(3) \text{ \AA}$ ;  $d[\text{C}(1)-\text{O}(1)] = 1.311(3) \text{ \AA}$ }, **3a** { $d[\text{C}(1)-\text{N}(1)] = 1.282(6) \text{ \AA}$ ;  $d[\text{C}(1)-\text{O}(1)] = 1.325(6) \text{ \AA}$ }, and {[ $(2,6\text{-}t\text{-Bu}_2\text{-C}_6\text{H}_3\text{O})(\text{N-}i\text{-Pr}_2)\text{CH}$ ]}<sup>+</sup>OTf<sup>-</sup> { $d[\text{C}(1)-\text{N}(2)] = 1.283(5) \text{ \AA}$ ;  $d[\text{C}(1)-\text{O}(1)] = 1.321(4) \text{ \AA}$ }<sup>31</sup> (Supporting Information, Figures S9 and S76 and Tables S1 and S5).

Quite interestingly, a comparison of the  $\angle\text{N}-\text{C}_{\text{carbene}}-\text{O}$  angle in **1b** [111.1(5)°] and **3b** [111.1(5)°] (Figure 2 and Supporting Information S17) with the structurally characterized methanaminium salts, **1a** [120.97(19)°], **3a** [119.9(5)°], and {[ $(2,6\text{-}t\text{-Bu}_2\text{-C}_6\text{H}_3\text{O})(\text{N-}i\text{-Pr}_2)\text{CH}$ ]}<sup>+</sup>OTf<sup>-</sup> [118.8(3)°]<sup>31</sup> (Supporting Information, Figures S9 and S76 and Table S5), revealed significant shortening of the  $\angle\text{N}-\text{C}_{\text{carbene}}-\text{O}$  angle by ca. 9° in the (AAOC)AuCl-type (1–4)**b** complexes arising from incorporation of bulky gold(I) atoms [ $r_{\text{cov}} = 1.36(6) \text{ \AA}$ ]<sup>32</sup> at the carbene center due to the metalation reaction. Several reported examples, {[ $(\text{O-1-Ad})(\text{N-1-Ad})(\text{N-C}_6\text{H}_5)$ ]}methylidene]AuCl [112.5(2)°],<sup>33</sup> {[ $(\text{O-1-Ad})(\text{N-2,6-}i\text{-Pr}_2\text{C}_6\text{H}_3)(\text{N-}i\text{-Pr})$ ]}methylidene]AuCl [110.7(3)°],<sup>33</sup> and {[ $(\text{O-Et})(\text{N-4-MeC}_6\text{H}_4)(\text{NH})$ ]}methylidene]AuCl [113 (3)°, 114 (4)°],<sup>34</sup> too exhibit a  $\angle\text{N}-\text{C}_{\text{carbene}}-\text{O}$  bond angle of around ca. 112° similar to the (1–4)**b** complexes.

The oxidation of the (AAOC)AuCl-type (1–4)**b** complexes with excess bromine yielded the corresponding gold(III) {[ $(4\text{-R}^2\text{-2,6-}t\text{-Bu}_2\text{-C}_6\text{H}_2\text{O})(\text{N}(\text{R}^1)_2)$ ]}methylidene]AuBr<sub>3</sub> (1–4)**c** complexes in ca. 35–95% yield. The diagnostic Au(III)–C<sub>carbene</sub> resonance appeared significantly upfield shifted by ( $\Delta\delta$ ) ca. 27.9 ppm, in the <sup>13</sup>C{<sup>1</sup>H} (100 MHz) NMR spectrum, appearing at 182.8 ppm (**1c**), 182.9 ppm (**2c**), 183.2 ppm (**3c**), and 183.9 ppm (**4c**) (Supporting Information, Figures S20, S21, S53, S54, S86, S87, S117, and S118) when compared to their starting gold(I) complexes at 210.3 ppm (**1b**), 211.6 ppm (**2b**), 210.5 ppm (**3b**), and 211.8 ppm (**4b**) (Supporting Information, Figures S12, S13, S45, S46, S79, S80, S109, and S110). To the best of our knowledge, no gold(III) (AAOC)AuBr<sub>3</sub>-type complexes have been reported for acyclic aminoxy carbene complexes. In the absence of any related examples bearing AAOC ligands, a comparison is made with respect to their N-heterocyclic carbene (NHC) counterpart. The Au(III)–C<sub>carbene</sub> resonance for (1–4)**c** was in contrast significantly downfield shifted by ( $\Delta\delta$ ) ca. 69.3 ppm with respect to the reported gold(III) N-heterocyclic carbene complexes, namely, [1-(*i*-propyl)-3-(benzyl)imidazol-2-ylidene]AuBr<sub>3</sub> (139.0),<sup>29</sup> [1-(benzyl)-3-(2,4,6-trimethylphenyl)imidazol-2-ylidene]AuBr<sub>3</sub> (140.9 ppm),<sup>29</sup> [1-(*i*-propyl)-3-(3,3-dimethyl-2-oxobutyl)imidazol-2-ylidene]AuBr<sub>3</sub> (136.6 ppm),<sup>29</sup> [1-(*tert*-butyl)-3-(3,3-dimethyl-2-oxobutyl)imidazol-2-ylidene]AuBr<sub>3</sub> (138.3 ppm),<sup>29</sup> [1-(diphenylmethyl)-3-(methyl)imidazol-2-ylidene]AuBr<sub>3</sub> (141.3 ppm),<sup>36</sup> and [1-(*tert*-butyl)-3-(2-(2-acetamido)-3-phenylalanine methylester)imidazol-2-ylidene]AuBr<sub>3</sub> (135.8 ppm).<sup>36</sup>

Structural characterization of (1–4)**c** revealed them to be monomeric square planar complexes in accordance with a *d*<sup>8</sup> configuration of the Au(III) center. It is surrounded by one acyclic aminoxy carbene (AAOC) ligand and three bromide ligands in concurrence with the four coordination geometry at the metal center (Figure 3 and Supporting Information Figures S24, S57 and S121). The Au(III)–C<sub>carbene</sub> bond distances of 2.047(12) Å (**1c**), 2.019(11) Å (**2c**), 1.986(13) Å (**3c**), and 2.043(8) Å (**4c**) are comparable to the sum of their individual covalent radii [ $d(\text{C}_{\text{sp}^2}-\text{Au}) = 2.09 \text{ \AA}$ ]<sup>32</sup> and are slightly longer

than the Au(I)–C<sub>carbene</sub> bond distances of 1.984(6) Å (**1b**), 1.993(3) Å (**2b**), 1.977(6) Å (**3b**), and 1.996(4) Å (**4b**) (Figure 2 and Supporting Information, Figures S17, S50, and S114). Several related structurally characterized gold(III) N-heterocyclic carbene complexes, namely, [1-(*i*-propyl)-3-(benzyl)imidazol-2-ylidene]AuBr<sub>3</sub> [2.002(15) Å],<sup>29</sup> [1-(benzyl)-3-(2,4,6-trimethylphenyl)imidazol-2-ylidene]AuBr<sub>3</sub> [2.047(11) Å],<sup>29</sup> [1-(*i*-propyl)-3-(3,3-dimethyl-2-oxobutyl)imidazol-2-ylidene]AuBr<sub>3</sub> [2.028(6) Å],<sup>29</sup> [1-(*tert*-butyl)-3-(3,3-dimethyl-2-oxobutyl)imidazol-2-ylidene]AuBr<sub>3</sub> [2.042(9) Å],<sup>29</sup> [1-(diphenylmethyl)-3-(methyl)imidazol-2-ylidene]AuBr<sub>3</sub> [2.016(8) Å],<sup>36</sup> and [1-(*tert*-butyl)-3-(2-(2-acetamido)-3-phenylalanine methylester)imidazol-2-ylidene]AuBr<sub>3</sub> [2.02(2) Å],<sup>36</sup> also exhibited comparable Au(III)–C<sub>carbene</sub> bond distances to that of (1–4)**c** complexes. The  $\angle\text{N}-\text{C}_{\text{carbene}}-\text{O}$  angle in **1c** [113.7(10)°], **2c** [112.8(10)°], **3c** [111.3(12)°], and **4c** [116.1(7)°] (Figure 3 and Supporting Information, Figures S24, S57, and S121) are similar to that of **1b** [111.1(5)°], **2b** [111.6(3)°], **3b** [111.1(5)°], and **4b** [112.4(3)°] (Figure 2 and Supporting Information, Figures S17, S50, and S114).

The perfluorinated aryl thiolato gold(I) complexes {[ $(4\text{-R}^2\text{-2,6-}t\text{-Bu}_2\text{-C}_6\text{H}_2\text{O})(\text{N}(\text{R}^1)_2)$ ]}methylidene]Au(SC<sub>6</sub>F<sub>5</sub>) (1–4)**d** were prepared by treating the (AAOC)AuCl-type (1–4)**b** complexes with excess C<sub>6</sub>F<sub>5</sub>SH in ca. 61–85% yield. The perfluorinated aryl thiolato gold(I) complexes and related phenolate complexes are known to be very sensitive.<sup>37</sup> Unlike the significant upfield shift by ( $\Delta\delta$ ) ca. 27.9 ppm in <sup>13</sup>C{<sup>1</sup>H} NMR in the case of the gold(III) (1–4)**c** complexes (Supporting Information, Figure S20, S21, S53, S54, S86, S87, S117, and S118), the perfluorinated aryl thiolato gold(I) complexes appeared further downfield shifted by ( $\Delta\delta$ ) ca. 7.3 ppm with regard to their chloro analogs (1–4)**b** (Supporting Information, Figures S12, S13, S45, S46, S79, S80, S109, and S110). Specifically, the diagnostic Au(I)–C<sub>carbene</sub> resonance appeared at 217.0 ppm (**1d**), 218.7 ppm (**2d**), 218.0 ppm (**3d**), and 219.6 ppm (**4d**) (Supporting Information Figure S27, S28, S60, S61, S92, S93, S124, and S125) than the chloro derivatives at 210.3 ppm (**1b**), 211.6 ppm (**2b**), 210.5 ppm (**3b**), and 211.8 ppm (**4b**) (Supporting Information, Figures S12, S13, S45, S46, S79, S80, S109, and S110).

Quite significantly, (1–4)**d** represent the only examples of gold(I) (AAOC)Au(SC<sub>6</sub>F<sub>5</sub>)-type complexes known in the literature, and in the absence of which, a comparison is made with regard to their imidazole based analogues, *i.e.*, a gold(I) (NHC)Au(SC<sub>6</sub>F<sub>5</sub>)-type complex<sup>38</sup> and gold(I) (NHC)Au(SC<sub>6</sub>H<sub>5</sub>)-type complexes<sup>39–44</sup> (Table 2). Specifically, the Au(I)–C<sub>carbene</sub> resonances at ca. 217.0–219.6 ppm for (1–4)**d** appeared significantly downfield shifted by ( $\Delta\delta$ ) ca. 36.5 ppm with respect to their imidazole-based NHC counterparts, namely, [1,3-(Mes)<sub>2</sub>-imidazol-2-ylidene]Au(SC<sub>6</sub>H<sub>4</sub>COOH) (184.6 ppm),<sup>39</sup> [1-(2-hydroxycyclohexyl)-3-(benzyl)imidazol-2-ylidene]Au(SC<sub>10</sub>H<sub>7</sub>) (181.0 ppm),<sup>43</sup> and [1,3-(Mes)<sub>2</sub>-imidazol-2-ylidene]Au(SC<sub>6</sub>F<sub>5</sub>) (182.0 ppm)<sup>38</sup> (Table 2).

The molecular structures of (1–4)**d** were isostructural with their chloro analogues (1–4)**b** exhibiting a linear geometry at the gold(I) center with the two sides flanked by an acyclic aminoxy carbene (AAOC) ligand and the perfluorophenyl thiolate (C<sub>6</sub>F<sub>5</sub>S) moiety (Figure 4 and Supporting Information, Figures S34, S67, and S131 and Table S4). The Au(I)–C<sub>carbene</sub> bond distances of 2.002(3) Å (**1d**), 2.028(2) Å (**2d**), 2.015(4) Å (**3d**), and 2.027(4) Å (**4d**) (Figure 4 and Supporting Information Figures S34, S67, and S131) are slightly shorter than the sum of their individual covalent radii [ $d(\text{C}_{\text{sp}^2}-\text{Au}) =$

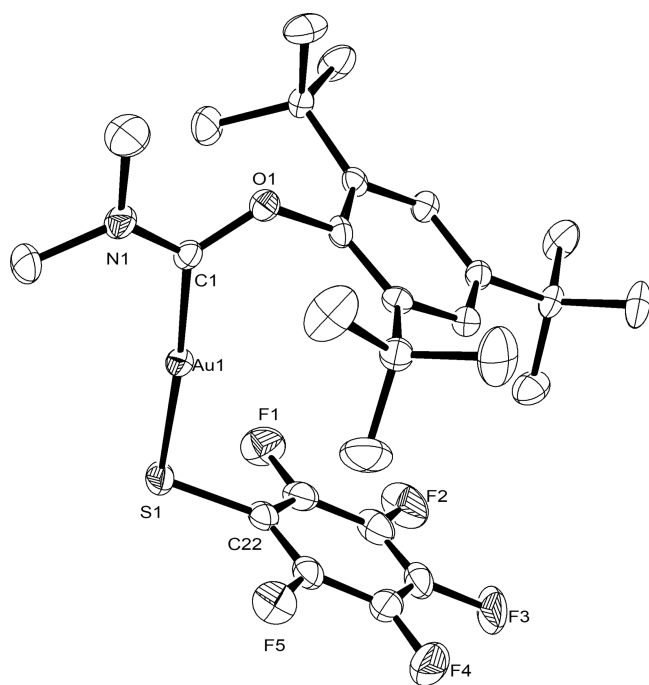


**Figure 4.** ORTEP of **3d** with thermal ellipsoids drawn at the 50% probability level. Hydrogen atoms are omitted for clarity. Selected bond lengths (Å) and angles (°): O(1)–C(1) 1.346(5), N(1)–C(1) 1.307(6), C(1)–Au(1) 2.015(4), Au(1)–S(1) 2.2927(12), S(1)–C(22) 1.770(5), N(1)–C(1)–O(1) 111.3(4), C(1)–Au(1)–S(1) 175.69(12), Au(1)–S(1)–C(22) 104.88(16).

2.09 Å]<sup>32</sup> but marginally longer than that in the chloro derivative, **1b** [1.984(6) Å], **2b** [1.993(3) Å], **3b** [1.977(6) Å], and **4b** [1.996(4) Å] (Figure 2 and Supporting Information, Figures S17, S50, and S114). For reference, the corresponding distance in the structurally characterized gold(I) *N*-heterocyclic carbene complexes are as follows: 1.995(6) Å in [1,3-(Mes)<sub>2</sub>-imidazol-2-ylidene]Au(SC<sub>6</sub>H<sub>4</sub>COOH),<sup>39</sup> 2.013(4) Å in [1-(2-hydroxycyclohexyl)-3-(benzyl)imidazol-2-ylidene]Au(SC<sub>10</sub>H<sub>7</sub>),<sup>43</sup> and 2.001(2) Å in [1,3-(Mes)<sub>2</sub>-imidazol-2-ylidene]Au(SC<sub>6</sub>F<sub>5</sub>)<sup>38</sup> (Table 2).

The Au–S bond distances of 2.2874(8) Å (**1d**), 2.2920(7) Å (**2d**), 2.2927(12) Å (**3d**), and 2.2785(11) Å (**4d**) (Figure 4 and Table 2 and Supporting Information, Figures S34, S67, and S131) are significantly shorter than the sum of their individual covalent radii [ $d(\text{Au}–\text{S}) = 2.41$  Å].<sup>32</sup> In the absence of any known structurally characterized example of (AAOC)Au(SC<sub>6</sub>F<sub>5</sub>)-type complexes (AAOC = acyclic aminoxy carbene) and (ADC)Au(SC<sub>6</sub>F<sub>5</sub>)-type complexes (ADC = acyclic diamino carbene), a comparison is made with the reported imidazole-based (NHC)Au(SC<sub>6</sub>F<sub>5</sub>)<sup>38</sup> and (NHC)Au(SC<sub>6</sub>H<sub>5</sub>)-type complexes<sup>39–44</sup> (Table 2).

The  $\angle\text{Au}–\text{S}–\text{C}_{\text{aryl}}$  angle in **1d** [99.20(10)°], **2d** [110.49(8)°], **3d** [104.88(16)°], and **4d** [109.28(15)°] (Figure 4 and Supporting Information, Figures S34, S67, and S131) compares well with structurally characterized gold(I) *N*-heterocyclic carbene complex analogues, namely, [1,3-(Mes)<sub>2</sub>-imidazol-2-ylidene]Au(SC<sub>6</sub>H<sub>4</sub>COOH) [105.92(19)°],<sup>39</sup> [1-(2-hydroxycyclohexyl)-3-(benzyl)imidazol-2-ylidene]Au(SC<sub>10</sub>H<sub>7</sub>) [101.18(14)°],<sup>43</sup> and [1,3-(Mes)<sub>2</sub>-imidazol-2-ylidene]Au(SC<sub>6</sub>F<sub>5</sub>) [106.43(7)°].<sup>38</sup>

Significantly enough, (1–4)**b** successfully catalyzed hydrohydrazination of terminal aryl acetylenes with *p*-toluenesulfonyl

hydrazide at 1 mol % of the catalyst loading in the presence of an equimolar amount of an additive at 95 °C (Table 3 and Supporting Information, Tables S6 and S7). In this regard, it is worth noting that significant interest has appeared on gold catalysis<sup>45</sup> lately and also on the nucleophilic additions to alkynes.<sup>46</sup> A series of catalyst optimization studies including blank runs performed on two representative substrates, phenylacetylene and *p*-toluenesulfonyl hydrazide (Supporting Information, Table S7), and control runs performed with (i) the representative ligand precursor, [(2,4,6-*t*-Bu<sub>3</sub>-C<sub>6</sub>H<sub>2</sub>O)(NCy<sub>2</sub>)]CH<sup>+</sup>OTf<sup>–</sup> (**4a**) (entry 2 and Supporting Information, Table S7), (ii) **4a** and AgSbF<sub>6</sub> (entry 3 and Supporting Information, Table S7), (iii) (Me<sub>2</sub>S)AuCl (entry 4 and Supporting Information, Table S7), (iv) (Me<sub>2</sub>S)AuCl and AgSbF<sub>6</sub> (entry 5 and Supporting Information, Table S7), (v) AgSbF<sub>6</sub> (entry 6 and Supporting Information, Table S7), (vi) representative catalyst [(2,4,6-*t*-Bu<sub>3</sub>-C<sub>6</sub>H<sub>2</sub>O)(NCy<sub>2</sub>)-methylidene]AuCl (**4b**) (entry 7 and Supporting Information, Table S7), and (vii) [(2,4,6-*t*-Bu<sub>3</sub>-C<sub>6</sub>H<sub>2</sub>O)(NCy<sub>2</sub>)-methylidene]AuBr<sub>3</sub> (**4c**) and AgSbF<sub>6</sub> (entry 10 and Supporting Information, Table S7) produced little or no product in all of the cases. In light of these results, the hydrohydrazination reaction between phenylacetylene and *p*-toluenesulfonyl hydrazide, when performed at 1 mol % **4b** in the presence of AgSbF<sub>6</sub> exhibited a significantly high product (**5**) yield of ca. 71% (entry 8 and Supporting Information, Table S7), thereby highlighting the influence of the acyclic aminoxy carbene-stabilized gold(I) complex (**4b**) in the catalysis. Interestingly, the perfluorophenylthiolato derivative (AAOC)Au(SC<sub>6</sub>F<sub>5</sub>) (**4d**) in the presence of AgSbF<sub>6</sub> produced ca. 38% of the product (**5**) (entry 11 and Supporting Information, Table S7). It is important to note that AgSbF<sub>6</sub> was chosen over other additives after performing a detailed additive variation study (Supporting Information, Tables S6 and S7).

The substrate scope was elaborated with several terminal alkynes by modulating the sterics and electronics with the aid of different substituents for all of the gold(I) chloro (1–4)**b** complexes. The sterically hindered **2b** and **4b** bearing cyclohexyl substituents performed better than **1b** and **3b** bearing sterically less demanding methyl substituents for a wide spectrum of electron-rich and electron-poor terminal alkynes substrates (Table 3).

In the absence of any hydrohydrazination of terminal alkynes reported for the acyclic aminoxy carbene based (AAOC)AuCl-type complexes, a comparison of the catalytic activity is made with that of the structurally characterized *N*-heterocyclic carbene-based (NHC)AuCl analogues.<sup>5,15,16,47</sup> However, an exact comparison of the catalysis performance of (1–4)**b** complexes cannot be made with the (NHC)AuCl complexes in the absence of a common substrate reported for these catalysts with the one used for the catalysis study of the (1–4)**b** complexes. Hence, for an exact comparison of the catalysis performance, the comparison of the activity of (1–4)**b** with the (NHC)AuOTf-type complex, [1,3-*bis*(2,6-diisopropylphenyl)hexahydro-2*H*-1,3-diazepine-2-ylidene]AuOTf<sup>12</sup> (Table 4), is made for the common pair of the substrates, phenylacetylene and *p*-toluenesulfonyl hydrazide, used in these two studies. In particular, at 1 mol % catalyst loading, the (NHC)AuOTf-type complex, [1,3-*bis*(2,6-diisopropylphenyl)hexahydro-2*H*-1,3-diazepine-2-ylidene]AuOTf<sup>12</sup> (Table 4), produced **5** in 95% yield at 110 °C in 12 h of reaction time in the absence of any additive in solvent-free conditions, while mixed yields of **5** were obtained for **1b** (8%), **2b** (40%), **3b** (18%), and **4b** (71%) at 1 mol %



**Table 3. Selected Results for the Chloro Derivative of Au(I) Acyclic Aminoxy Carbene (AAOC) (1–4)b Complex-Catalyzed Hydrohydrazination of Terminal Alkynes<sup>a</sup>**

$R^1 = \text{Me}, R^2 = \text{H}$  (1)  
 $R^1 = \text{Cy}, R^2 = \text{H}$  (2)  
 $R^1 = \text{Me}, R^2 = t\text{-Bu}$  (3)  
 $R^1 = \text{Cy}, R^2 = t\text{-Bu}$  (4)

entry	reagent		product	yield <sup>b</sup>											
	(1b)	(2b)		(3b)	(4b)	(5)	(6)	(7)	(8)	(9)	(10)	(11)	(12)	(13)	(14)
1.				8	40	18	71								
2.				58	66	70	51								
3.				39	29	48	25								
4.				18	77	16	70								
5.				0	66	5	57								
6.				0	25	15	62								
7.				0	41	19	65								
8.				0	54	12	60								
9.				0	61	10	53								
10.				0	20	9	25								

<sup>a</sup>Reaction conditions: 1:1 ratio of terminal alkynes:hydrazide derivatives; 1 mol % of catalyst (1–4)b; 1 mol % AgSbF<sub>6</sub>; 5 mL of CH<sub>3</sub>CN at 95 °C for 6 h. <sup>b</sup>Isolated yields (%).

catalyst loading in 6 h of reaction time in CH<sub>3</sub>CN at 95 °C and in the presence of AgSbF<sub>6</sub> as an additive. Hence, the (NHC)-AuOTf-type complex, [1,3-bis(2,6-diisopropylphenyl)-

hexahydro-2H-1,3-diazepine-2-ylidene]AuOTf<sup>12</sup> (Table 4), exhibited superior activity to the (1–4)b complexes. Additionally, at 1 mol % catalyst loading in the presence of 1 mol %

**Table 4.** Comparison of the Reaction Yield of the Product  $p$ -CH<sub>3</sub>C<sub>6</sub>H<sub>4</sub>SO<sub>2</sub>NHNC(CH<sub>3</sub>)C<sub>6</sub>H<sub>5</sub> (**5**) Formed in the Hydrohydrazination Reaction of the Representative Phenylacetylene and  $p$ -Toluenesulfonyl Hydrazide Substrates as Catalyzed by (1–4)**b** Complexes with the Other Well-Defined Gold–Heteroatom-Stabilized Singlet Carbene Complexes in the Literature

(5)

entry	catalyst	additive	time (h)	solvent	catalyst loading (mol %)	temperature (°C)	yield <sup>a</sup> (%)	reference
1.			12	solvent-free condition	1	110	95	[12]
2.		AgSbF <sub>6</sub>	6	CH <sub>3</sub> CN	1	95	63	present work
3.		AgSbF <sub>6</sub>	6	CH <sub>3</sub> CN	1	95	55	present work
4.		AgSbF <sub>6</sub>	6	CH <sub>3</sub> CN	1	95	8	present work
5.		AgSbF <sub>6</sub>	6	CH <sub>3</sub> CN	1	95	40	present work
6.		AgSbF <sub>6</sub>	6	CH <sub>3</sub> CN	1	95	18	present work
7.		AgSbF <sub>6</sub>	6	CH <sub>3</sub> CN	1	95	71	present work

<sup>a</sup>Isolated yield.

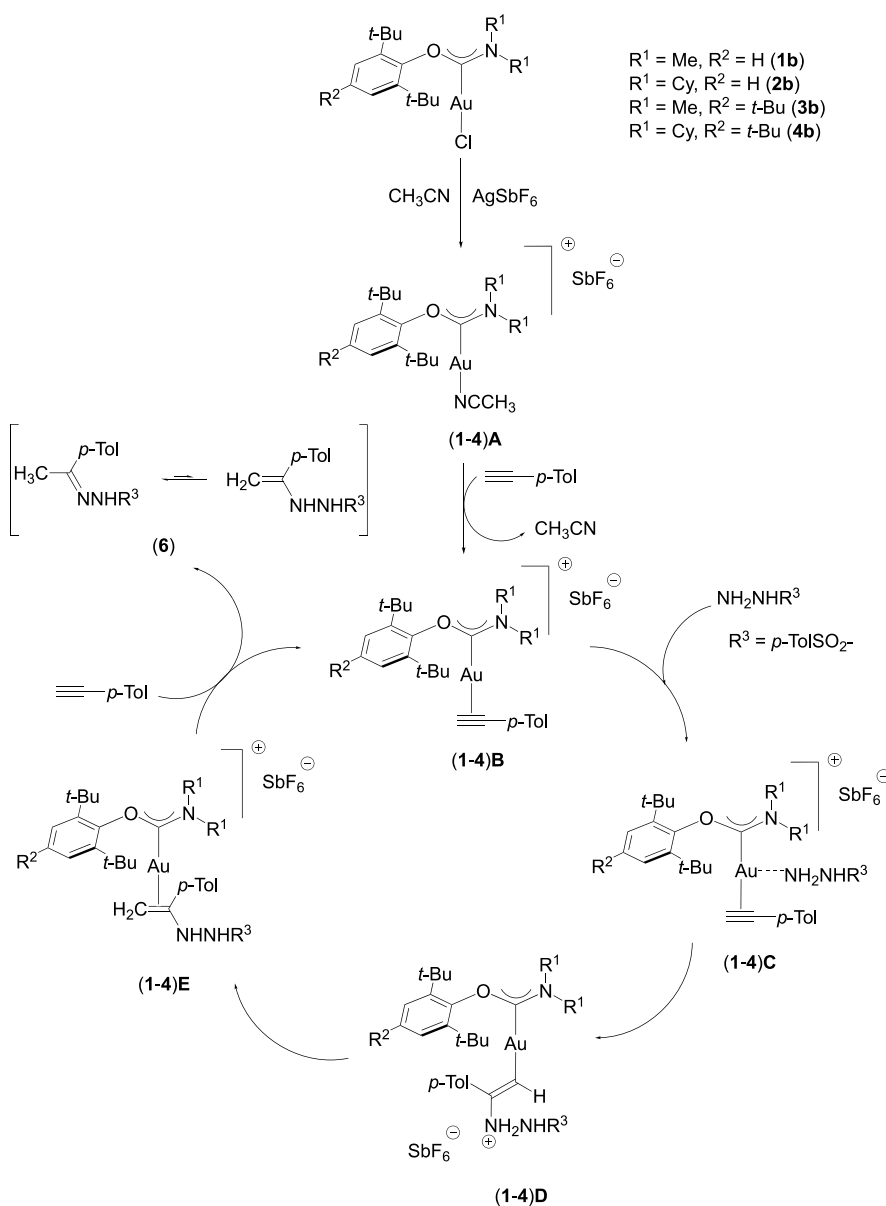
AgSbF<sub>6</sub>, the following two benchmark catalysts, [1,3-bis(2,6-diisopropylphenyl)imidazol-2-ylidene]AuCl<sup>48</sup> and [1,3-bis(mesityl)imidazol-2-ylidene]AuCl,<sup>48</sup> exhibited 63% (entry 2 in Table 4) and 55% (Entry 3 in Table 4) yields, respectively, under analogous catalysis conditions. Nonetheless, (1–4)**b** represent the first catalytic utility of the acyclic aminoxy carbene-based (AAOC)AuCl-type complexes in the hydrohydrazination of terminal alkynes, thereby opening new avenues for exploration in this newly developed carbene platform.

Based on the mass spectrometry studies, a mechanistic pathway has been proposed for the hydrohydrazination of terminal alkynes by the (1–4)**b** complexes (Scheme 2).

A proposed catalytic cycle<sup>49</sup> for the hydrohydrazination reaction initiates the formation of the CH<sub>3</sub>CN bound

gold(I) species of the type [(AAOC)Au(CH<sub>3</sub>CN)]SbF<sub>6</sub> (1–4)**A**, upon the treatment of the (AAOC)AuCl-type complexes with AgSbF<sub>6</sub> in CH<sub>3</sub>CN along with the formation of AgCl precipitates (Scheme 2). Quite significantly, all of the [(AAOC)Au(CH<sub>3</sub>CN)]SbF<sub>6</sub>-type (1–4)**A** species have been characterized by mass spectrometry (Figure 5 and Supporting Information, Figures S188–S192, S194, and S195). Subsequent addition of 4-ethynyltoluene to (1–4)**A** yields the  $\pi$ -complexes of gold(I) species coordinated to alkyne of the type [(AAOC)-Au(HC $\equiv$ CPhMe)]SbF<sub>6</sub> (1–4)**B**, which too have been characterized by mass spectrometry for the representative **3B** species (Figure 6 and Supporting Information, Figure S193).<sup>50</sup> The activation of  $p$ -toluenesulfonyl hydrazide by coordination to the metal center in (1–4)**B** yields the hydrazide-coordinated

**Scheme 2. Proposed Mechanism for the Chloro Derivative of Au(I) Acyclic Aminooxy Carbene (AAOC) (1–4)-Catalyzed Hydrohydrazination of the Representative Substrates, Namely, 4-Ethynyltoluene and *p*-Toluenesulfonyl Hydrazide**



[(AAOC)Au(HC≡CPhMe)(NH<sub>2</sub>NHSO<sub>2</sub>C<sub>6</sub>H<sub>4</sub>CH<sub>3</sub>)]SbF<sub>6</sub> (**1–4**)C, which undergo intramolecular hydroamination to give (**1–4**)D (Scheme 2). Finally, the hydrogen transfer in (**1–4**)D that proceeds via a two-step sequence as corroborated by DFT studies gives the alkene-coordinated (**1–4**)E, which in the presence of 4-ethynyltoluene results in the regeneration of (**1–4**)B along with the release of the hydrohydrazinated product (**6**) (Scheme 2).<sup>51</sup>

The isotopic labeling study performed with deuterated phenylacetylene-*d* (PhC≡CD), synthesized using a modified procedure,<sup>52</sup> showed Markovnikov's type of hydroamination reaction resulting in formation of a deuterated analogue (CH<sub>3</sub>C<sub>6</sub>H<sub>4</sub>SO<sub>2</sub>NHN=C(CH<sub>2</sub>D)Ph) (**5-d**<sub>1</sub>) along with the protonated analogue (**5**) in a *ca.* 1:2 ratio (Figure 7). The characteristic resonance for the CH<sub>2</sub>D moiety in (**5-d**<sub>1</sub>) appeared as a triplet at 2.18 ppm<sup>53</sup> in the <sup>1</sup>H NMR (Figure 7 and Supporting Information, Figures S196–S199). Similarly, in the <sup>13</sup>C{<sup>1</sup>H} NMR spectrum, the CH<sub>2</sub>D moiety in **5-d**<sub>1</sub> appeared

at 13.5 ppm (Figure 7 and Supporting Information, Figures S196–S199).<sup>53</sup>

The hydrohydrazination reaction is attracting interest mainly for their utility in accessing a large variety of organic compound having anticonvulsant properties.<sup>54</sup> These compounds are primarily used for treating neurological disorders including epilepsy.<sup>54–56</sup> In this backdrop, it is but significant that the representative gold(I) **2b** complex successfully carry out the hydrohydrazination reaction between a series of terminal alkynes, namely, phenylacetylene, 4-ethynyltoluene, 1-ethynyl-4-chlorobenzene, and 1-ethynyl-4-bromobenzene, and acetohydrazide giving access to several anticonvulsant compounds (**15–18**) (Table 5 and Supporting Information, Figures S172–S187).<sup>55</sup> The two benchmark catalysts 1,3-bis(2,6-diisopropylphenyl)imidazol-2-ylidene]AuCl<sup>48</sup> and [1,3-bis(mesityl)imidazol-2-ylidene]AuCl<sup>48</sup> exhibited comparable yields for the substrates, phenylacetylene, 4-ethynyltoluene, and 1-ethynyl-4-bromobenzene, but showed no product with 1-

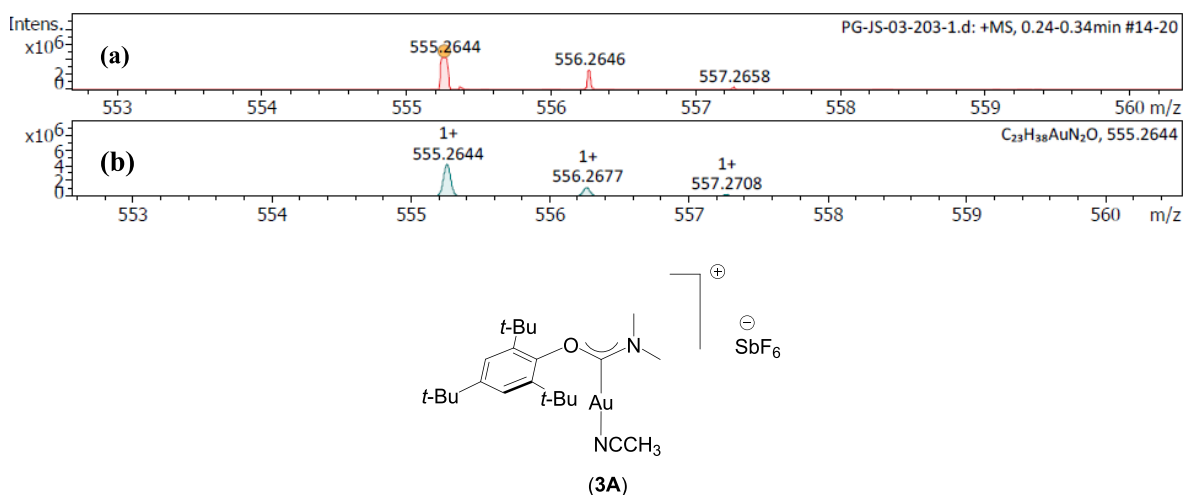


**Figure 5.** HRMS data of the  $\{[(2,4,6\text{-}t\text{-Bu}_3\text{-C}_6\text{H}_2\text{O})(\text{NMe}_2)\text{methylidene}]\text{Au}(\text{CH}_3\text{CN})\}\text{SbF}_6$  species (**3A**), detected in the reaction mixture of 1 mol % catalyst (**3b**) and 1 mol %  $\text{AgSbF}_6$ , 2.5 mL of  $\text{CH}_3\text{CN}$  at room temperature. (a) Experimental and (b) simulated pattern of ESI-MS data.

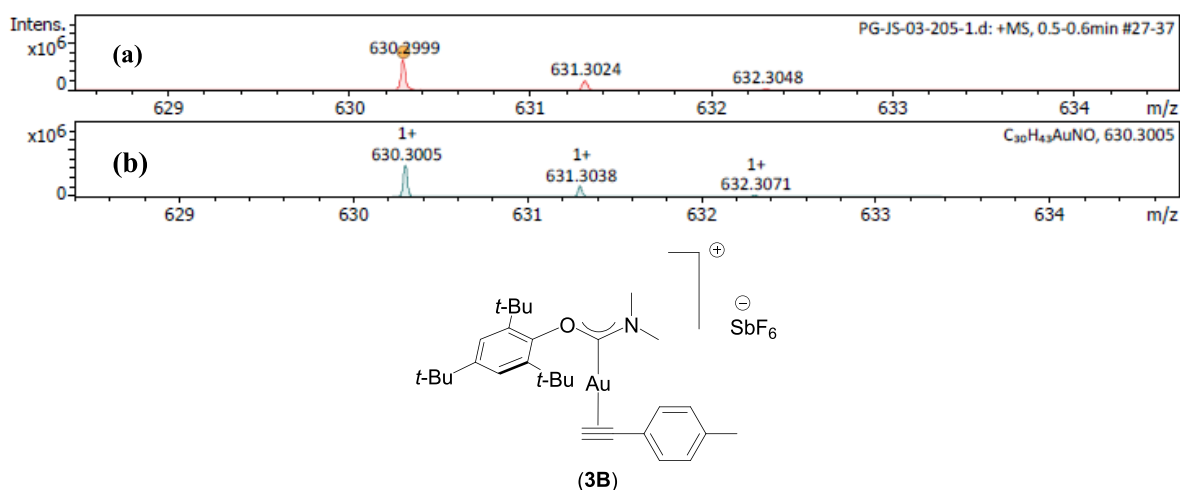


**Figure 6.** HRMS data of the  $\{[(2,4,6\text{-}t\text{-Bu}_3\text{-C}_6\text{H}_2\text{O})(\text{NMe}_2)\text{methylidene}]\text{Au}(\text{HC}\equiv\text{CPhMe})\}\text{SbF}_6$  species (**3B**), detected in the reaction mixture of 4-ethynyltoluene (0.156 mmol), 1 mol % catalyst (**3b**), and 1 mol %  $\text{AgSbF}_6$ , 2.5 mL of  $\text{CH}_3\text{CN}$  at room temperature. (a) Experimental and (b) simulated pattern of ESI-MS data.

ethynyl-4-chlorobenzene in the reaction with acetohydrazide (Table 5).

**Density Functional Theory Studies.** All DFT calculations have been performed in the Gaussian suite of program g09.<sup>57</sup> The methodology that has been used is the B3LYP-D3 functional along with the basis set SDD for Au atom<sup>58</sup> and 6-31G\*<sup>59</sup> for other atoms.<sup>60,61</sup> Functional choice has been made on the basis of our previous work<sup>62</sup> and some similar work in this area.<sup>63</sup> The single point energies were computed on optimized geometries with the combination of the B3LYP-D3 functional and def2-TZVP basis set for all atoms.<sup>64</sup> For refining the gas-phase electronic energies, the Gibbs free energy correction has been added to the single-point energies obtained from the higher basis set. The solvation has been modeled in the polarizable continuum model (PCM),<sup>65</sup> and acetonitrile has been taken as the solvent. The natural bond orbital (NBO) analysis<sup>66</sup> and Wiberg bond order (WBI) analysis<sup>67</sup> have been performed with the same methodology. The optimization of the structures of all of the (1–4)**b** precatalysts and two benchmarks (NHC)AuCl analogues, namely, [1,3-bis(2,6-diisopropylphenyl)imidazol-2-ylidene]AuCl<sup>48</sup> and [1,3-bis(mesityl)imidazol-2-ylidene]AuCl,<sup>48</sup> showed good agreement with the single-crystal X-ray

diffraction data of these complexes (Supporting Information, Figures S202 and S203 and Tables S31–S37), thereby strengthening our confidence in our computational methods and also leading us to search all possible pathways of the hydrohydrazination reaction.

**<sup>13</sup>C NMR Chemical Shift Analysis.** The <sup>13</sup>C NMR spectroscopic calculations have been performed in ORCA 4.2<sup>68</sup> version software (Supporting Information, Table S42). The starting coordinates for the <sup>13</sup>C NMR calculations have been obtained by DFT calculations in the Gaussian09 suite of programs as stated earlier.<sup>57</sup> The B3LYP hybrid functional<sup>60,61</sup> has been used along with the RIJK approximation.<sup>69</sup> The Sapporo-DKH3-DZP-2012 basis set has been used for gold transition metal,<sup>70</sup> DKH-def2-TZVP(-f) was used for Cl,<sup>70</sup> IGLO-II was used for C,<sup>71</sup> and DKH-def2-SVP was used for the rest of the atoms (O, N, and H).<sup>64,72</sup> The same method is also employed for <sup>13</sup>C NMR calculations in the case of TMS.

The computed <sup>13</sup>C NMR chemical shifts for (1–4)**b** and two benchmarks (NHC)AuCl analogues, namely, [1,3-bis(2,6-diisopropylphenyl)imidazol-2-ylidene]AuCl<sup>48</sup> and [1,3-bis(mesityl)imidazol-2-ylidene]AuCl,<sup>48</sup> agree well with the experimentally reported values (Supporting Information, Table

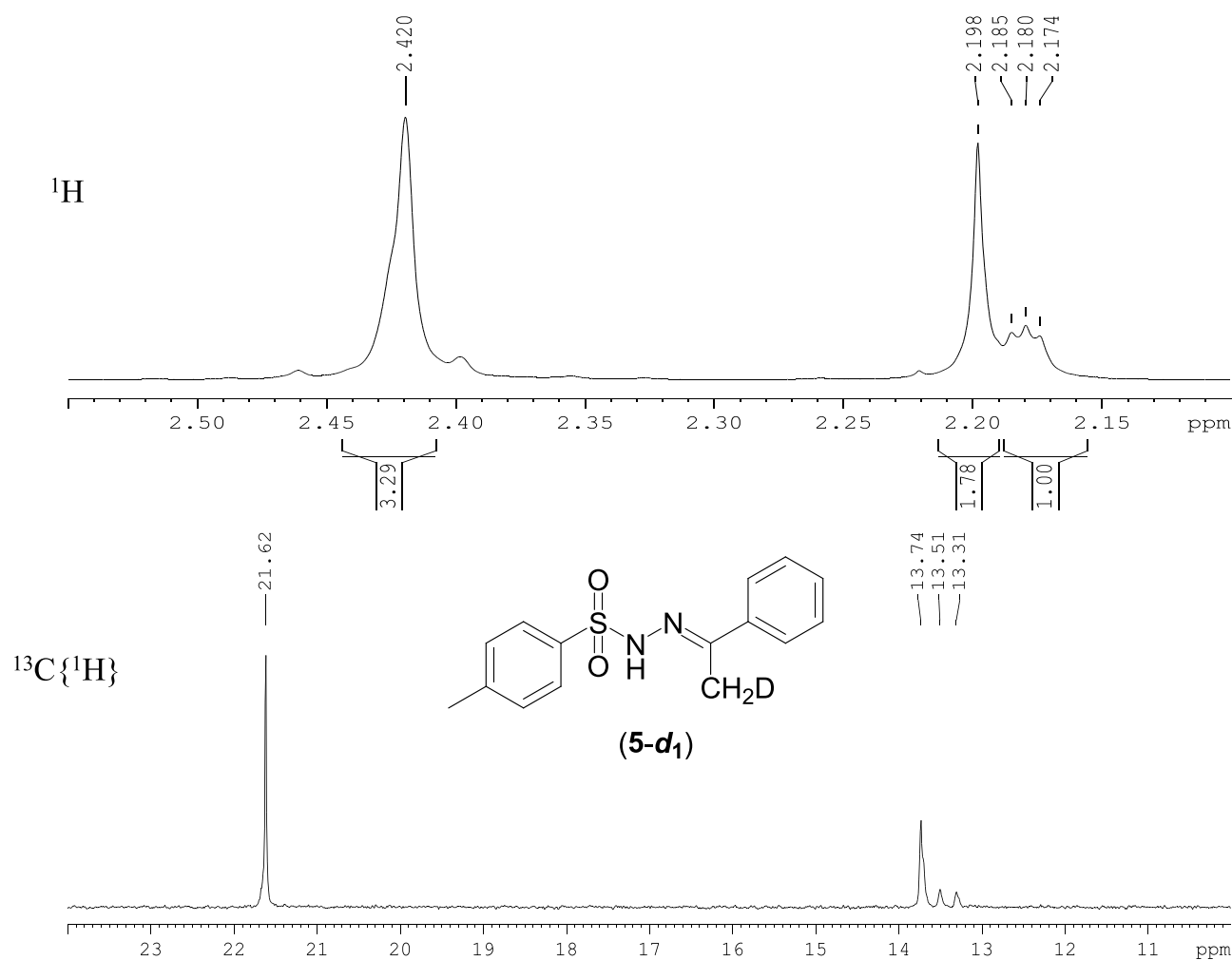


**Figure 7.**  $^1\text{H}$  NMR (400 MHz) and  $^{13}\text{C}\{^1\text{H}\}$  NMR (100 MHz) spectra of  $5\text{-}d_1$  containing deuterium in its methyl group.

S42). For example, for the **2b** and **4b** complexes that showed higher yields for the hydrohydrazination reaction, the experimentally observed ( $\text{Au}-\underline{\text{C}}_{\text{carbene}}$ ) resonance appeared at  $\delta$  ca. 211.6 and 211.8 ppm, respectively, while the computed values were at  $\delta$ . 220.5 and 220.6 ppm, respectively, and were in line with the similar difference between the observed and computed chemical shifts reported earlier.<sup>73</sup> The computed deshielding observed suggested that the dominant contribution to the  $\text{Au}-\underline{\text{C}}_{\text{carbene}}$  bond arise from the  $\sigma$  character of the corresponding occupied MO bond as expected. The large deshielding contributions to our complexes compared to the benchmark system were found to arise from the paramagnetic spin-orbit term while other contributions are nearly equal.<sup>74</sup> The difference in chemical shift has been attributed to the predictive power of the generalized gradient approximation (GGA) functionals in the case of  $\pi$ -donating carbenic carbon atoms. Another interesting observation is that for the (**1–4**)**b** complexes, this difference in chemical shift between the observed and the computed values decreases gradually on moving from deshielding to the shielding region.

**Steric Parameter (% Buried Volume) Analysis.** The steric map plot and buried volume (%  $V_{\text{Bur}}$ ) of the precatalyst (**1–4**)**b** have been computed using SambVca 2.0 (a web tool for analyzing catalytic pockets with topographic steric maps).<sup>75</sup> The steric map plot gives the calculated %  $V_{\text{Bur}}$ , which correlates to the steric factor. Generally, in the steric map plots, an area with a

greater red color indicates a greater steric factor of the catalyst, while an area with a greater blue color indicates a less steric factor of the catalyst. Hence, the steric effect of the catalytic pocket is reduced by moving from the red to blue region. The calculated steric map plot was generated by entering the default values of the SambVca 2.0 web tool. The Cartesian coordinate representation of the steric map plot is given in Figure S200.

The steric map and percent buried volume (%  $V_{\text{Bur}}$ ) calculations for (**1–4**)**b** and the two benchmark (NHC)AuCl analogues, namely, [1,3-bis(2,6-diisopropylphenyl)imidazol-2-ylidene]AuCl<sup>48</sup> and [1,3-bis(mesityl)imidazol-2-ylidene]AuCl-type complexes,<sup>48</sup> were computed, and a comparison was made as shown in Table 6. A careful scrutiny of the results showed that sterically demanding precatalysts (**4b**) having large buried volumes (%  $V_{\text{Bur}}$ ) of 90.0% exhibited a higher yield of 71%. However, another sterically demanding precatalyst (**2b**), having a large-buried volume (%  $V_{\text{Bur}}$ ) of 91.3%, showed a modest yield of 40%, thereby suggesting that apart from the sterics, the electronics and other factors too play a pivotal role in the hydrohydrazination catalysis.

**Catalytic Pathway.** The DFT calculation of a simplified model species (**4b'**) and its catalytically relevant  $\text{CH}_3\text{CN}$  coordinated species (**A**) of the most active (**4b**) precatalyst was undertaken in order to reduce the computational cost<sup>28a</sup> (Supporting Information, Figures S203 and S204 and Table S38). The computed structural parameters of these models



**Table 5. Synthesis of a Variety of Anticonvulsant Active Compounds by Using Hydrohydrazination of Terminal Alkynes Catalyzed by the Representative **2b**, [1,3-bis(2,6-Diisopropylphenyl)imidazol-2-ylidene]AuCl and [1,3-bis(Mesityl)imidazol-2-ylidene]AuCl Complexes<sup>a</sup>**

1 mol % Au(I)  
1 mol % AgSbF<sub>6</sub>  
CH<sub>3</sub>CN  
reflux, 95 °C

R = H (**15**)  
= *p*-Me (**16**)  
= *p*-Cl (**17**)  
= *p*-Br (**18**)

entry	reagent	reagent	product			
			<p><b>(2b)</b></p>	yield <sup>b</sup>	yield <sup>b</sup>	yield <sup>b</sup>
1.			<p><b>(15)</b></p>	16	10	6
2.			<p><b>(16)</b></p>	24	27	22
3.			<p><b>(17)</b></p>	9	0	0
4.			<p><b>(18)</b></p>	15	20	13

<sup>a</sup>Reaction conditions: 1:1 ratio of terminal alkynes:acetohydrazide; 1 mol % of catalyst **2b** or [1,3-bis(2,6-diisopropylphenyl)imidazol-2-ylidene]AuCl or [1,3-bis(mesityl)imidazol-2-ylidene]AuCl; 1 mol % AgSbF<sub>6</sub>; 5 mL of CH<sub>3</sub>CN at 95 °C for 6 h. <sup>b</sup>Isolated yields (%).

generally agreed with the X-ray structure reported. The DFT result showed that the formation of CH<sub>3</sub>CN-coordinated species (**A**) [(AAOC)Au(NCMe)] formed from the species **4b'** is more favorable than its acetylene coordinated species (**A'**) [(AAOC)Au(HC=CPhMe)] with an energy difference of 5.8 kJ/mol with respect to species **4b'** (Supporting Information, Figure S213). Therefore, for the catalytic process CH<sub>3</sub>CN-coordinated species, **A** has been considered as the starting precursor<sup>28a</sup> (see Figure S201 for bond parameters, WBI, and NBO analysis).

The natural bond order (NBO) analysis of **A** shows that the N(1)–C(19) bond has *p<sub>x</sub>*–*p<sub>x</sub>* and *p<sub>z</sub>*–*p<sub>z</sub>* characters having 63.7% and 73.9% occupancy of N(1) orbitals and 36.3% and

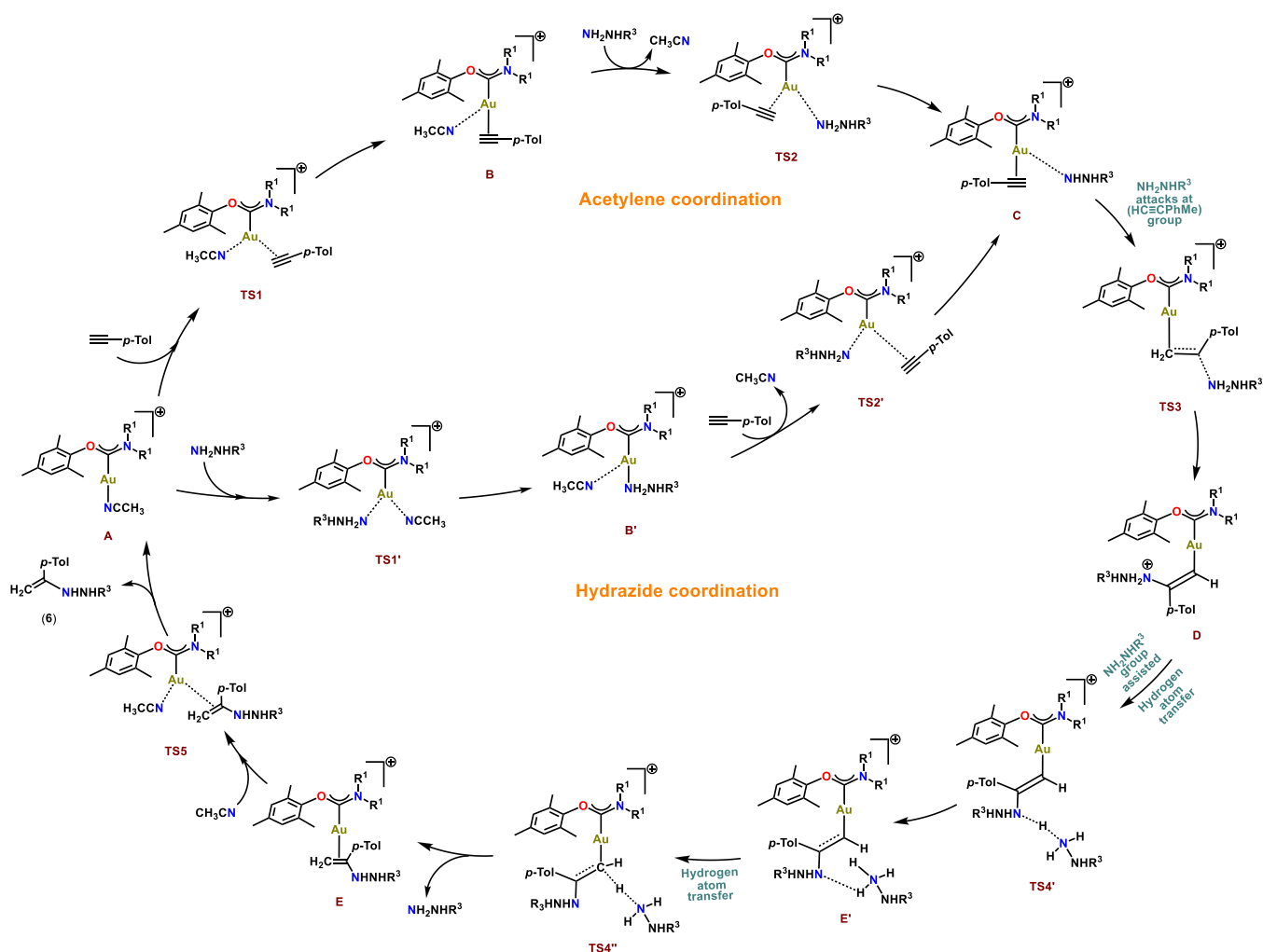
26.1% occupancy of C(19) orbitals (Supporting Information, Figure S206), in concurrence with the double bonded nature of the N(1)–C(19) bond. In contrast, the other O(1)–C(19) bond exhibited an overlap between the *p<sub>y</sub>*–*p<sub>y</sub>* orbitals with an occupancy of 68.7% and 31.3% for the O(1) and C(19) orbitals, respectively, implying a single bond character. The gold(I) metal center bound to the carbenic C(19) atom showed the 6s orbital of Au(1) with 26.7% occupancy interacting with the *p<sub>y</sub>* orbital of C(19) with 73.3% occupancy. NBO analysis results are further validated by Wiberg bond index (WBI) analysis that showed a 1.48 bond index for the N(1)–C(19) bond, consistent with a double bond character, and a single bond value of 1.10 for the O(1)–C(19) bond, similar to the NBO results. A single bond

**Table 6.** Comparison between Computationally Calculated %  $V_{\text{Bur}}$  and Experimentally Observed % Yield of Product  $p\text{-CH}_3\text{C}_6\text{H}_4\text{SO}_2\text{NHNC}(\text{CH}_3)\text{C}_6\text{H}_5$  (**5**) Formed in the Hydrohydrazination Reaction of the Representative Phenylacetylene and  $p$ -Toluenesulfonyl Hydrazide Substrates as Catalyzed by (1–4)b Precatalyst and (NHC)AuCl Analogues [1,3-bis(2,6-Diisopropylphenyl)imidazol-2-ylidene]AuCl and [1,3-bis(Mesityl)imidazol-2-ylidene]AuCl

(5)

entry	catalyst	steric map plot	% $V_{\text{Bur}}$	% yield
1.	<p>(2b)</p>		91.3	40
2.	<p>(4b)</p>		90.0	71
3.			89.9	63
4.	<p>(1b)</p>		86.9	8
5.	<p>(3b)</p>		84.9	18
6.			83.4	55

**Scheme 3. Proposed Mechanism for Hydrohydrazination of 4-Ethynyltoluene (HC≡CPhMe) and *p*-Toluenesulfonyl Hydrazide (NH<sub>2</sub>NHSO<sub>2</sub>C<sub>6</sub>H<sub>4</sub>CH<sub>3</sub>) by Solvent-Coordinated Starting Species A, Exhibiting an Acetylene and Hydrazide Coordination Pathway and Proton Transfer Occurring *via* Another Hydrazide Group Assistance**



character with a 0.71 Wiberg bond index was observed for the Au(1)–C(19) bond (Supporting Information, Table S39).

The catalytic cycle is proposed to proceed through any of the following two pathways: (i) acetylene (HC≡CPhMe) coordination to the gold(I) center in the first step and (ii) the hydrazide (NH<sub>2</sub>NHSO<sub>2</sub>C<sub>6</sub>H<sub>4</sub>CH<sub>3</sub>) coordination to the gold(I) center in the first step (Scheme 3).

**Acetylene Coordination Pathway.** In this route, the first step involves the attack of 4-ethynyltoluene (HC≡CPhMe) on the solvent-coordinated gold(I) metal center of A, resulting in the transition state TS1 with the release of the coordinated CH<sub>3</sub>CN. In this transition state (TS1), gold(I) was three-coordinated, being bound to the amino alkoxy carbene ligand, 4-ethynyltoluene (HC≡CPhMe), and CH<sub>3</sub>CN, with an energy barrier of 62.6 kJ/mol, and produced cationic acetylene bound gold(I) [(AAOC)Au(HC≡CPhMe)]<sup>+</sup>-type species (B). In TS1, the detachment of the CH<sub>3</sub>CN moiety occurs, as evidenced by a longer Au(1)–N(2) bond length of 2.424 Å with respect to that of 2.065 Å in the starting reactant species (A). Simultaneously, the approach of acetylene to the gold(I) center is observed from a Au(1)–C(a) bond length of 2.481 Å. The transition state (TS1) leads to a cationic intermediate species (B) of the type [(AAOC)Au(HC≡CPhMe)]<sup>+</sup> that display a weak interaction with the outgoing CH<sub>3</sub>CN molecule as

observed from a distance of 3.245 Å (Supporting Information, Figure S204). Intermediate B has an energy barrier of 30.6 kJ/mol with regard to the starting reactant species (A). The acetylene (HC≡CPhMe) moiety is bound more tightly to the gold(I) center in intermediate B as seen from a shorter Au(1)–C(a) bond distance of 2.190 Å as opposed to that of 2.481 Å in the TS1 transition state. Subsequent attack of the hydrazide (NH<sub>2</sub>NHSO<sub>2</sub>C<sub>6</sub>H<sub>4</sub>CH<sub>3</sub>) moiety results in transition state TS2 having an energy margin of 53.5 kJ/mol with respect to the reactant species (A). The ∠C(a)–Au(1)–N(3) bond angle that the acetylene and hydrazide moieties make with the gold(I) center is 78.5°. The Au(1)–C(a) bond 2.384 Å is extended in (TS2) as compared to the intermediate species (B) (2.190 Å). Similarly, an interaction of the approaching hydrazide (NH<sub>2</sub>NHSO<sub>2</sub>C<sub>6</sub>H<sub>4</sub>CH<sub>3</sub>) moiety and the gold(I) center is observed from an extended Au(1)–N(3) distance of 2.492 Å. The Au(1)–C(19) distance increases by 0.009 Å in transition state TS2, as compared to TS1, indicating a greater *trans*-effect of the hydrazide (NH<sub>2</sub>NHSO<sub>2</sub>C<sub>6</sub>H<sub>4</sub>CH<sub>3</sub>) moiety than that of the CH<sub>3</sub>CN moiety. The transition state TS2 leads to the formation of the intermediate C species, containing a strongly bound acetylene (HC≡CPhMe) moiety, and a weakly bound hydrazide (NH<sub>2</sub>NHSO<sub>2</sub>C<sub>6</sub>H<sub>4</sub>CH<sub>3</sub>) moiety. However, another possibility exists for the proposed mechanism, in which TS2 may

lead directly to the formation of intermediate **D**. Such a possible mechanism has also been reported in the previous literature.<sup>23</sup> In this study, intermediate **C** formation was found to be more exothermic by *ca.* 7.6 kJ/mol than intermediate **D** formation. Thus, it can be concluded that intermediate **C** is more likely to be formed as it is more stable owing to the energy margin of 23.3 kJ/mol. In particular, the acetylene (HC≡CPhMe)-bound gold(I) center in **C** exhibits a Au(1)–C(a) bond length of 2.186 Å, while the hydrazide (NH<sub>2</sub>NHSO<sub>2</sub>C<sub>6</sub>H<sub>4</sub>CH<sub>3</sub>) moiety can be seen weakly interacting with the metal center at a Au(1)⋯N(3) distance of 3.754 Å. The Wiberg bond index analysis gives a value of 2.51 for the C(a)–C(b) bond consistent with the triple bond character for the C(a)–C(b) bond of acetylene (HC≡CPhMe) moiety and Wiberg index value of 0.02 for the Au(1)⋯N(3) distance, thus indicating a fragile interaction, or a no bond character, of the hydrazide (NH<sub>2</sub>NHSO<sub>2</sub>C<sub>6</sub>H<sub>4</sub>CH<sub>3</sub>) moiety with the gold(I) center. From intermediate **C**, the catalytic cycle further proceeds by a common mechanism for both the acetylene and hydrazide coordination pathways.

**Hydrazide Coordination Pathway.** This pathway proceeds by hydrazide (NH<sub>2</sub>NHSO<sub>2</sub>C<sub>6</sub>H<sub>4</sub>CH<sub>3</sub>) coordination to the gold(I) metal center along with the cleavage of the gold(I) coordinated CH<sub>3</sub>CN solvent, giving rise to the transition state **TS1'** with an energy barrier of 64.3 kJ/mol. Here too, the bond distance between Au(1) and the leaving CH<sub>3</sub>CN moiety, *i.e.*, the Au(1)–N(2) bond is extended as observed from the distance of 2.411 Å as compared to that of 2.065 Å in reactant **A**. The approaching hydrazide (NH<sub>2</sub>NHSO<sub>2</sub>C<sub>6</sub>H<sub>4</sub>CH<sub>3</sub>) moiety interacts with the gold(I) center at a distance of 2.403 Å. Compared to the transition state **TS1**, where the acetylene (HC≡CPhMe) moiety coordinates first instead of the hydrazide (NH<sub>2</sub>NHSO<sub>2</sub>C<sub>6</sub>H<sub>4</sub>CH<sub>3</sub>) moiety, the bond length between the gold(I) metal and the solvent CH<sub>3</sub>CN and between the Au(1)–C(19) bond is comparatively shorter in the transition state **TS1'** (Supporting Information, Figure S205). Therefore, it can be seen that the hydrazide (NH<sub>2</sub>NHSO<sub>2</sub>C<sub>6</sub>H<sub>4</sub>CH<sub>3</sub>) moiety coordination makes the Au(1)–C(19) bond order stronger in the transition state **TS1'** than the acetylene (HC≡CPhMe) moiety coordination in the transition state **TS1**. It is noteworthy that the transition state (**TS1**) is found to be more stable than the transition state **TS1'** by 1.7 kJ/mol, favoring path a (acetylene coordination pathway). The transition state **TS1'** converts to the intermediate species (**B'**), displaying an energy barrier of 13.2 kJ/mol with respect to the reactant species (**A**). In this cationic [(AAOC)Au(NH<sub>2</sub>NHSO<sub>2</sub>C<sub>6</sub>H<sub>4</sub>CH<sub>3</sub>)]<sup>+</sup>-type species (**B'**), the hydrazide (NH<sub>2</sub>NHSO<sub>2</sub>C<sub>6</sub>H<sub>4</sub>CH<sub>3</sub>) moiety is closely associated with the gold(I) center at a distance of 2.155 Å and the outgoing CH<sub>3</sub>CN moiety is disposed far away at a distance of 3.362 Å. The WBI analysis showed a single bond character for the Au(1)–N(3) bond due to the bound hydrazide (NH<sub>2</sub>NHSO<sub>2</sub>C<sub>6</sub>H<sub>4</sub>CH<sub>3</sub>) moiety with a WBI value of 0.31 and the absence of a bond for the outgoing CH<sub>3</sub>CN moiety having a WBI value of 0.05 for the Au(1)⋯N(2) interaction. The intermediate **B'** is thermodynamically more stable by 17.4 kJ/mol than the intermediate **B**.

The intermediate **B'** undergoes an attack by the acetylene (HC≡CPhMe) moiety to yield the transition state **TS2'** with an energy barrier of 41.5 kJ/mol. In this three-coordinated hydrazide–acetylene–gold [(AAOC)Au(HC≡CPhMe)–(NH<sub>2</sub>NHSO<sub>2</sub>C<sub>6</sub>H<sub>4</sub>CH<sub>3</sub>)]<sup>+</sup>-type transition state (**TS2'**), the gold–hydrazide bond is 2.437 Å as compared to 2.155 Å in the intermediate **B'**, and the acetylene (HC≡CPhMe) moiety is attached to the gold(I) center at a distance of 2.511 Å. The

transition state **TS2'** is more stable by 12.0 kJ/mol than the transition state **TS2**. The bond lengths of both the Au(1)–C(a) bond and the Au(1)–N(3) bond are observed to be different in both transition states, and this may be the reason for the energy difference between the two transition states. The **TS2'** leads to the intermediate **C**, after which the catalytic cycle proceeds with a common pathway.

In the next step, the transition state **TS3** is formed from the intermediate species **C**. In this transition state (**TS3**), the hydrazide moiety attacks the acetylene moiety's second carbon center C(b) in anti-fashion and forms an acetylene-bonded hydrazine species as the transition state (**TS3**) having an energy penalty of 62.1 kJ/mol with respect to the reactant species (**A**). In 1998, Teles et al. observed that the syn addition of alcohols to the alkyls via nucleophilic attack of the oxygen is more favorable in the proposed mechanism.<sup>76</sup> However, in 2004, Hashmi et al. found that *anti*-addition is more favorable in the stereospecific reaction of the intramolecular carbonyl-oxygen nucleophile attacks toward the  $\pi$ -coordinated alkyne.<sup>77</sup> This contrast from Teles's work can be explained by the absence of solvation free-energy in the earlier study. Our calculations favor the *anti*-addition of the hydrazide group with acetylene which is also supported by the experiments. The barrier computed for the **TS3** is nearly equal to the one computed for the rate-determining transition (**TS1**). Hence, it can be said that the formation of intermediate species **D** is an important step toward the intermolecular hydroamination reaction. During the formation of the transition state, the hydrazide group approaches the acetylene group at a distance of 2.430 Å, and simultaneously the C(a)–C(b) distance elongates by 0.030 Å with respect to **C**. The addition of the hydrazide proceeds in a Markovnikov fashion via *anti*-addition with the C(a)–N(3) bond formation in the transition state (**TS3**) that eventually leads to the intermediate species **D**. To further investigate, the outer sphere mechanism also has been attempted by modeling the **TS3'**<sub>OS</sub>. As our attempt to obtain the corresponding transition state is unsuccessful, we perform a relaxed scan along the reaction coordinate to estimate the corresponding barrier. During this transition state, hydrazide group nitrogen N(3) attacks the C(a) center instead of the C(b) center of the acetylene group. The calculated energy barrier from the scan suggests that the outer sphere attack on C(a) center is found to be higher in energy by 20.3 kJ/mol from the transition state **TS3**. While this is the maximum barrier one can obtain, this and experiments suggested that this mechanistic route is unfavorable (Supporting Information, Figure S216). The formation of intermediate species **D** is observed with an energy barrier of 30.9 kJ/mol with respect to the reactant species (**A**). The bond distance between the N(3) atom of the hydrazide moiety and the C(b) atom of the acetylene moiety is 1.549 Å and is consistent with the formation of the C–N bond. Also, the elongation of the C(a)–C(b) distance bond distance 1.269 Å in **TS3** to 1.332 Å in **D** is in agreement with the reduction in the bond order of the acetylene group in the intermediate species **D**, which too has been validated with WBI and NBO analyses (Supporting Information, Figure S210 and Table S39).

This intermediate species **D** undergoes a proton transfer that may proceed by (a) water-assisted proton transfer (Supporting Information, Scheme S1 and Figure S214) (b) assistance by another hydrazide molecule (Scheme 3), and (c) a direct proton transfer from the N(3)-atom of hydrazide moiety to the C(a)-atom of the acetylene moiety (Supporting Information, Scheme S2 and Figure S215).

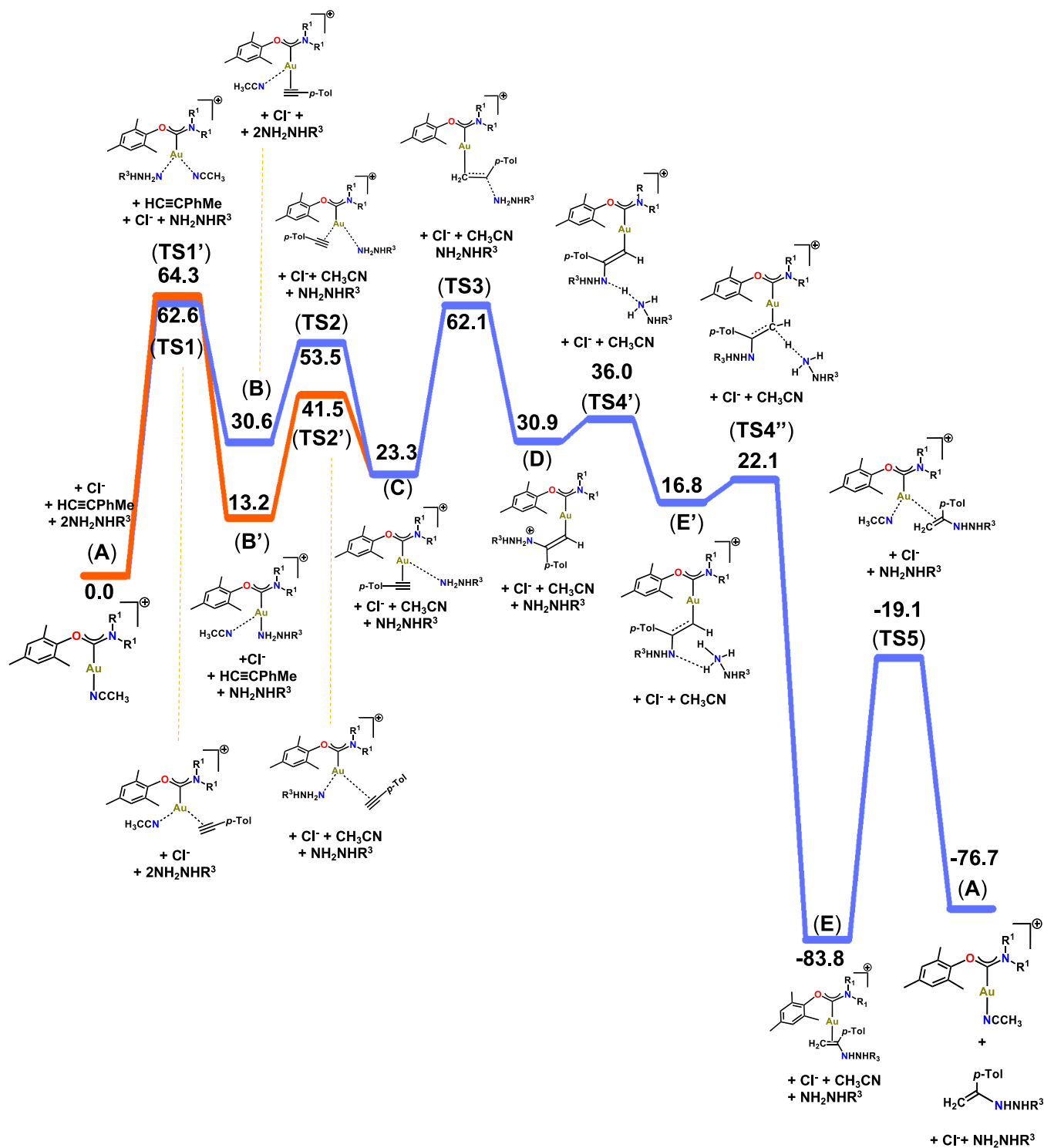


**Figure 8.** Energy profile diagram of the computed solvent phase free energies ( $\Delta G$ ), at the B3LYP-D3/def2-TZVP level of theory, exhibiting acetylene coordination pathway (in light blue color) and hydrazide coordination pathway (in orange color) proceeding via another hydrazide group assisted proton transfer pathway for the hydrohydrazination reaction of 4-ethynyltoluene ( $\text{HC}\equiv\text{CPhMe}$ ) and *p*-toluenesulfonyl hydrazide ( $\text{NH}_2\text{NHSO}_2\text{C}_6\text{H}_4\text{CH}_3$ ) by a gold(I) catalyst (A) (energy in kJ/mol).

**Water-Assisted Proton Transfer.** The water-assisted proton-transfer proceeds via the five-membered transition state **TS4**, in which a water molecule takes up the hydrogen atom from the N(3) center of the hydrazide moiety and simultaneously transfers it to the C(a)-atom of the acetylene moiety to form the alkene product, which has an energy penalty of 82.8 kJ/mol. This step is found to be the rate-determining

step for the proposed pathway. In this 5-membered ring transition state, the O(w)–H(a) bond of water is elongated to 1.125 Å, and the C(a)–H(a) bond is formed at 1.625 Å. Also, the C(a)–C(b) bond distance increases to 1.360 Å from 1.332 Å in intermediate(D, in line with the formation of the alkene product. In the next step, the transition state **TS4** converts to the highly stable intermediate E.



**Hydrazide-Assisted Proton Transfer.** In this course of proton transfer after the formation of intermediate **D**, another hydrazide molecule assists in transferring the proton from the N(3)-atom of the hydrazide moiety to the C(a)-atom of the acetylene group in a two-step process (Figure 8). In this hydrogen transfer process, the first step is the formation of a transition state (TS4') with an energy barrier of 36.0 kJ/mol. The energy difference between the intermediate **D** and the transition state TS4' is 5.1 kJ/mol. The very small energy barrier value indicates the ease of the hydrazide-assisted proton transfer process as compared to H<sub>2</sub>O-assisted hydrogen transfer pathway. In this hydrogen atom transfer, the N(3)-H bond is elongated to 1.295 Å, and the second nitrogen center N(5) of a second hydrazide molecule abstracts the hydrogen atom as seen from the bond distance of 1.310 Å. The transition state TS4' culminates in the intermediate (E'). The formation of the intermediate species E' is exhibited with an energy barrier of 16.8 kJ/mol with respect to the reactant species (A). The optimized geometry of the intermediate E' shows a bond length of 1.080 Å for the N(5)-H bond, and the bond distance between acetylene carbon-C(a) atom and hydrogen H-atom attached from the other hydrazide moiety is 1.845 Å. The intermediate E', with the closest distance of the C(a)-H bond and activated N(5)-H bond, triggers the formation of TS4'', where a hydrogen transfer from the second hydrazide species to the carbon center of acetylene occurs. As a result, the intermediate E' quickly leads to the transition state TS4'' with a very low energy barrier of 5.3 kJ/mol with respect to the intermediate E'. The transition state TS4'' exhibits an extended N(5)-H bond of 1.338 Å, and hydrogen transfer occurs on the carbon atom of the acetylene moiety at a distance of 1.387 Å. Thus, the pre-activation of the N(5)-H bond in the intermediate E' facilitates hydrogen atom transfer in the hydrazide-assisted route than in the H<sub>2</sub>O-assisted pathway.

**Direct Proton Transfer.** Furthermore, a possibility exists that after the formation of intermediate **D**, the proton directly transfers from the nitrogen atom of the hydrazide moiety to the carbon of the acetylene moiety and leads to the formation of the transition state TS4'''. The calculated output for the transition state TS4''' reveals an extremely high energy barrier of 207.6 kJ/mol as compared to the water-assisted and the other hydrazide group-assisted pathways, thereby making this possibility highly unlikely to occur. The high barrier is due to the formation of a constrained four-membered ring transition state with a  $\angle$ C(a)-H(d)-N(3) bond angle of 102.5°, in which the proton migrates from the N(3) atom of the hydrazide moiety at a distance of 1.426 Å to the C(a)-atom of the acetylene moiety at a distance of 1.496 Å. Hence, the direct proton transfer via this transition state TS4''' is not a favorable pathway for the hydrohydrazination reaction.

Thus, the intermolecular hydrogen transfer by all the above-discussed three pathways leads to the intermediate **E**. The formation of alkene species from acetylene leads to an increase in the  $\sigma$ -interaction as observed by NBO analysis (Supporting Information, Figure S211). Additionally, the formation of this more saturated alkene species makes the intermediate **E** more stable, as observed from its highly exothermic energy value of -83.8 kJ/mol. The WBI value of 1.37 clearly points toward the double bonded character of the C(a)-C(b) bond and also is in agreement with the observed distance of 1.418 Å for the C(a)-C(b) bond in tune with the alkene formation. In the next step, the CH<sub>3</sub>CN solvent coordinates with the gold(I) center, resulting in the transition state TS5 having an energy barrier

of -19.1 kJ/mol. The coordination of the solvent CH<sub>3</sub>CN concurrently occurs with the bond breaking of the hydrohydrazinated species with the gold(I) center in the transition state (TS5). In particular, the CH<sub>3</sub>CN initiates bonding with the Au(I) metal center at 2.328 Å bond length, and the alkene product begins to cleave at 2.569 Å bond length. In the final step of the mechanism, the alkene product is completely dissociated from the Au(I) metal center and again regenerates the reactive species (A). This regeneration step is found to be very exothermic by an energy margin of -76.7 kJ/mol. This exothermicity explains the feasibility of the alkene product formation of compound **6**.

## CONCLUSIONS

In summary, a series four acyclic aminoxy carbene (AAOC) ligand precursors, namely,  $\{(4\text{-R}^2\text{-}2,6\text{-}t\text{-Bu}_2\text{-C}_6\text{H}_2\text{O})(\text{N}(\text{R}^1)_2)\text{-CH}\}^+\text{OTf}^-$  (where R<sup>2</sup> = H, R<sup>1</sup> = Me; R<sup>2</sup> = H, R<sup>1</sup> = Cy; R<sup>2</sup> = *t*-Bu, R<sup>1</sup> = Me; R<sup>2</sup> = *t*-Bu, R<sup>1</sup> = Cy) (1-4)a, were synthesized and successfully employed as a platform for developing the gold(I) and gold(III) chemistry through a series reactivity studies. Specifically, the gold(I) (AAOC)AuCl-type (1-4)b complexes were synthesized from the AAOC ligand precursors (1-4)a by direct metalation with (Me<sub>2</sub>)AuCl and NaH as a base. Further treatment of (1-4)b with molecular bromine yielded the gold(III) (AAOC)AuBr<sub>3</sub>-type (1-4)c complexes while the gold(I) (AAOC)Au(SC<sub>6</sub>F<sub>5</sub>)-type (1-4)d complexes were synthesized by the treatment of (1-4)b with C<sub>6</sub>F<sub>5</sub>SH. Quite significantly, the gold(III) (AAOC)AuBr<sub>3</sub>-type (1-4)c complexes and the gold(I) (AAOC)Au(SC<sub>6</sub>F<sub>5</sub>)-type (1-4)d complexes represent the only reported structurally characterized examples supported over any acyclic aminoxy carbene (AAOC) ligand. Significantly enough, the gold(I) (AAOC)-AuCl-type (1-4)b complexes successfully catalyzed the hydrohydrazination of terminal alkynes with *p*-toluenesulfonyl hydrazide yielding several substituted hydrazone derivatives (5-14). Several important catalytic intermediates, like [(AAOC)Au(CH<sub>3</sub>CN)]SbF<sub>6</sub> species (1-4)A and alkyne coordinated intermediate  $\{[(2,4,6\text{-}t\text{-Bu}_3\text{-C}_6\text{H}_2\text{O})(\text{NMe}_2)\text{-methylidene}]\text{Au}(\text{HC}\equiv\text{CPhMe})\}\text{SbF}_6$  species (3B) have been detected by mass spectrometry.

Additionally, two mechanistic pathways have been explored by employing DFT methods. The first step, which is the acetylene coordination pathway or hydrazide coordination pathway, leads to two mechanistic pathways named the acetylene coordination pathway and hydrazide coordination pathway, respectively. It is mainly concluded from the computed results of these two pathways that the acetylene coordination pathway was more favorable than the hydrazide coordination pathway by a 1.7 kJ/mol energy difference. Both the acetylene and hydrazide coordination pathways end with the formation of the common intermediate **C**. After which, the reaction proceeds with a common transition state TS3, and intermediate **D**. After intermediate **D** formation, intermolecular proton transfer occurs through three pathways, including the water-assisted pathway, another hydrazide group-assisted pathway, and the direct proton transfer pathway. The DFT calculations showed the hydrazide coordination pathway to be the most favorable pathway. The total energy passage through the hydrazide-assisted pathway is found to be exothermic by -76.7 kJ/mol. The major factor that plays an important role in the fast reactivity of the hydrazide-assisted pathway case is the pre-activation of the N-H bond in the intermediate E'. Finally, it should be mentioned that steric

effects have played a role along with the electronic effects in the whole mechanistic pathway.

Furthermore, gold(I) (AAOC)AuCl-type (**2b**) complexes were successfully employed in synthesizing a series of bioactive acetylhydrazone derivatives (**15–18**) with anticonvulsant properties. The results obtained in the current study would push forward the cause of gold catalysis with acyclic aminoxy carbene ligands.

## EXPERIMENTAL SECTION

**General Procedures.** All manipulations were carried out using standard Schlenk techniques. Solvents were purified and degassed by standard procedures. Phenylacetylene-*d* was synthesized with the help of a procedure reported in the literature.<sup>52</sup> Dicyclohexyl amine, *N,N*-dimethylformamide, *N,N*-di-*i*-propylethylamine, trifluoromethanesulfonic anhydride, 2,6-di-*t*-butylphenol, and NaH were purchased from Spectrochem Chemicals (India), and 2,4,6-tri-*t*-butylphenol was purchased from Sigma Aldrich Chemicals (India) and used without any further purification. <sup>1</sup>H, <sup>13</sup>C{<sup>1</sup>H}, and <sup>19</sup>F{<sup>1</sup>H} NMR spectra were recorded on Bruker 400 MHz and Bruker 500 MHz NMR spectrometers. <sup>1</sup>H NMR peaks are labeled as singlet (s), doublet (d), triplet (t), and multiplet (m). *N,N*-dicyclohexylformamide was synthesized with the help of procedures reported in the literature.<sup>78</sup> Gold precursor (Me<sub>2</sub>S)AuCl was synthesized with the help of a procedure reported in the literature.<sup>79</sup> [1,3-bis(2,6-diisopropylphenyl)imidazol-2-ylidene]AuCl and [1,3-bis(mesityl)imidazol-2-ylidene]AuCl were synthesized with the help of a procedure reported in the literature.<sup>48</sup> High-resolution mass spectrometry measurements were done on a Micromass Q-ToF spectrometer and a Bruker maxis impact spectrometer. Infrared spectra were recorded on a Perkin Elmer Spectrum One FT-IR spectrometer. Elemental analysis was carried out on a Thermo Quest FLASH 1112 SERIES (CHNS) Elemental Analyser. X-ray diffraction data were collected for compounds **1a**, **1b**, **2b**, **2c**, **3a**, **4b**, and **4c** on a Rigaku Saturn 724+ CCD single crystal X-ray diffractometer with Mo K $\alpha$  (0.71073) radiation, whereas for compounds **1c**, **1d**, **2d**, **3b**, **3c**, **3d**, and **4d**, the X-ray data were collected on a Bruker D8 QUEST single crystal X-ray diffractometer with Mo K $\alpha$  (0.71073) radiation. Both the Bruker D8 QUEST and Rigaku Saturn 724+ CCD single crystal X-ray diffractometer were equipped with an Oxford liquid nitrogen cryostream. Crystals were mounted on a nylon loop with paraffin oil. The structures were solved via the direct method using SHELXT and refined via the full matrix least-squares method with SHELXL-2018/3, refining on  $F^2$ .<sup>80</sup> Crystal data collection and refinement parameters are summarized in Tables S1–S4, and CCDC for the AAOC ligand precursor CCDC-1936844 (for **1a**), CCDC-1949239 (for **3a**), and for the gold complexes CCDC-1949238 (for **1b**), CCDC-2071056 (for **1c**), CCDC-2152819 (for **1d**), CCDC-1974061 (for **2b**), CCDC-1989852 (for **2c**), CCDC-2102959 (for **2d**), CCDC-1980626 (for **3b**), CCDC-2071055 (for **3c**), CCDC-2156345 (for **3d**), CCDC-1974062 (for **4b**), CCDC-1989853 (for **4c**), CCDC-2099515 (for **4d**) contain the supplementary crystallographic data for this paper. These data can be obtained free of charge from the Cambridge Crystallographic Data Centre via [www.ccdc.cam.ac.uk/data\\_request/cif](http://www.ccdc.cam.ac.uk/data_request/cif).

**Synthesis of [(2,6-*t*-Bu<sub>2</sub>-C<sub>6</sub>H<sub>3</sub>O)(NMe<sub>2</sub>)CH]<sup>+</sup>OTf<sup>-</sup> (**1a**).** (CH<sub>3</sub>)<sub>2</sub>NCHO (10.1 g, 136 mmol) was dissolved in dry CH<sub>2</sub>Cl<sub>2</sub> (*ca.* 15 mL) and cooled to *ca.* -78 °C. Tf<sub>2</sub>O (14.8 g, 52.6 mmol) was added dropwise and then stirred at the same temperature for 15 min. The reaction mixture was then allowed to warm to room

temperature and further stirred for 1 h until a colorless solid precipitated. The precipitation was completed by the addition of Et<sub>2</sub>O (*ca.* 10 mL). After the removal of the solvent by cannula filtration, the residue was further washed with Et<sub>2</sub>O (*ca.* 2 × 10 mL). After addition of CH<sub>2</sub>Cl<sub>2</sub> (10 mL), the resultant suspension was cooled to *ca.* -78 °C and then a solution of 2,6-di-*tert*-butylphenol (14.2 g, 68.8 mmol) and <sup>i</sup>Pr<sub>2</sub>NEt (8.82 g, 68.2 mmol) in CH<sub>2</sub>Cl<sub>2</sub> (*ca.* 5 mL) was added dropwise. The reaction mixture was further stirred for 30 min at the same temperature and then allowed to stir for 2 h at room temperature, during which a red solid was obtained. The volatiles were removed *in vacuo*, and the residue was redissolved in CH<sub>2</sub>Cl<sub>2</sub> (*ca.* 150 mL) and washed with water (*ca.* 2 × 50 mL). The collected organic layer was dried over anhydrous Na<sub>2</sub>SO<sub>4</sub> and evaporated *in vacuo*. The pure product (**1a**) was obtained by the trituration in CHCl<sub>3</sub>/Et<sub>2</sub>O as a colorless solid (4.26 g, 20%). <sup>1</sup>H NMR (CDCl<sub>3</sub>, 400 MHz, 25 °C):  $\delta$  ppm, 9.01 (s, 1H, NCHO), 7.36 (d, 2H, <sup>3</sup>J<sub>HH</sub> = 8 Hz, C<sub>6</sub>H<sub>3</sub>), 7.26 (t, 1H, <sup>3</sup>J<sub>HH</sub> = 6 Hz, C<sub>6</sub>H<sub>3</sub>), 3.73 (s, 3H, NCH<sub>3</sub>), 3.60 (s, 3H, NCH<sub>3</sub>), 1.33 (s, 18H, 2C(CH<sub>3</sub>)<sub>3</sub>). <sup>13</sup>C{<sup>1</sup>H} NMR (CDCl<sub>3</sub>, 100 MHz, 25 °C):  $\delta$  ppm, 168.1 (NCHO), 152.3 (*ipso*-C<sub>6</sub>H<sub>3</sub>), 141.6 (*o*-C<sub>6</sub>H<sub>3</sub>), 128.4 (*p*-C<sub>6</sub>H<sub>3</sub>), 127.4 (*m*-C<sub>6</sub>H<sub>3</sub>), 120.3 (q, <sup>1</sup>J<sub>CF</sub> = 318 Hz, CF<sub>3</sub>SO<sub>3</sub>), 42.1 (NCH<sub>3</sub>), 37.6 (NCH<sub>3</sub>), 35.1 (2C(CH<sub>3</sub>)<sub>3</sub>), 31.7 (2C(CH<sub>3</sub>)<sub>3</sub>). <sup>19</sup>F{<sup>1</sup>H} NMR (CDCl<sub>3</sub>, 470 MHz, 25 °C):  $\delta$  ppm, -78.69 (s, 3F, CF<sub>3</sub>SO<sub>3</sub>). IR data (cm<sup>-1</sup>) KBr pellet: 3421 (br), 2973 (m), 1705 (s), 1410 (m), 1277 (s), 1254 (s), 1156 (m), 1096 (w), 1032 (w), 750 (w), 639 (w). HRMS (ESI): *m/z* 262.2159 [C<sub>17</sub>H<sub>28</sub>NO]<sup>+</sup>, Calcd. 262.2165. Anal. Calcd. for C<sub>18</sub>H<sub>28</sub>F<sub>3</sub>NO<sub>4</sub>S: C, 52.54; H, 6.86; N, 3.40; S, 7.79. Found: C, 52.80; H, 6.82; N, 2.94; S, 7.55%.

**Synthesis of [(2,6-*t*-Bu<sub>2</sub>-C<sub>6</sub>H<sub>3</sub>O)(NMe<sub>2</sub>)methylidene]AuCl (**1b**).** [(2,6-*t*-Bu<sub>2</sub>-C<sub>6</sub>H<sub>3</sub>O)(NMe<sub>2</sub>)CH]<sup>+</sup>OTf<sup>-</sup> (**1a**) (0.150 g, 0.364 mmol), NaH (0.087 g, 3.64 mmol), and (Me<sub>2</sub>S)AuCl (0.107 g, 0.364 mmol) were taken in a round-bottom flask under a nitrogen atmosphere, and dry THF (*ca.* 30 mL) was added to it at *ca.* -78 °C. The reaction mixture was stirred for 30 min at the same temperature and further stirred for the 2 h at room temperature. The volatiles were removed *in vacuo*, and the residue was purified by column chromatography using neutral alumina as the stationary phase and CH<sub>2</sub>Cl<sub>2</sub> as the mobile phase to give the pure product (**1b**) as a colorless solid (0.076 g, 43%). <sup>1</sup>H NMR (CDCl<sub>3</sub>, 400 MHz, 25 °C):  $\delta$  ppm, 7.34 (d, 2H, <sup>3</sup>J<sub>HH</sub> = 8 Hz, C<sub>6</sub>H<sub>3</sub>), 7.21 (t, 1H, <sup>3</sup>J<sub>HH</sub> = 8 Hz, C<sub>6</sub>H<sub>3</sub>), 3.71 (s, 3H, NCH<sub>3</sub>), 3.36 (s, 3H, NCH<sub>3</sub>), 1.37 (s, 18H, 2C(CH<sub>3</sub>)<sub>3</sub>). <sup>13</sup>C{<sup>1</sup>H} NMR (CDCl<sub>3</sub>, 100 MHz, 25 °C):  $\delta$  ppm, 210.3 (Au-C<sub>carbene</sub>), 153.6 (*ipso*-C<sub>6</sub>H<sub>3</sub>), 142.1 (*o*-C<sub>6</sub>H<sub>3</sub>), 127.2 (*m*-C<sub>6</sub>H<sub>3</sub>), 126.5 (*p*-C<sub>6</sub>H<sub>3</sub>), 44.7 (NCH<sub>3</sub>), 37.1 (NCH<sub>3</sub>), 35.5 (2C(CH<sub>3</sub>)<sub>3</sub>), 32.6 (2C(CH<sub>3</sub>)<sub>3</sub>). IR data (cm<sup>-1</sup>) KBr pellet: 3446 (w), 2967 (s), 2873 (w), 1582 (s), 1571 (w), 1482 (w), 1407 (s), 1361 (w), 1278 (s), 1262 (w), 1212 (s), 1140 (w), 1111 (m), 1047 (w), 926 (w), 883 (w), 801 (w), 760 (w), 592 (w). HRMS (ESI): *m/z* 516.1330 [C<sub>17</sub>H<sub>27</sub>AuClNO + Na]<sup>+</sup> Calcd. 516.1339. Anal. Calcd. for C<sub>17</sub>H<sub>27</sub>AuClNO: C, 41.35; H, 5.51; N, 2.84. Found: C, 41.35; H, 5.34; N, 2.76%.

**Synthesis of [(2,6-*t*-Bu<sub>2</sub>-C<sub>6</sub>H<sub>3</sub>O)(NMe<sub>2</sub>)methylidene]AuBr<sub>3</sub> (**1c**).** A mixture of [(2,6-*t*-Bu<sub>2</sub>-C<sub>6</sub>H<sub>3</sub>O)(NMe<sub>2</sub>)methylidene]AuCl (**1b**) (0.030 g, 0.061 mmol) and Br<sub>2</sub> (0.031 g, 0.194 mmol) in CH<sub>2</sub>Cl<sub>2</sub> (*ca.* 10 mL) was stirred for the 1 h at room temperature, after which the volatiles were removed *in vacuo*. The residue was washed with pentane (*ca.* 3 × 5 mL) and dried under vacuum to give the product **1c** as an orange solid (0.041 g, 95%). <sup>1</sup>H NMR (CDCl<sub>3</sub>, 400 MHz, 25 °C):  $\delta$  ppm, 7.38–7.30 (m, 3H, C<sub>6</sub>H<sub>3</sub>), 3.81 (s, 3H, NCH<sub>3</sub>),



3.63 (s, 3H, NCH<sub>3</sub>), 1.56 (s, 9H, C(CH<sub>3</sub>)<sub>3</sub>), 1.45 (s, 9H, C(CH<sub>3</sub>)<sub>3</sub>). <sup>13</sup>C{<sup>1</sup>H} NMR (CDCl<sub>3</sub>, 100 MHz, 25 °C): δ ppm, 182.8 (Au-C<sub>carbene</sub>), 149.5 (*ipso*-C<sub>6</sub>H<sub>3</sub>), 142.6 (*p*-C<sub>6</sub>H<sub>3</sub>), 128.1 (*o*-C<sub>6</sub>H<sub>3</sub>), 127.7 (*m*-C<sub>6</sub>H<sub>3</sub>), 45.7 (NCH<sub>3</sub>), 41.7 (NCH<sub>3</sub>), 32.9 (2C(CH<sub>3</sub>)<sub>3</sub>), 32.7 (2C(CH<sub>3</sub>)<sub>3</sub>). IR data (cm<sup>-1</sup>) KBr pellet: 3328 (m), 2965 (s), 2872 (w), 2186 (w), 1715 (s), 1582 (s), 1481 (m), 1408 (m), 1362 (m), 1262 (s), 1211 (s), 1111 (w), 1022 (w), 941 (w), 883 (w), 842 (w), 801 (w), 771 (w), 760 (w). Anal. Calcd. for C<sub>17</sub>H<sub>27</sub>AuBr<sub>3</sub>NO: C, 29.25; H, 3.90; N, 2.01. Found: C, 29.63; H, 4.23; N, 2.55%.

**Synthesis of [(2,6-*t*-Bu<sub>2</sub>-C<sub>6</sub>H<sub>3</sub>O)(NMe<sub>2</sub>)]methylidene]-Au(SC<sub>6</sub>F<sub>5</sub>) (1d).** The [(2,6-*t*-Bu<sub>2</sub>-C<sub>6</sub>H<sub>3</sub>O)(NMe<sub>2</sub>)]methylidene]AuCl (1b) (0.075 g, 0.151 mmol) and C<sub>6</sub>F<sub>5</sub>SH (0.091 g, 0.453 mmol) was stirred in the presence of K<sub>2</sub>CO<sub>3</sub> (0.208 g, 1.51 mmol) in CH<sub>2</sub>Cl<sub>2</sub> (ca. 20 mL) at room temperature for 4 h. The reaction mixture was filtered through Celite, and the solvent was evaporated. The residue was dried under vacuum to give the product (1d) as a colorless solid (0.065 g, 65%). <sup>1</sup>H NMR (CDCl<sub>3</sub>, 500 MHz, 25 °C): δ ppm, 7.14 (d, 2H, <sup>3</sup>J<sub>HH</sub> = 8 Hz, C<sub>6</sub>H<sub>3</sub>), 6.95 (t, 1H, <sup>3</sup>J<sub>HH</sub> = 8 Hz, C<sub>6</sub>H<sub>3</sub>), 3.69 (s, 3H, NCH<sub>3</sub>), 3.33 (s, 3H, NCH<sub>3</sub>), 1.34 (s, 18H, 2C(CH<sub>3</sub>)<sub>3</sub>). <sup>13</sup>C{<sup>1</sup>H} NMR (CDCl<sub>3</sub>, 125 MHz, 25 °C): δ ppm, 217.0 (Au-C<sub>carbene</sub>), 153.3 (*ipso*-C<sub>6</sub>H<sub>3</sub>), 142.1 (*o*-C<sub>6</sub>H<sub>3</sub>), 126.6 (*m*-C<sub>6</sub>H<sub>3</sub>), 125.6 (*p*-C<sub>6</sub>H<sub>3</sub>), 44.2 (NCH<sub>3</sub>), 36.9 (NCH<sub>3</sub>), 35.5 (2C(CH<sub>3</sub>)<sub>3</sub>), 32.5 (2C(CH<sub>3</sub>)<sub>3</sub>). <sup>19</sup>F{<sup>1</sup>H} NMR (CDCl<sub>3</sub>, 376 MHz, 25 °C): δ ppm, -132.09 (dd, 2F, <sup>3</sup>J<sub>FF</sub> = 26 Hz, <sup>4</sup>J<sub>FF</sub> = 8 Hz, *o*-C<sub>6</sub>F<sub>5</sub>), -163.22 (t, 1F, <sup>3</sup>J<sub>FF</sub> = 23 Hz, *p*-C<sub>6</sub>F<sub>5</sub>), -164.87 (t, 2F, <sup>3</sup>J<sub>FF</sub> = 20 Hz, *m*-C<sub>6</sub>F<sub>5</sub>). IR data (cm<sup>-1</sup>) KBr pellet: 2963 (s), 1580 (s), 1504 (s), 1477 (s), 1407 (m), 1363 (w), 1278 (m), 1203 (s), 1140 (w), 1109 (w), 1080 (m), 1013 (m), 970 (s), 854 (m), 803 (w), 762 (w). HRMS (ESI): *m/z* 680.1294 [C<sub>23</sub>H<sub>27</sub>AuF<sub>5</sub>NOS + Na]<sup>+</sup> Calcd. 680.1291. Anal. Calcd. for C<sub>23</sub>H<sub>27</sub>AuF<sub>5</sub>NOS: C, 42.02; H, 4.14; N, 2.13; S, 4.88. Found: C, 41.71; H, 4.16; N, 1.91; S, 4.70%.

**Synthesis of [(2,6-*t*-Bu<sub>2</sub>-C<sub>6</sub>H<sub>3</sub>O)(NCy<sub>2</sub>)]CH<sup>+</sup>OTf<sup>-</sup> (2a).** Cy<sub>2</sub>NCHO (4.05 g, 19.3 mmol) was dissolved in dry CH<sub>2</sub>Cl<sub>2</sub> (ca. 10 mL) and cooled to ca. -78 °C. Tf<sub>2</sub>O (2.72 g, 9.65 mmol) was added dropwise and then stirred at the same temperature for 20 min. The reaction mixture was then allowed to warm to room temperature and further stirred for 2 h until a colorless solid precipitated. The precipitation was completed by the addition of Et<sub>2</sub>O (ca. 10 mL). After the removal of the solvent by cannula filtration, the residue was further washed with Et<sub>2</sub>O (ca. 2 × 10 mL). After addition of CH<sub>2</sub>Cl<sub>2</sub> (15 mL), the resultant suspension was cooled to ca. -78 °C and then a solution of 2,6-di-*tert*-butylphenol (1.98 g, 9.65 mmol) and <sup>1</sup>Pr<sub>2</sub>NEt (1.24 g, 9.65 mmol) in CH<sub>2</sub>Cl<sub>2</sub> (ca. 5 mL) was added dropwise. The reaction mixture was further stirred for the 30 min at the same temperature and then allowed to stir for 2 h at room temperature, during which a red solid was obtained. The volatiles were removed *in vacuo*, and the residue was redissolved in CH<sub>2</sub>Cl<sub>2</sub> (ca. 100 mL) and washed with water (ca. 2 × 30 mL). The collected organic layer was dried over anhydrous Na<sub>2</sub>SO<sub>4</sub> and evaporated *in vacuo*. The pure product (2a) was obtained by trituration in CHCl<sub>3</sub>/Et<sub>2</sub>O as a colorless solid (2.68 g, 51%). <sup>1</sup>H NMR (CDCl<sub>3</sub>, 400 MHz, 25 °C): δ ppm, 9.25 (s, 1H, NCH<sub>3</sub>O), 7.37 (d, 2H, <sup>3</sup>J<sub>HH</sub> = 8 Hz, C<sub>6</sub>H<sub>3</sub>), 7.28 (t, 1H, <sup>3</sup>J<sub>HH</sub> = 7 Hz, C<sub>6</sub>H<sub>3</sub>), 4.64–4.60 (m, 1H, NC<sub>6</sub>H<sub>11</sub>), 3.75–3.69 (m, 1H, NC<sub>6</sub>H<sub>11</sub>), 2.05–1.79 (m, 16H, 2C<sub>6</sub>H<sub>11</sub>), 1.61–1.41 (m, 4H, 2C<sub>6</sub>H<sub>11</sub>), 1.34 (s, 18H, 2C(CH<sub>3</sub>)<sub>3</sub>). <sup>13</sup>C{<sup>1</sup>H} NMR (CDCl<sub>3</sub>, 100 MHz, 25 °C): δ ppm, 169.0 (NCH<sub>3</sub>O), 152.5 (*ipso*-C<sub>6</sub>H<sub>3</sub>), 141.1 (*o*-C<sub>6</sub>H<sub>3</sub>), 128.3 (*p*-C<sub>6</sub>H<sub>3</sub>), 127.3 (*m*-C<sub>6</sub>H<sub>3</sub>), 120.4, (q, <sup>1</sup>J<sub>CF</sub> = 319 Hz, CF<sub>3</sub>SO<sub>3</sub>), 60.0 (NC<sub>6</sub>H<sub>11</sub>), 59.4 (NC<sub>6</sub>H<sub>11</sub>), 35.0 (2C(CH<sub>3</sub>)<sub>3</sub>),

33.3 (C<sub>6</sub>H<sub>11</sub>), 31.6 (2C(CH<sub>3</sub>)<sub>3</sub>), 29.0 (C<sub>6</sub>H<sub>11</sub>), 25.8 (C<sub>6</sub>H<sub>11</sub>), 24.9 (C<sub>6</sub>H<sub>11</sub>), 24.3 (C<sub>6</sub>H<sub>11</sub>), 23.4 (C<sub>6</sub>H<sub>11</sub>). <sup>19</sup>F{<sup>1</sup>H} NMR (CDCl<sub>3</sub>, 470 MHz, 25 °C): δ ppm, -78.38 (s, 3F, CF<sub>3</sub>SO<sub>3</sub>). IR data (cm<sup>-1</sup>) KBr pellet: 2939 (s), 2868 (w), 1651 (s), 1452 (w), 1409 (w), 1322 (w), 1257 (s), 1157 (s), 1110 (w), 1033 (w), 638 (m). HRMS (ESI): *m/z* 398.3421 [C<sub>27</sub>H<sub>44</sub>NO]<sup>+</sup> Calcd. 398.3417. Anal. Calcd. for C<sub>28</sub>H<sub>44</sub>F<sub>3</sub>NO<sub>4</sub>S: C, 61.40; H, 8.10; N, 2.56; S, 5.85. Found: C, 61.40; H, 7.83; N, 2.10; S, 5.80%.

**Synthesis of [(2,6-*t*-Bu<sub>2</sub>-C<sub>6</sub>H<sub>3</sub>O)(NCy<sub>2</sub>)]methylidene]-AuCl (2b).** [(2,6-*t*-Bu<sub>2</sub>-C<sub>6</sub>H<sub>3</sub>O)(NCy<sub>2</sub>)]CH<sup>+</sup>OTf<sup>-</sup> (2a) (0.150 g, 0.273 mmol), NaH (0.065 g, 2.73 mmol), and (Me<sub>2</sub>S)AuCl (0.079 g, 0.273 mmol) were taken in a round-bottom flask under a nitrogen atmosphere, and dry THF (ca. 30 mL) was added to it at ca. -78 °C. The reaction mixture was stirred for 30 min at same temperature and further stirred for 2 h at room temperature. After that, the reaction mixture was evaporated. The volatiles were removed *in vacuo*, and the residue was purified by column chromatography using neutral alumina as the stationary phase and CH<sub>2</sub>Cl<sub>2</sub> as the mobile phase to give the pure product (2b) as a colorless solid (0.107 g, 62%). <sup>1</sup>H NMR (CDCl<sub>3</sub>, 400 MHz, 25 °C): δ ppm, 7.33 (d, 2H, <sup>3</sup>J<sub>HH</sub> = 8 Hz, C<sub>6</sub>H<sub>3</sub>), 7.21 (t, 1H, <sup>3</sup>J<sub>HH</sub> = 8 Hz, C<sub>6</sub>H<sub>3</sub>), 4.93–4.87 (m, 1H, NC<sub>6</sub>H<sub>11</sub>), 3.21 (br, 1H, NC<sub>6</sub>H<sub>11</sub>), 1.95–1.64 (m, 13H, 2C<sub>6</sub>H<sub>11</sub>), 1.61–1.42 (m, 7H, 2C<sub>6</sub>H<sub>11</sub>), 1.37 (s, 18H, 2C(CH<sub>3</sub>)<sub>3</sub>). <sup>13</sup>C{<sup>1</sup>H} NMR (CDCl<sub>3</sub>, 100 MHz, 25 °C): δ ppm, 211.6 (Au-C<sub>carbene</sub>), 155.4 (*ipso*-C<sub>6</sub>H<sub>3</sub>), 141.8 (*o*-C<sub>6</sub>H<sub>3</sub>), 127.1 (*m*-C<sub>6</sub>H<sub>3</sub>), 126.3 (*p*-C<sub>6</sub>H<sub>3</sub>), 59.3 (NC<sub>6</sub>H<sub>11</sub>), 58.4 (NC<sub>6</sub>H<sub>11</sub>), 35.4 (2C(CH<sub>3</sub>)<sub>3</sub>), 34.3 (C<sub>6</sub>H<sub>11</sub>), 32.3 (2C(CH<sub>3</sub>)<sub>3</sub>), 29.7 (C<sub>6</sub>H<sub>11</sub>), 26.5 (C<sub>6</sub>H<sub>11</sub>), 25.3 (C<sub>6</sub>H<sub>11</sub>), 25.0 (C<sub>6</sub>H<sub>11</sub>), 24.8 (C<sub>6</sub>H<sub>11</sub>). IR data (cm<sup>-1</sup>) KBr pellet: 3444 (m), 2934 (s), 2854 (w), 1628 (w), 1524 (s), 1449 (w), 1414 (w), 1378 (w), 1319 (w), 1270 (w), 1218 (m), 1191 (m), 1144 (w), 1118 (w), 1033 (w), 898 (w), 753 (w), 622 (w). HRMS (ESI): *m/z* 652.2597 [C<sub>27</sub>H<sub>43</sub>AuClNO + Na]<sup>+</sup> Calcd. 652.2591. Anal. Calcd. for C<sub>27</sub>H<sub>43</sub>AuClNO: C, 51.47; H, 6.88; N, 2.22. Found: C, 52.08; H, 7.34; N, 1.84%.

**Synthesis of [(2,6-*t*-Bu<sub>2</sub>-C<sub>6</sub>H<sub>3</sub>O)(NCy<sub>2</sub>)]methylidene]-AuBr<sub>3</sub> (2c).** A mixture of [(2,6-*t*-Bu<sub>2</sub>-C<sub>6</sub>H<sub>3</sub>O)(NCy<sub>2</sub>)]methylidene]AuCl (2b) (0.050 g, 0.079 mmol) and Br<sub>2</sub> (0.037 g, 0.237 mmol) in CH<sub>2</sub>Cl<sub>2</sub> (ca. 15 mL) was stirred for 1.5 h at room temperature, after which the volatiles were removed *in vacuo*. The residue was washed with pentane and dried under vacuum to give the product 2c as an orange solid (0.049 g, 75%). <sup>1</sup>H NMR (CDCl<sub>3</sub>, 400 MHz, 25 °C): δ ppm, 7.39 (d, 2H, <sup>3</sup>J<sub>HH</sub> = 8 Hz, C<sub>6</sub>H<sub>3</sub>), 7.33 (t, 1H, <sup>3</sup>J<sub>HH</sub> = 8 Hz, C<sub>6</sub>H<sub>3</sub>), 5.14 (br, 1H, NC<sub>6</sub>H<sub>11</sub>), 4.97 (br, 1H, NC<sub>6</sub>H<sub>11</sub>), 2.28–1.95 (m, 12H, 2C<sub>6</sub>H<sub>11</sub>), 1.91–1.70 (m, 8H, 2C<sub>6</sub>H<sub>11</sub>), 1.45 (s, 9H, C(CH<sub>3</sub>)<sub>3</sub>), 1.43 (s, 9H, C(CH<sub>3</sub>)<sub>3</sub>). <sup>13</sup>C{<sup>1</sup>H} NMR (CDCl<sub>3</sub>, 100 MHz, 25 °C): δ ppm, 182.9 (Au-C<sub>carbene</sub>), 150.1 (*ipso*-C<sub>6</sub>H<sub>3</sub>), 142.9 (*p*-C<sub>6</sub>H<sub>3</sub>), 128.6 (*o*-C<sub>6</sub>H<sub>3</sub>), 127.7 (*m*-C<sub>6</sub>H<sub>3</sub>), 70.4 (NC<sub>6</sub>H<sub>11</sub>), 64.3 (NC<sub>6</sub>H<sub>11</sub>), 37.7 (C<sub>6</sub>H<sub>11</sub>), 37.1 (C<sub>6</sub>H<sub>11</sub>), 33.0 (C(CH<sub>3</sub>)<sub>3</sub>), 32.7 (C(CH<sub>3</sub>)<sub>3</sub>), 26.4 (C<sub>6</sub>H<sub>11</sub>), 26.3 (C<sub>6</sub>H<sub>11</sub>), 25.1 (C<sub>6</sub>H<sub>11</sub>), 25.0 (C<sub>6</sub>H<sub>11</sub>). IR data (cm<sup>-1</sup>) KBr pellet: 3853 (w), 3444 (w), 2933 (s), 2855 (w), 2355 (w), 1525 (w), 1449 (w), 1412 (w), 1319 (w), 1269 (w), 1206 (m), 989 (w), 897 (w), 782 (w). Anal. Calcd. for C<sub>27</sub>H<sub>43</sub>AuBr<sub>3</sub>NO: C, 38.87; H, 5.20; N, 1.68. Found: C, 38.10; H, 4.73; N, 1.69%.

**Synthesis of [(2,6-*t*-Bu<sub>2</sub>-C<sub>6</sub>H<sub>3</sub>O)(NCy<sub>2</sub>)]methylidene]-Au(SC<sub>6</sub>F<sub>5</sub>) (2d).** [(2,6-*t*-Bu<sub>2</sub>-C<sub>6</sub>H<sub>3</sub>O)(NCy<sub>2</sub>)]methylidene]-AuCl (2b) (0.040 g, 0.072 mmol) and C<sub>6</sub>F<sub>5</sub>SH (0.043 g, 0.219 mmol) were stirred in the presence of K<sub>2</sub>CO<sub>3</sub> (0.101 g, 0.727 mmol) in CH<sub>2</sub>Cl<sub>2</sub> (ca. 30 mL) at room temperature for 3.5 h. The reaction mixture was filtered through Celite, and the solvent was evaporated. The residue was dried under vacuum to give the

product **2d** as a colorless solid (0.031 g, 61%).  $^1\text{H}$  NMR ( $\text{CDCl}_3$ , 400  $\text{MHz}$ , 25  $^\circ\text{C}$ ):  $\delta$  ppm, 7.11 (d, 2H,  $^3J_{\text{HH}} = 8$  Hz,  $\text{C}_6\text{H}_3$ ), 6.87 (t, 1H,  $^3J_{\text{HH}} = 8$  Hz,  $\text{C}_6\text{H}_3$ ), 4.88–4.82 (m, 1H,  $\text{NC}_6\text{H}_{11}$ ), 3.12–3.10 (m, 1H,  $\text{NC}_6\text{H}_{11}$ ), 1.95–1.74 (m, 11H,  $2\text{C}_6\text{H}_{11}$ ), 1.64–1.38 (m, 9H,  $2\text{C}_6\text{H}_{11}$ ), 1.35 (s, 18H,  $2\text{C}(\text{CH}_3)_3$ ).  $^{13}\text{C}\{^1\text{H}\}$  NMR ( $\text{CDCl}_3$ , 100  $\text{MHz}$ , 25  $^\circ\text{C}$ ):  $\delta$  ppm, 218.7 (Au- $\text{C}_{\text{carbene}}$ ), 154.9 (*ipso*- $\text{C}_6\text{H}_3$ ), 142.0 (*o*- $\text{C}_6\text{H}_3$ ), 126.4 (*m*- $\text{C}_6\text{H}_3$ ), 125.1 (*p*- $\text{C}_6\text{H}_3$ ), 59.1 ( $\text{NC}_6\text{H}_{11}$ ), 58.1 ( $\text{NC}_6\text{H}_{11}$ ), 35.4 ( $2\text{C}(\text{CH}_3)_3$ ), 34.4 ( $\text{C}_6\text{H}_{11}$ ), 32.3 ( $2\text{C}(\text{CH}_3)_3$ ), 29.7 ( $\text{C}_6\text{H}_{11}$ ), 26.5 ( $\text{C}_6\text{H}_{11}$ ), 25.3 ( $\text{C}_6\text{H}_{11}$ ), 25.0 ( $\text{C}_6\text{H}_{11}$ ), 24.8 ( $\text{C}_6\text{H}_{11}$ ).  $^{19}\text{F}\{^1\text{H}\}$  NMR ( $\text{CDCl}_3$ , 376  $\text{MHz}$ , 25  $^\circ\text{C}$ ):  $\delta$  ppm, -132.15 (dd, 2F,  $^3J_{\text{FF}} = 26$  Hz,  $^4J_{\text{FF}} = 8$  Hz, *o*- $\text{C}_6\text{F}_5$ ), -163.55 (t, 1F,  $^3J_{\text{FF}} = 22$  Hz, *p*- $\text{C}_6\text{F}_5$ ), -165.14 (t, 2F,  $^3J_{\text{FF}} = 26$  Hz, *m*- $\text{C}_6\text{F}_5$ ). IR data ( $\text{cm}^{-1}$ ) KBr pellet: 2938 (s), 2854 (w), 1532 (w), 1507 (m), 1475 (s), 1415 (w), 1264 (m), 1196 (s), 1076 (w), 1033 (w), 971 (w), 859 (w), 644 (w). HRMS (ESI):  $m/z$  816.2541 [ $\text{C}_{33}\text{H}_{43}\text{AuF}_5\text{NOS} + \text{Na}$ ] $^+$  Calcd. 816.2543. Anal. Calcd. for  $\text{C}_{33}\text{H}_{43}\text{AuF}_5\text{NOS}$ : C, 49.94; H, 5.46; N, 1.75; S, 4.04. Found: C, 50.01; H, 5.15; N, 1.37, S, 4.25%.

**Synthesis of [(2,4,6-*t*-Bu $_3$ -C $_6$ H $_2$ O)(NMe $_2$ )CH] $^+$ OTf $^-$  (3a).** ( $\text{CH}_3$ ) $_2\text{NCHO}$  (5.01 g, 68.4 mmol) was dissolved in dry  $\text{CH}_2\text{Cl}_2$  (ca. 10 mL) and cooled to ca. -78  $^\circ\text{C}$ .  $\text{TiF}_2\text{O}$  (9.64 g, 34.2 mmol) was added dropwise and then stirred at the same temperature for 20 min. The reaction mixture was then allowed to warm to room temperature and further stirred for 1 h until a colorless solid precipitated. The precipitation was completed by the addition of  $\text{Et}_2\text{O}$  (ca. 10 mL). After the removal of the solvent by cannula filtration, the residue was further washed with  $\text{Et}_2\text{O}$  (ca. 2  $\times$  10 mL). After addition of  $\text{CH}_2\text{Cl}_2$  (10 mL), the resultant suspension was cooled to ca. -78  $^\circ\text{C}$  and then a solution of 2,4,6-tri-*tert*-butylphenol (8.97 g, 34.2 mmol) and  $^i\text{Pr}_2\text{NEt}$  (4.42 g, 34.2 mmol) in  $\text{CH}_2\text{Cl}_2$  (ca. 10 mL) was added dropwise. The reaction mixture was further stirred for 30 min at the same temperature and then allowed to stir for 2 h at room temperature, during which a red solid was obtained. The volatiles were removed *in vacuo*, and the residue was redissolved in  $\text{CH}_2\text{Cl}_2$  (ca. 100 mL) and washed with water (ca. 2  $\times$  30 mL). The collected organic layer was dried over anhydrous  $\text{Na}_2\text{SO}_4$  and evaporated *in vacuo*. The pure product (**3a**) was obtained by trituration in  $\text{CHCl}_3/\text{Et}_2\text{O}$  as a light-yellow solid (2.34 g, 14%).  $^1\text{H}$  NMR ( $\text{CDCl}_3$ , 400  $\text{MHz}$ , 25  $^\circ\text{C}$ ):  $\delta$  ppm, 8.93 (s, 1H,  $\text{NCHO}$ ), 7.36 (s, 2H,  $\text{C}_6\text{H}_2$ ), 3.75 (s, 3H,  $\text{NCH}_3$ ), 3.60 (s, 3H,  $\text{NCH}_3$ ), 1.34 (s, 18H,  $2\text{C}(\text{CH}_3)_3$ ), 1.31 (s, 9H,  $\text{C}(\text{CH}_3)_3$ ).  $^{13}\text{C}\{^1\text{H}\}$  NMR ( $\text{CDCl}_3$ , 100  $\text{MHz}$ , 25  $^\circ\text{C}$ ):  $\delta$  ppm, 68.2 ( $\text{NCHO}$ ), 150.6 (*ipso*- $\text{C}_6\text{H}_2$ ), 150.1 (*p*- $\text{C}_6\text{H}_2$ ), 140.6 (*o*- $\text{C}_6\text{H}_2$ ), 124.3 (*m*- $\text{C}_6\text{H}_2$ ), 120.3 (q,  $^1J_{\text{CF}} = 318$  Hz,  $\text{CF}_3\text{SO}_3$ ), 42.2 ( $\text{NCH}_3$ ), 37.5 ( $\text{NCH}_3$ ), 35.3 ( $2\text{C}(\text{CH}_3)_3$ ), 35.1 ( $2\text{C}(\text{CH}_3)_3$ ), 31.8 ( $2\text{C}(\text{CH}_3)_3$ ), 31.2 ( $\text{C}(\text{CH}_3)_3$ ).  $^{19}\text{F}\{^1\text{H}\}$  NMR ( $\text{CDCl}_3$ , 470  $\text{MHz}$ , 25  $^\circ\text{C}$ ):  $\delta$  ppm, -78.70 (s, 3F,  $\text{CF}_3\text{SO}_3$ ). IR data ( $\text{cm}^{-1}$ ) KBr pellet: 3585 (m), 3514 (w), 2965 (s), 1703 (s), 1426 (w), 1364 (w), 1276 (s), 1247 (m), 1165 (m), 1094 (w), 1031 (w), 808 (w), 645 (w), 518 (w). HRMS (ESI):  $m/z$  318.2794 [ $\text{C}_{21}\text{H}_{36}\text{NO}$ ] $^+$  Calcd 318.2791. Anal. Calcd. for  $\text{C}_{22}\text{H}_{36}\text{F}_3\text{NO}_4\text{S}$ : C, 56.51; H, 7.76; N, 3.00; S, 6.86. Found: C, 55.69; H, 6.90; N, 2.42; S, 7.38%.

**Synthesis of [(2,4,6-*t*-Bu $_3$ -C $_6$ H $_2$ O)(NMe $_2$ )-methylidene]AuCl (3b).** [(2,4,6-*t*-Bu $_3$ -C $_6$ H $_2$ O)(NMe $_2$ )-CH] $^+$ OTf $^-$  (**3a**) (0.150 g, 0.321 mmol), NaH (0.077 g, 3.21 mmol), and (Me $_2\text{S})\text{AuCl}$  (0.094 g, 0.321 mmol) were taken in a round-bottom flask under a nitrogen atmosphere, and dry THF (ca. 30 mL) was added to it at ca. -78  $^\circ\text{C}$ . The reaction mixture was stirred for 30 min at the same temperature and further

stirred for 2 h at room temperature. The volatiles were removed *in vacuo*, and the residue was purified by column chromatography using neutral alumina as the stationary phase and  $\text{CH}_2\text{Cl}_2$  as the mobile phase to give the pure product **3b** as a colorless solid (0.059 g, 33%).  $^1\text{H}$  NMR ( $\text{CDCl}_3$ , 400  $\text{MHz}$ , 25  $^\circ\text{C}$ ):  $\delta$  ppm, 7.33 (s, 2H,  $\text{C}_6\text{H}_2$ ), 3.70 (s, 3H,  $\text{NCH}_3$ ), 3.34 (s, 3H,  $\text{NCH}_3$ ), 1.37 (s, 18H,  $2\text{C}(\text{CH}_3)_3$ ), 1.32 (s, 9H,  $\text{C}(\text{CH}_3)_3$ ).  $^{13}\text{C}\{^1\text{H}\}$  NMR ( $\text{CDCl}_3$ , 125  $\text{MHz}$ , 25  $^\circ\text{C}$ ):  $\delta$  ppm, 210.5 (Au- $\text{C}_{\text{carbene}}$ ), 151.4 (*ipso*- $\text{C}_6\text{H}_2$ ), 148.5 (*p*- $\text{C}_6\text{H}_2$ ), 140.9 (*o*- $\text{C}_6\text{H}_2$ ), 124.1 (*m*- $\text{C}_6\text{H}_2$ ), 44.7 ( $\text{NCH}_3$ ), 37.1 ( $\text{NCH}_3$ ), 35.7 ( $2\text{C}(\text{CH}_3)_3$ ), 34.9 ( $\text{C}(\text{CH}_3)_3$ ), 32.7 ( $2\text{C}(\text{CH}_3)_3$ ), 31.4 ( $\text{C}(\text{CH}_3)_3$ ). IR data ( $\text{cm}^{-1}$ ) KBr pellet: 3853 (w), 3735 (w), 3444 (w), 3005 (w), 2963 (s), 2907 (w), 2872 (w), 1596 (m), 1578 (s), 1477 (m), 1450 (m), 1428 (m), 1409 (m), 1395 (w), 1362 (w), 1282 (m), 1220 (s), 1138 (w), 1107 (w), 1051 (w), 926 (w), 882 (w), 816 (w), 768 (w), 588 (w). HRMS (ESI):  $m/z$  572.1958 [ $\text{C}_{21}\text{H}_{35}\text{AuClNO} + \text{Na}$ ] $^+$  Calcd. 572.1965. Anal. Calcd. for  $\text{C}_{21}\text{H}_{35}\text{AuClNO}$ : C, 45.87; H, 6.42; N, 2.55. Found: C, 45.87; H, 6.25; N, 2.41%.

**Synthesis of [(2,4,6-*t*-Bu $_3$ -C $_6$ H $_2$ O)(NMe $_2$ )-methylidene]AuBr $_3$  (3c).** A mixture of [(2,4,6-*t*-Bu $_3$ -C $_6$ H $_2$ O)(NMe $_2$ )-methylidene]AuCl (**3b**) (0.060 g, 0.109 mmol) and  $\text{Br}_2$  (0.052 g, 0.327 mmol) in  $\text{CH}_2\text{Cl}_2$  (ca. 15 mL) was stirred for 1.5 h at room temperature, after which the volatiles were removed *in vacuo*. The residue was washed with pentane and dried under vacuum to give the product **3c** as an orange solid (0.028 g, 35%).  $^1\text{H}$  NMR ( $\text{CDCl}_3$ , 400  $\text{MHz}$ , 25  $^\circ\text{C}$ ):  $\delta$  ppm, 7.32 (s, 2H,  $\text{C}_6\text{H}_2$ ), 3.74 (s, 3H,  $\text{NCH}_3$ ), 3.62 (s, 3H,  $\text{NCH}_3$ ), 1.46 (s, 18H,  $2\text{C}(\text{CH}_3)_3$ ), 1.32 (s, 9H,  $\text{C}(\text{CH}_3)_3$ ).  $^{13}\text{C}\{^1\text{H}\}$  NMR ( $\text{CDCl}_3$ , 100  $\text{MHz}$ , 25  $^\circ\text{C}$ ):  $\delta$  ppm, 183.2 (Au- $\text{C}_{\text{carbene}}$ ), 148.4 (*ipso*- $\text{C}_6\text{H}_2$ ), 147.7 (*p*- $\text{C}_6\text{H}_2$ ), 140.9 (*o*- $\text{C}_6\text{H}_2$ ), 124.1 (*m*- $\text{C}_6\text{H}_2$ ), 45.9 ( $\text{NCH}_3$ ), 41.7 ( $\text{NCH}_3$ ), 37.7 ( $\text{C}(\text{CH}_3)_3$ ), 34.8 ( $\text{C}(\text{CH}_3)_3$ ), 32.9 ( $2\text{C}(\text{CH}_3)_3$ ), 31.4 ( $2\text{C}(\text{CH}_3)_3$ ). IR data ( $\text{cm}^{-1}$ ) KBr pellet: 3855 (w), 3747 (w), 3444 (w), 2962 (s), 2907 (w), 2872 (w), 2370 (w), 1612 (s), 1463 (w), 1424 (w), 1412 (w), 1396 (w), 1363 (w), 1283 (s), 1237 (s), 1137 (w), 1093 (w), 1048 (w), 924 (w), 879 (w), 813 (w), 757 (w), 650 (w), 605 (w), 540 (w). Anal. Calcd. for  $\text{C}_{21}\text{H}_{35}\text{AuBr}_3\text{NO}$ : C, 33.44; H, 4.68; N, 1.86. Found: C, 33.40; H, 4.73; N, 1.86%.

**Synthesis of [(2,4,6-*t*-Bu $_3$ -C $_6$ H $_2$ O)(NMe $_2$ )-methylidene]Au(SC $_6$ F $_5$ ) (3d).** [(2,4,6-*t*-Bu $_3$ -C $_6$ H $_2$ O)(NMe $_2$ )-methylidene]AuCl (**3b**) (0.045 g, 0.082 mmol) and  $\text{C}_6\text{F}_5\text{SH}$  (0.049 g, 0.246 mmol) was stirred in the presence of  $\text{K}_2\text{CO}_3$  (0.113 g, 0.821 mmol) in  $\text{CH}_2\text{Cl}_2$  (ca. 20 mL) at room temperature for 4 h. The reaction mixture was filtered through Celite, and the solvent was evaporated. The residue was dried under vacuum to give the product (**3d**) as a colorless solid (0.039 g, 68%).  $^1\text{H}$  NMR ( $\text{CDCl}_3$ , 400  $\text{MHz}$ , 25  $^\circ\text{C}$ ):  $\delta$  ppm, 7.31 (s, 2H,  $\text{C}_6\text{H}_2$ ), 3.71 (s, 3H,  $\text{NCH}_3$ ), 3.35 (s, 3H,  $\text{NCH}_3$ ), 1.37 (s, 18H,  $2\text{C}(\text{CH}_3)_3$ ), 1.29 (s, 9H,  $\text{C}(\text{CH}_3)_3$ ).  $^{13}\text{C}\{^1\text{H}\}$  NMR ( $\text{CDCl}_3$ , 100  $\text{MHz}$ , 25  $^\circ\text{C}$ ):  $\delta$  ppm, 218.0 (Au- $\text{C}_{\text{carbene}}$ ), 151.1 (*ipso*- $\text{C}_6\text{H}_2$ ), 148.4 (*o*- $\text{C}_6\text{H}_2$ ), 140.9 (*p*- $\text{C}_6\text{H}_2$ ), 123.9 (*m*- $\text{C}_6\text{H}_2$ ), 44.1 ( $\text{NCH}_3$ ), 37.0 ( $\text{NCH}_3$ ), 35.7 ( $2\text{C}(\text{CH}_3)_3$ ), 34.8 ( $\text{C}(\text{CH}_3)_3$ ), 32.6 ( $2\text{C}(\text{CH}_3)_3$ ), 31.3 ( $\text{C}(\text{CH}_3)_3$ ).  $^{19}\text{F}\{^1\text{H}\}$  NMR ( $\text{CDCl}_3$ , 376  $\text{MHz}$ , 25  $^\circ\text{C}$ ):  $\delta$  ppm, -132.48 (dd, 2F,  $^3J_{\text{FF}} = 26$  Hz,  $^4J_{\text{FF}} = 8$  Hz, *o*- $\text{C}_6\text{F}_5$ ), -163.76 (t, 1F,  $^3J_{\text{FF}} = 22$  Hz, *p*- $\text{C}_6\text{F}_5$ ), -164.91 (t, 2F,  $^3J_{\text{FF}} = 26$  Hz, *m*- $\text{C}_6\text{F}_5$ ). IR data ( $\text{cm}^{-1}$ ) KBr pellet: 3443 (w), 2966 (s), 1570 (m), 1508 (m), 1476 (s), 1363 (w), 1280 (m), 1223 (s), 1080 (w), 972 (m), 856 (m). HRMS (ESI):  $m/z$  752.1656 [ $\text{C}_{27}\text{H}_{35}\text{AuF}_5\text{NOS} + \text{K}$ ] $^+$  Calcd. 752.1657. Anal. Calcd. for  $\text{C}_{27}\text{H}_{35}\text{AuF}_5\text{NOS}$ : C, 45.45; H, 4.94; N, 1.96; S, 4.49. Found: C, 45.39; H, 4.45; N, 1.57; S, 4.74%.



**Synthesis of [(2,4,6-*t*-Bu<sub>3</sub>-C<sub>6</sub>H<sub>2</sub>O)(NCy<sub>2</sub>)]CH<sup>+</sup>OTf<sup>-</sup> (4a).** Cy<sub>2</sub>NCHO (6.09 g, 29.1 mmol) was dissolved in dry CH<sub>2</sub>Cl<sub>2</sub> (ca. 10 mL) and cooled to ca. -78 °C. Tf<sub>2</sub>O (4.10 g, 14.5 mmol) was added dropwise and then stirred at the same temperature for 15 min. The reaction mixture was then allowed to warm to room temperature and further stirred for 1 h until a colorless solid precipitated. The precipitation was completed by the addition of Et<sub>2</sub>O (ca. 10 mL). After the removal of the solvent by cannula filtration, the residue was further washed with Et<sub>2</sub>O (ca. 2 × 10 mL). After addition of CH<sub>2</sub>Cl<sub>2</sub> (10 mL), the resultant suspension was cooled to ca. -78 °C and then a solution of 2,4,6-tri-*tert*-butylphenol (3.82 g, 14.5 mmol) and <sup>1</sup>Pr<sub>2</sub>NEt (1.88 g, 14.5 mmol) in CH<sub>2</sub>Cl<sub>2</sub> (ca. 5 mL) was added dropwise. The reaction mixture was further stirred for 30 min at the same temperature and then allowed to stir for 2 h at room temperature, during which a yellow-colored solid was obtained. The volatiles were removed *in vacuo*, and the residue was redissolved in CH<sub>2</sub>Cl<sub>2</sub> (ca. 100 mL) and washed with water (ca. 2 × 30 mL). The collected organic layer was dried over anhydrous Na<sub>2</sub>SO<sub>4</sub> and evaporated *in vacuo*. The pure product (4a) was obtained by trituration in CHCl<sub>3</sub>/Et<sub>2</sub>O as a colorless solid (2.88 g, 32%). <sup>1</sup>H NMR (CDCl<sub>3</sub>, 400 MHz, 25 °C): δ ppm, 9.11 (s, 1H, NCHO), 7.38 (s, 2H, C<sub>6</sub>H<sub>2</sub>), 4.66–4.59 (m, 1H, NC<sub>6</sub>H<sub>11</sub>), 3.80–3.74 (m, 1H, NC<sub>6</sub>H<sub>11</sub>), 2.06–1.79 (m, 13H, 2C<sub>6</sub>H<sub>11</sub>), 1.62–1.38 (m, 7H, 2C<sub>6</sub>H<sub>11</sub>), 1.36 (s, 18H, 2C(CH<sub>3</sub>)<sub>3</sub>), 1.33 (s, 9H, C(CH<sub>3</sub>)<sub>3</sub>). <sup>13</sup>C{<sup>1</sup>H} NMR (CDCl<sub>3</sub>, 100 MHz, 25 °C): δ ppm, 168.8 (NCHO), 150.5 (*ipso*-C<sub>6</sub>H<sub>2</sub>), 150.3 (*o*-C<sub>6</sub>H<sub>2</sub>), 140.1 (*p*-C<sub>6</sub>H<sub>2</sub>), 124.3 (*m*-C<sub>6</sub>H<sub>2</sub>), 120.5, (q, <sup>1</sup>J<sub>CF</sub> = 319 Hz, CF<sub>3</sub>SO<sub>3</sub>), 60.1 (NC<sub>6</sub>H<sub>11</sub>), 59.5 (NC<sub>6</sub>H<sub>11</sub>), 35.2 (2C(CH<sub>3</sub>)<sub>3</sub>), 35.1 (C(CH<sub>3</sub>)<sub>3</sub>), 33.3 (C<sub>6</sub>H<sub>11</sub>), 31.7 (2C(CH<sub>3</sub>)<sub>3</sub>), 31.3 (C(CH<sub>3</sub>)<sub>3</sub>), 29.1 (C<sub>6</sub>H<sub>11</sub>), 25.8 (C<sub>6</sub>H<sub>11</sub>), 24.9 (C<sub>6</sub>H<sub>11</sub>), 24.3 (C<sub>6</sub>H<sub>11</sub>), 23.5 (C<sub>6</sub>H<sub>11</sub>). <sup>19</sup>F{<sup>1</sup>H} NMR (CDCl<sub>3</sub>, 376 MHz, 25 °C): δ ppm, -78.45 (s, 3F, CF<sub>3</sub>SO<sub>3</sub>). IR data (cm<sup>-1</sup>) KBr pellet: 2952 (s), 2869 (w), 1654 (s), 1452 (m), 1365 (w), 1323 (w), 1255 (s), 1154 (s), 1108 (w), 1032 (m), 637 (m). HRMS (ESI): *m/z* 454.4046 [C<sub>31</sub>H<sub>52</sub>NO]<sup>+</sup> Calcd. 454.4043. Anal. Calcd. for C<sub>32</sub>H<sub>52</sub>F<sub>3</sub>NO<sub>4</sub>S: C, 63.65; H, 8.68; N, 2.32; S, 5.31. Found: C, 62.80; H, 8.41; N, 2.08; S, 5.28%.

**Synthesis of [(2,4,6-*t*-Bu<sub>3</sub>-C<sub>6</sub>H<sub>2</sub>O)(NCy<sub>2</sub>)}-methylidene]AuCl (4b).** [(2,4,6-*t*-Bu<sub>3</sub>-C<sub>6</sub>H<sub>2</sub>O)(NCy<sub>2</sub>)]-CH<sup>+</sup>OTf<sup>-</sup> (4a) (0.150 g, 0.248 mmol), NaH (0.059 g, 2.48 mmol), and (Me<sub>2</sub>S)AuCl (0.073 g, 0.248 mmol) were taken in a round-bottom flask under a nitrogen atmosphere, and dry THF (ca. 30 mL) was added to it at ca. -78 °C. The reaction mixture was stirred for 30 min at the same temperature and further stirred for 2 h at room temperature. The volatiles were removed *in vacuo*, and the residue was purified by column chromatography using neutral alumina as the stationary phase and CH<sub>2</sub>Cl<sub>2</sub> as the mobile phase to give the pure product (4b) as a colorless solid (0.045 g, 26%). <sup>1</sup>H NMR (CDCl<sub>3</sub>, 400 MHz, 25 °C): δ ppm, 7.33 (s, 2H, C<sub>6</sub>H<sub>2</sub>), 4.89 (br, 1H, NC<sub>6</sub>H<sub>11</sub>), 3.21 (br, 1H, NC<sub>6</sub>H<sub>11</sub>), 1.90–1.73 (m, 10H, 2C<sub>6</sub>H<sub>11</sub>), 1.63–1.41 (m, 10H, 2C<sub>6</sub>H<sub>11</sub>), 1.37 (s, 18H, 2C(CH<sub>3</sub>)<sub>3</sub>), 1.33 (s, 9H, C(CH<sub>3</sub>)<sub>3</sub>). <sup>13</sup>C{<sup>1</sup>H} NMR (CDCl<sub>3</sub>, 125 MHz, 25 °C): δ ppm, 211.8 (Au-C<sub>carbene</sub>), 153.1 (*ipso*-C<sub>6</sub>H<sub>2</sub>), 148.2 (*p*-C<sub>6</sub>H<sub>2</sub>), 140.7 (*o*-C<sub>6</sub>H<sub>2</sub>), 123.9 (*m*-C<sub>6</sub>H<sub>2</sub>), 59.3 (NC<sub>6</sub>H<sub>11</sub>), 58.4 (NC<sub>6</sub>H<sub>11</sub>), 35.6 (2C(CH<sub>3</sub>)<sub>3</sub>), 34.9 (C(CH<sub>3</sub>)<sub>3</sub>), 34.3 (C<sub>6</sub>H<sub>11</sub>), 32.4 (2C(CH<sub>3</sub>)<sub>3</sub>), 31.5 (C(CH<sub>3</sub>)<sub>3</sub>), 29.7 (C<sub>6</sub>H<sub>11</sub>), 26.6 (C<sub>6</sub>H<sub>11</sub>), 25.4 (C<sub>6</sub>H<sub>11</sub>), 25.1 (C<sub>6</sub>H<sub>11</sub>), 24.8 (C<sub>6</sub>H<sub>11</sub>). IR data (cm<sup>-1</sup>) KBr pellet: 3446 (w), 2961 (w), 2931 (s), 2858 (m), 1594 (w), 1531 (s), 1479 (w), 1449 (m), 1429 (w), 1378 (w), 1362 (w), 1319 (w), 1265 (w), 1247 (w), 1205 (s), 1135 (m), 1115 (m), 1085 (w), 1032 (w), 1017 (w), 986 (w), 897 (w), 830 (w), 787 (w), 752 (w), 620

(w). HRMS (ESI): *m/z* 724.2958 [C<sub>31</sub>H<sub>51</sub>AuClNO + K]<sup>+</sup> Calcd. 724.2956. Anal. Calcd. for C<sub>31</sub>H<sub>51</sub>AuClNO: C, 54.26; H, 7.49; N, 2.04. Found: C, 53.70; H, 7.32; N, 1.96%.

**Synthesis of [(2,4,6-*t*-Bu<sub>3</sub>-C<sub>6</sub>H<sub>2</sub>O)(NCy<sub>2</sub>)}-methylidene]AuBr<sub>3</sub> (4c).** A mixture of [(2,4,6-*t*-Bu<sub>3</sub>-C<sub>6</sub>H<sub>2</sub>O)(NCy<sub>2</sub>)}methylidene]AuCl (4b) (0.050 g, 0.072 mmol) and Br<sub>2</sub> (0.034 g, 0.216 mmol) in CH<sub>2</sub>Cl<sub>2</sub> (ca. 15 mL) was stirred for 1.5 h at room temperature, after which the volatiles were removed *in vacuo*. The residue was washed with pentane and dried under vacuum to give the product 4c as an orange solid (0.045 g, 70%). <sup>1</sup>H NMR (CDCl<sub>3</sub>, 400 MHz, 25 °C): δ ppm, 7.31 (s, 2H, C<sub>6</sub>H<sub>2</sub>), 5.05 (br, 1H, NC<sub>6</sub>H<sub>11</sub>), 4.94 (br, 1H, NC<sub>6</sub>H<sub>11</sub>), 2.25–1.85 (m, 14H, 2C<sub>6</sub>H<sub>11</sub>), 1.74–1.43 (m, 6H, 2C<sub>6</sub>H<sub>11</sub>), 1.44 (s, 18H, C(CH<sub>3</sub>)<sub>3</sub>), 1.31 (s, 9H, C(CH<sub>3</sub>)<sub>3</sub>). <sup>13</sup>C{<sup>1</sup>H} NMR (CDCl<sub>3</sub>, 100 MHz, 25 °C): δ ppm, 183.9 (Au-C<sub>carbene</sub>), 149.7 (*ipso*-C<sub>6</sub>H<sub>2</sub>), 148.1 (*p*-C<sub>6</sub>H<sub>2</sub>), 141.7 (*o*-C<sub>6</sub>H<sub>2</sub>), 124.8 (*m*-C<sub>6</sub>H<sub>2</sub>), 70.2 (NC<sub>6</sub>H<sub>11</sub>), 64.0 (NC<sub>6</sub>H<sub>11</sub>), 37.4 (2C(CH<sub>3</sub>)<sub>3</sub>), 34.7 (C(CH<sub>3</sub>)<sub>3</sub>), 33.0 (2C(CH<sub>3</sub>)<sub>3</sub>), 32.6 (C<sub>6</sub>H<sub>11</sub>), 32.3 (C<sub>6</sub>H<sub>11</sub>), 31.4 (C(CH<sub>3</sub>)<sub>3</sub>), 27.0 (C<sub>6</sub>H<sub>11</sub>), 26.3 (C<sub>6</sub>H<sub>11</sub>), 25.3 (C<sub>6</sub>H<sub>11</sub>), 25.1 (C<sub>6</sub>H<sub>11</sub>). IR data (cm<sup>-1</sup>) KBr pellet: 3851 (w), 3444 (m), 2933 (s), 2859 (m), 2361 (w), 1637 (w), 1527 (w), 1449 (w), 1206 (m), 1136 (w), 1114 (w), 1013 (w), 642 (w). Anal. Calcd. for C<sub>31</sub>H<sub>51</sub>AuBr<sub>3</sub>NO: C, 41.82; H, 5.77; N, 1.57. Found: C, 41.12; H, 5.61; N, 1.46%.

**Synthesis of [(2,4,6-*t*-Bu<sub>3</sub>-C<sub>6</sub>H<sub>2</sub>O)(NCy<sub>2</sub>)}-methylidene]Au(SC<sub>6</sub>F<sub>5</sub>) (4d).** [(2,4,6-*t*-Bu<sub>3</sub>-C<sub>6</sub>H<sub>2</sub>O)(NCy<sub>2</sub>)}methylidene]AuCl (4b) (0.040 g, 0.058 mmol) and C<sub>6</sub>F<sub>5</sub>SH (0.075 g, 0.374 mmol) was stirred in the presence of K<sub>2</sub>CO<sub>3</sub> (0.801 g, 0.582 mmol) in CH<sub>2</sub>Cl<sub>2</sub> (ca. 25 mL) at room temperature for 3.5 h. The reaction mixture was filtered through Celite, and the solvent was evaporated. The residue was dried under vacuum to give the product 4d as a colorless solid (0.042 g, 85%). <sup>1</sup>H NMR (CDCl<sub>3</sub>, 500 MHz, 25 °C): δ ppm, 7.31 (s, 2H, C<sub>6</sub>H<sub>2</sub>), 4.89 (br, 1H, NC<sub>6</sub>H<sub>11</sub>), 3.05 (br, 1H, NC<sub>6</sub>H<sub>11</sub>), 1.96–1.80 (m, 12H, 2C<sub>6</sub>H<sub>11</sub>), 1.75–1.66 (m, 8H, 2C<sub>6</sub>H<sub>11</sub>), 1.39 (s, 18H, 2C(CH<sub>3</sub>)<sub>3</sub>), 1.31 (s, 9H, C(CH<sub>3</sub>)<sub>3</sub>). <sup>13</sup>C{<sup>1</sup>H} NMR (CDCl<sub>3</sub>, 100 MHz, 25 °C): δ ppm, 219.6 (Au-C<sub>carbene</sub>), 153.0 (*ipso*-C<sub>6</sub>H<sub>2</sub>), 148.2 (*p*-C<sub>6</sub>H<sub>2</sub>), 140.8 (*o*-C<sub>6</sub>H<sub>2</sub>), 123.8 (*m*-C<sub>6</sub>H<sub>2</sub>), 60.0 (NC<sub>6</sub>H<sub>11</sub>), 58.1 (NC<sub>6</sub>H<sub>11</sub>), 35.6 (2C(CH<sub>3</sub>)<sub>3</sub>), 34.8 (C<sub>6</sub>H<sub>11</sub>), 34.2 (C(CH<sub>3</sub>)<sub>3</sub>), 32.3 (2C(CH<sub>3</sub>)<sub>3</sub>), 31.33 (C(CH<sub>3</sub>)<sub>3</sub>), 29.7 (C<sub>6</sub>H<sub>11</sub>), 26.5 (C<sub>6</sub>H<sub>11</sub>), 25.4 (C<sub>6</sub>H<sub>11</sub>), 25.1 (C<sub>6</sub>H<sub>11</sub>), 24.6 (C<sub>6</sub>H<sub>11</sub>). <sup>19</sup>F{<sup>1</sup>H} NMR (CDCl<sub>3</sub>, 376 MHz, 25 °C): δ ppm, -132.22 (dd, 2F, <sup>3</sup>J<sub>FF</sub> = 26 Hz, <sup>4</sup>J<sub>FF</sub> = 8 Hz, *o*-C<sub>6</sub>F<sub>5</sub>), -163.88 (t, 1F, <sup>3</sup>J<sub>FF</sub> = 22 Hz, *p*-C<sub>6</sub>F<sub>5</sub>), -165.23 (t, 2F, <sup>3</sup>J<sub>FF</sub> = 26 Hz, *m*-C<sub>6</sub>F<sub>5</sub>). IR data (cm<sup>-1</sup>) KBr pellet: 2948 (s), 2857 (w), 1524 (w), 1508 (m), 1476 (s), 1363 (w), 1314 (w), 1248 (w), 1204 (s), 1134 (w), 1115 (m), 1076 (w), 1033 (w), 972 (w), 859 (w). HRMS (ESI): *m/z* 888.2906 [C<sub>37</sub>H<sub>51</sub>AuF<sub>5</sub>NOS + K]<sup>+</sup> Calcd. 888.2909. Anal. Calcd. for C<sub>37</sub>H<sub>51</sub>AuF<sub>5</sub>NOS: C, 52.29; H, 6.05; N, 1.65; S, 3.77. Found: C, 51.98; H, 5.83; N, 1.21; S, 3.85%.

**General Procedure for the Blank Experiment.** In a typical blank run, a mixture of the phenylacetylene (1.00 mmol) and *p*-toluenesulfonyl hydrazide (1.00 mmol) in ca. 5 mL of CH<sub>3</sub>CN was refluxed at 95 °C for 6 h. The reaction mixture was cooled to room temperature. The volatiles were removed *in vacuo* and the residue was analyzed by <sup>1</sup>H NMR and mass spectrometry (entry 1 in Table S7).

**General Procedure for the Control Experiment.** The following control experiments were performed.

- (i) In a typical control run, a mixture of phenylacetylene (1.00 mmol), *p*-toluenesulfonyl hydrazide (1.00 mmol), and ligand precursor (4a) (0.01 mmol, 1 mol %) in ca. 5



mL of CH<sub>3</sub>CN at 95 °C for the 6 h was prepared. The reaction mixture was cooled to room temperature. The volatiles were removed *in vacuo*, and the residue was analyzed by <sup>1</sup>H NMR and mass spectrometry (entry 2 in Table S7).

- (ii) In a typical control run, a mixture of phenylacetylene (1.00 mmol), *p*-toluenesulfonyl hydrazide (1.00 mmol), AgSbF<sub>6</sub> (0.01 mmol, 1 mol %), and ligand precursor (**4a**) (0.01 mmol, 1 mol %) in *ca.* 5 mL of CH<sub>3</sub>CN at 95 °C for the 6 h was prepared. The reaction mixture was cooled to room temperature. The volatiles were removed *in vacuo*, and the residue was analyzed by <sup>1</sup>H NMR and mass spectrometry (entry 3 in Table S7).
- (iii) In a typical control run, a mixture of phenylacetylene (1.00 mmol), *p*-toluenesulfonyl hydrazide (1.00 mmol), and (Me<sub>2</sub>S)AuCl (0.01 mmol, 1 mol %) in *ca.* 5 mL of CH<sub>3</sub>CN at 95 °C for 6 h was prepared. The reaction mixture was cooled to room temperature. The volatiles were removed *in vacuo*, and the residue was analyzed by <sup>1</sup>H NMR and mass spectrometry (entry 4 in Table S7).
- (iv) In a typical control run, a mixture of phenylacetylene (1.00 mmol), *p*-toluenesulfonyl hydrazide (1.00 mmol), AgSbF<sub>6</sub> (0.01 mmol, 1 mol %), and (Me<sub>2</sub>S)AuCl (0.01 mmol, 1 mol %) in *ca.* 5 mL of CH<sub>3</sub>CN was refluxed at 95 °C for 6 h. The reaction mixture was cooled to room temperature. The volatiles were removed *in vacuo*, and the residue was purified by column chromatography using neutral alumina as the stationary phase and a mixed medium of petroleum ether and EtOAc as the mobile phase to give pure product (**5**) that was confirmed by <sup>1</sup>H NMR, mass spectrometry, and elemental analysis (entry 5 in Table S7 and Figures S132–S135).
- (v) In a typical control run, a mixture of phenylacetylene (1.00 mmol), *p*-toluenesulfonyl hydrazide (1.00 mmol), and AgSbF<sub>6</sub> (0.01 mmol, 1 mol %) in *ca.* 5 mL of CH<sub>3</sub>CN was refluxed at 95 °C for 6 h. The reaction mixture was cooled to room temperature. The volatiles were removed *in vacuo* and the residue was analyzed by <sup>1</sup>H NMR and mass spectrometry (entry 6 in Table S7).
- (vi) In a typical control run, a mixture of phenylacetylene (1.00 mmol), *p*-toluenesulfonyl hydrazide (1.00 mmol), and (AAOC)AuCl (**4b**) (0.01 mmol, 1 mol %) in *ca.* 5 mL of CH<sub>3</sub>CN was refluxed at 95 °C for 6 h. The reaction mixture was cooled to room temperature. The volatiles were removed *in vacuo*, and the residue was analyzed by <sup>1</sup>H NMR and mass spectrometry (entry 7 in Table S7).
- (vii) In a typical control run, a mixture of phenylacetylene (1.00 mmol), *p*-toluenesulfonyl hydrazide (1.00 mmol), AgSbF<sub>6</sub> (0.01 mmol, 1 mol %), and (AAOC)AuCl (**4b**) (0.01 mmol, 1 mol %) in *ca.* 5 mL of CH<sub>3</sub>CN was refluxed at 95 °C for 6 h. The reaction mixture was cooled to room temperature. The volatiles were removed *in vacuo*, and the residue was purified by column chromatography using neutral alumina as the stationary phase and a mixed medium of petroleum ether and EtOAc as the mobile phase to give pure product (**5**) that was confirmed by <sup>1</sup>H NMR, mass spectrometry, and elemental analysis (entry 8 in Table S7 and Figures S132–S135).
- (viii) In a typical control run, a mixture of phenylacetylene (1.00 mmol), *p*-toluenesulfonyl hydrazide (1.00 mmol), AgSbF<sub>6</sub> (0.01 mmol, 1 mol %) and (AAOC)AuBr<sub>3</sub> (**4c**) (0.01 mmol, 1 mol %) in *ca.* 5 mL of CH<sub>3</sub>CN was refluxed at 95 °C for 6 h. The reaction mixture was cooled to room temperature. The volatiles were removed *in vacuo*, and the residue was purified by column chromatography using neutral alumina as the stationary phase and a mixed medium of petroleum ether and EtOAc and analyzed by <sup>1</sup>H NMR, mass spectrometry, and elemental analysis (entry 10 in Table S7).
- (ix) In a typical control run, a mixture of phenylacetylene (1.00 mmol), *p*-toluenesulfonyl hydrazide (1.00 mmol), AgSbF<sub>6</sub> (0.01 mmol, 1 mol %), and (AAOC)Au(SC<sub>6</sub>F<sub>5</sub>) (**4d**) (0.01 mmol, 1 mol %) in *ca.* 5 mL of CH<sub>3</sub>CN was refluxed at 95 °C for 6 h. The reaction mixture was cooled to room temperature. The volatiles were removed *in vacuo* and the residue was purified by column chromatography using neutral alumina as the stationary phase and a mixed medium of petroleum ether and EtOAc as the mobile phase to give pure product (**5**) that was confirmed by <sup>1</sup>H NMR, mass spectrometry, and elemental analysis (entry 11 in Table S7 and Figures S131–S134).
- (x) In a typical control run, a mixture of phenylacetylene (1.00 mmol), *p*-toluenesulfonyl hydrazide (1.00 mmol), AgSbF<sub>6</sub> (0.01 mmol, 1 mol %), and [1,3-bis(2,6-diisopropylphenyl)imidazol-2-ylidene]AuCl (0.01 mmol, 1 mol %) in *ca.* 5 mL of CH<sub>3</sub>CN was refluxed at 95 °C for 6 h. The reaction mixture was cooled to room temperature. The volatiles were removed *in vacuo*, and the residue was purified by column chromatography using neutral alumina as the stationary phase and a mixed medium of petroleum ether and EtOAc as the mobile phase to give pure product (**5**) that was confirmed by <sup>1</sup>H NMR, mass spectrometry, and elemental analysis (entry 2 in Table 8 and Figures S132–S135).
- (xi) In a typical control run, a mixture of phenylacetylene (1.00 mmol), *p*-toluenesulfonyl hydrazide (1.00 mmol), AgSbF<sub>6</sub> (0.01 mmol, 1 mol %), and [1,3-bis(mesityl)imidazol-2-ylidene]AuCl (0.01 mmol, 1 mol %) in *ca.* 5 mL of CH<sub>3</sub>CN was refluxed at 95 °C for 6 h. The reaction mixture was cooled to room temperature. The volatiles were removed *in vacuo*, and the residue was purified by column chromatography using neutral alumina as the stationary phase and a mixed medium of petroleum ether and EtOAc as the mobile phase to give pure product **5** that was confirmed by <sup>1</sup>H NMR, mass spectrometry, and elemental analysis (entry 3 in Table 8 and Figures S132–S135).

**General Procedure for the Hg Drop Experiment.** In a typical Hg-drop experiment, a mixture of the terminal alkyne (1.00 mmol), *p*-toluenesulfonyl hydrazide (1.00 mmol), AgSbF<sub>6</sub> (0.01 mmol, 1 mol %), and [(AAOC)AuCl] (**4b**) (0.01 mmol, 1 mol %) in *ca.* 5 mL of CH<sub>3</sub>CN was taken along with one drop of Hg. The reaction mixture was refluxed for 6 h at 95 °C and then cooled to room temperature. The volatiles were removed *in vacuo*, and the residue was purified by column chromatography using neutral alumina as the stationary phase and a mixed medium of petroleum ether and EtOAc as the mobile phase to give pure product **5** that was confirmed by <sup>1</sup>H NMR, mass spectrometry, and elemental analysis (entry 9 in Table S7 and Figures S132–S135).

**General Procedure of the Additive Variation Experiment.** In catalysis run, a mixture of phenylacetylene (1.00 mmol), *p*-toluenesulfonyl hydrazide (1.00 mmol) taken with different additives (AgSbF<sub>6</sub>/AgOTf/AgBF<sub>4</sub>/AgClO<sub>4</sub>/AgO-COCF<sub>3</sub>/AgOCOCH<sub>3</sub>) (0.01 mmol, 1 mol %), and [(AAOC)-

AuCl] (**4b**) (0.01 mmol, 1 mol %) in *ca.* 5 mL of CH<sub>3</sub>CN was refluxed at 95 °C for 6 h. The reaction mixture was cooled to room temperature. The volatiles were removed *in vacuo*, and the residue was purified by column chromatography using neutral alumina as the stationary phase and a mixed medium of petroleum ether and EtOAc as the mobile phase to give the pure product **5** that was confirmed by <sup>1</sup>H NMR, mass spectrometry, and elemental analysis (Table S6 and Figures S131–S134).

**General Procedure for the Mass Experiment for the Detection of the Catalytic Intermediates.** In the typical mass experiment for (1–4)A, a mixture of catalyst AAOC-Au(I) chloride (1–4)b (0.01 mmol, 1 mol %) and AgSbF<sub>6</sub> (0.01 mmol, 1 mol %) was taken in *ca.* 2.5 mL of CH<sub>3</sub>CN and immediately subjected to mass analysis. ESI-MS data of CH<sub>3</sub>CN bound Au(I)(AAOC) species (1–4)A were recorded (Figure 5 and Figures S188–S192, S194, and S195).

In the typical mass experiment for **3B**, an excess of 4-ethynyltoluene (0.018 g, 0.156 mmol), AAOC-Au(I) chloride (**3b**) (1 mol %), and AgSbF<sub>6</sub> (1 mol %) was taken in *ca.* 2.5 mL of CH<sub>3</sub>CN and immediately subjected to mass analysis. ESI-MS data of 4-ethynyltoluene bound Au(I)(AAOC) species (**3B**) were recorded (Figure 6 and Figure S193).

**General Procedure of Hydrohydrazination of the Terminal Alkynes Catalyzed by the Chloro Derivative of Au(I) Acyclic Aminoxy Carbene (AAOC) (1–4)b Complexes.** In typical catalysis run, a mixture of the terminal alkyne (1.00 mmol), *p*-toluenesulfonyl hydrazide (1.00 mmol), AgSbF<sub>6</sub> (0.01 mmol, 1 mol %), and [(AAOC)AuCl] (1–4)b (0.01 mmol, 1 mol %) in *ca.* 5 mL of CH<sub>3</sub>CN was refluxed at 95 °C for 6 h. The reaction mixture was cooled to room temperature. The volatiles were removed *in vacuo*, and the residue was purified by column chromatography using neutral alumina as the stationary phase and a mixed medium of petroleum ether and EtOAc as the mobile phase to give the pure products (**5–14**) (Table 7) that was confirmed by <sup>1</sup>H NMR, mass spectrometry, and elemental analysis (Figures S132–S171). The characterization data of compounds **5–14** is shown in Figures 9–19.

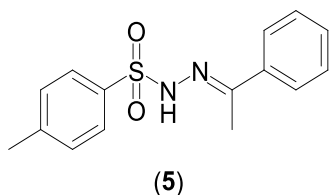


Figure 9. Characterization data of **5**.

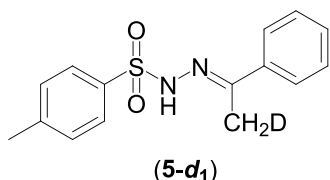


Figure 10. Characterization data of **5-d<sub>1</sub>**.

**Deuteration Experiment.** In typical catalysis run, a mixture of phenylacetylene-*d* (1.00 mmol), *p*-toluenesulfonyl hydrazide (1.00 mmol), AgSbF<sub>6</sub> (0.01 mmol, 1 mol %), and [(AAOC)-AuCl] (**2b**) (0.01 mmol, 1 mol %) in *ca.* 5 mL of CH<sub>3</sub>CN was refluxed at 95 °C for 6 h. The reaction mixture was cooled to room temperature. The volatiles were removed *in vacuo*, and the

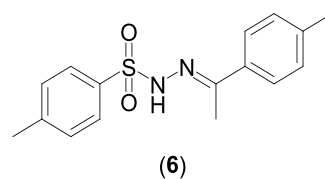


Figure 11. Characterization data of **6**.

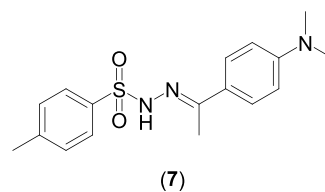


Figure 12. Characterization data of **7**.

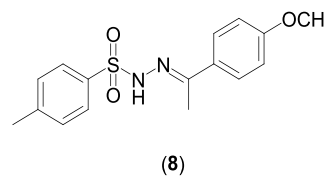


Figure 13. Characterization data of **8**.

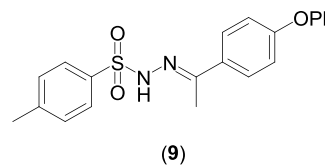


Figure 14. Characterization data of **9**.

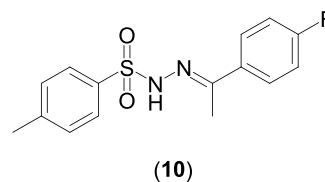


Figure 15. Characterization data of **10**.

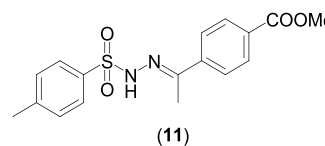


Figure 16. Characterization data of **11**

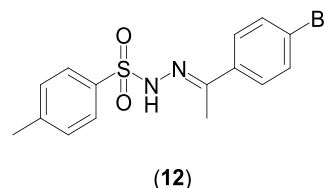
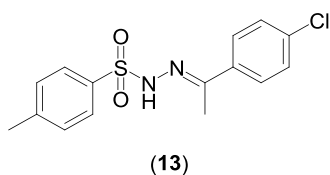


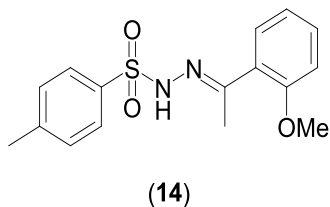
Figure 17. Characterization data of **12**.

residue was purified by column chromatography using neutral alumina as the stationary phase and a mixed medium of petroleum ether and EtOAc as the mobile phase to give the products **5** and **5-d** in a 2:1 ratio as confirmed by <sup>1</sup>H NMR and



(13)

Figure 18. Characterization data of 13



(14)

Figure 19. Characterization data of 14.

$^{13}\text{C}\{^1\text{H}\}$  NMR (Figures S196–S199). The characterization data of compound **5-d**<sub>1</sub> is shown in Figure 10.

(*E*)-4-Methyl-*N'*-(1-phenylethylidene)-benzenesulfonohydrazide (**5**).<sup>12</sup> Yields: 0.021 g, 8% (**1b**), 0.113 g, 40% (**2b**), 0.051 g, 18% (**3b**), 0.201 g, 71% (**4b**).

$^1\text{H}$  NMR ( $\text{CDCl}_3$ , 400 MHz, 25 °C):  $\delta$  ppm, 7.94 (d, 2H,  $^3J_{\text{HH}} = 8$  Hz, *o*- $\text{CH}_3\text{C}_6\text{H}_4\text{SO}_2$ ), 7.73 (s, 1H,  $\text{NH}$ ), 7.68–7.66 (m, 2H, *m*- $\text{CH}_3\text{C}_6\text{H}_4\text{SO}_2$ ), 7.38–7.33 (m, 5H,  $\text{C}_6\text{H}_5$ ), 2.44 (s, 3H,  $\text{CH}_3\text{C}_6\text{H}_4\text{SO}_2$ ), 2.17 (s, 3H,  $\text{N}=\text{C}(\text{CH}_3)$ ). HRMS (ESI):  $m/z$  289.1009 [ $\text{C}_{15}\text{H}_{16}\text{N}_2\text{O}_2\text{S} + \text{H}^+$ ] Calcd. 289.1005. Anal. Calcd. for  $\text{C}_{15}\text{H}_{16}\text{N}_2\text{O}_2\text{S}$ : C, 62.48; H, 5.59; N, 9.71; S, 11.12. Found: C, 62.08; H, 5.30; N, 9.62; S, 10.60%.

(*E*)-4-Methyl-*N'*-(1-phenylethylidene-2-*d*)-benzenesulfonohydrazide (**5-d**<sub>1</sub>).  $^1\text{H}$  NMR ( $\text{CDCl}_3$ , 400 MHz, 25 °C):  $\delta$  ppm, 7.97 (d, 2H,  $^3J_{\text{HH}} = 8$  Hz, *o*- $\text{CH}_3\text{C}_6\text{H}_4\text{SO}_2$ ), 7.66–7.64 (m, 2H, *m*- $\text{CH}_3\text{C}_6\text{H}_4\text{SO}_2$ ), 7.36–7.33 (m, 5H,  $\text{C}_6\text{H}_5$ ), 2.42 (s, 3H,  $\text{CH}_3\text{C}_6\text{H}_4\text{SO}_2$ ), 2.18 (t, 3H,  $^2J_{\text{HD}} = 2.4$  Hz,  $\text{N}=\text{C}(\text{CH}_2\text{D})$ ).  $^{13}\text{C}\{^1\text{H}\}$  NMR ( $\text{CDCl}_3$ , 100 MHz, 25 °C):  $\delta$  ppm, 153.5 (*ipso*- $\text{C}_6\text{H}_4\text{CH}_3$ ), 144.2 (*p*- $\text{C}_6\text{H}_4\text{CH}_3$ ), 137.4 (*ipso*- $\text{C}_6\text{H}_5$ ), 135.4 (*p*- $\text{C}_6\text{H}_4\text{CH}_3$ ), 129.7 (*o*- $\text{C}_6\text{H}_4\text{CH}_3$ ), 129.6 ( $\text{N}=\text{CCH}_2\text{DPh}$ ), 128.4 (*o*- $\text{C}_6\text{H}_5$ ), 128.2 (*m*- $\text{C}_6\text{H}_4\text{CH}_3$ ), 126.3 (*m*- $\text{C}_6\text{H}_5$ ), 21.6 ( $\text{C}_6\text{H}_4\text{CH}_3$ ), 13.5 (t,  $^1J_{\text{CD}} = 20$  Hz,  $\text{N}=\text{CCH}_2\text{DPh}$ ).

(*E*)-4-Methyl-*N'*-(1-*p*-tolylethylidene)-benzenesulfonohydrazide (**6**).<sup>12</sup> Yields: 0.152 g, 58% (**1b**), 0.171 g, 66% (**2b**), 0.183 g, 70% (**3b**), 0.135 g, 51% (**4b**).

$^1\text{H}$  NMR ( $\text{CDCl}_3$ , 400 MHz, 25 °C):  $\delta$  ppm, 7.91 (d, 2H,  $^3J_{\text{HH}} = 8$  Hz, *o*- $\text{CH}_3\text{C}_6\text{H}_4\text{SO}_2$ ), 7.54 (d, 2H,  $^3J_{\text{HH}} = 8$  Hz, *m*- $\text{CH}_3\text{C}_6\text{H}_4\text{SO}_2$ ), 7.31 (d, 2H,  $^3J_{\text{HH}} = 8$  Hz, *o*- $\text{C}_6\text{H}_4\text{CH}_3$ ), 7.14 (d, 2H,  $^3J_{\text{HH}} = 8$  Hz, *m*- $\text{C}_6\text{H}_4\text{CH}_3$ ), 2.41 (s, 3H,  $\text{CH}_3\text{C}_6\text{H}_4\text{SO}_2$ ), 2.35 (s, 3H,  $\text{C}_6\text{H}_4\text{CH}_3$ ), 2.12 (s, 3H,  $\text{N}=\text{C}(\text{CH}_3)$ ). HRMS (ESI):  $m/z$  303.1168 [ $\text{C}_{16}\text{H}_{18}\text{N}_2\text{O}_2\text{S} + \text{H}^+$ ] Calcd. 303.1162. Anal. Calcd. for  $\text{C}_{16}\text{H}_{18}\text{N}_2\text{O}_2\text{S}$ : C, 63.55; H, 6.00; N, 9.26; S, 10.60. Found: C, 62.56; H, 5.48; N, 9.09; S, 11.20%.

(*E*)-*N'*-(1-(4-(dimethylamino)phenyl)ethylidene)-4-methylbenzenesulfonohydrazide (**7**).<sup>12</sup> Yields: 0.090 g, 39% (**1b**), 0.067 g, 29% (**2b**), 0.111 g, 48% (**3b**), 0.058 g, 25% (**4b**).

$^1\text{H}$  NMR ( $\text{CDCl}_3$ , 400 MHz, 25 °C):  $\delta$  ppm, 7.93 (d, 2H,  $^3J_{\text{HH}} = 8$  Hz, *o*- $\text{CH}_3\text{C}_6\text{H}_4\text{SO}_2$ ), 7.58 (d, 2H,  $^3J_{\text{HH}} = 9$  Hz, *m*- $\text{CH}_3\text{C}_6\text{H}_4\text{SO}_2$ ), 7.32 (d, 2H,  $^3J_{\text{HH}} = 8$  Hz, *o*- $\text{C}_6\text{H}_4\text{N}(\text{CH}_3)_2$ ), 6.65 (d, 2H,  $^3J_{\text{HH}} = 9$  Hz, *m*- $\text{C}_6\text{H}_4\text{N}(\text{CH}_3)_2$ ), 3.00 (s, 6H,  $\text{N}(\text{CH}_3)_2$ ), 2.43 (s, 3H,  $\text{CH}_3\text{C}_6\text{H}_4\text{SO}_2$ ), 2.12 (s, 3H,  $\text{N}=\text{C}(\text{CH}_3)$ ). HRMS (ESI):  $m/z$  332.1427 [ $\text{C}_{17}\text{H}_{21}\text{N}_3\text{O}_2\text{S} + \text{H}^+$ ] Calcd. 332.1427. Anal. Calcd. for  $\text{C}_{17}\text{H}_{21}\text{N}_3\text{O}_2\text{S}$ : C, 61.61; H, 6.39; N, 12.68; S, 9.67. Found: C, 60.77; H, 5.63; N, 12.23; S, 10.02%.

(*E*)-*N'*-(1-(4-methoxyphenyl)ethylidene)-4-methylbenzenesulfonohydrazide (**8**).<sup>12</sup> Yields: 0.044 g, 18% (**1b**), 0.186 g, 77% (**2b**), 0.040 g, 16% (**3b**), 0.169 g, 70% (**4b**).

$^1\text{H}$  NMR ( $\text{CDCl}_3$ , 400 MHz, 25 °C):  $\delta$  ppm, 7.93 (d, 2H,  $^3J_{\text{HH}} = 8$  Hz, *o*- $\text{CH}_3\text{C}_6\text{H}_4\text{SO}_2$ ), 7.63 (d, 2H,  $^3J_{\text{HH}} = 7$  Hz, *m*- $\text{CH}_3\text{C}_6\text{H}_4\text{SO}_2$ ), 7.34 (d, 2H,  $^3J_{\text{HH}} = 8$  Hz, *o*- $\text{C}_6\text{H}_4(\text{OCH}_3)$ ), 6.87 (d, 2H,  $^3J_{\text{HH}} = 9$  Hz, *m*- $\text{C}_6\text{H}_4(\text{OCH}_3)$ ), 3.84 (s, 3H,  $\text{OCH}_3$ ), 2.44 (s, 3H,  $\text{CH}_3\text{C}_6\text{H}_4\text{SO}_2$ ), 2.15 (s, 3H,  $\text{N}=\text{C}(\text{CH}_3)$ ). HRMS (ESI):  $m/z$  319.1113 [ $\text{C}_{16}\text{H}_{18}\text{N}_2\text{O}_3\text{S} + \text{H}^+$ ] Calcd. 319.1111. Anal. Calcd. for  $\text{C}_{16}\text{H}_{18}\text{N}_2\text{O}_3\text{S}$ : C, 60.36; H, 5.70; N, 8.80; S, 10.07. Found: C, 59.98; H, 6.00; N, 8.43; S, 9.51%.

(*E*)-4-Methyl-*N'*-(1-(4-phenoxyphenyl)ethylidene)-benzenesulfonohydrazide (**9**).<sup>12</sup> Yields: 0.000 g, 0% (**1b**), 0.132 g, 66% (**2b**), 0.009 g, 5% (**3b**), 0.112 g, 57% (**4b**).

$^1\text{H}$  NMR ( $\text{CDCl}_3$ , 400 MHz, 25 °C):  $\delta$  ppm, 7.93 (d, 2H,  $^3J_{\text{HH}} = 8$  Hz, *o*- $\text{CH}_3\text{C}_6\text{H}_4\text{SO}_2$ ), 7.64 (d, 2H,  $^3J_{\text{HH}} = 9$  Hz, *m*- $\text{CH}_3\text{C}_6\text{H}_4\text{SO}_2$ ), 7.40–7.33 (m, 4H, *o*- $\text{C}_6\text{H}_4(\text{OC}_6\text{H}_5)$ ) and *m*- $\text{C}_6\text{H}_4(\text{OC}_6\text{H}_5)$ ), 7.17 (t, 1H,  $^3J_{\text{HH}} = 7$  Hz, *p*- $(\text{OC}_6\text{H}_5)$ ), 7.04 (d, 2H,  $^3J_{\text{HH}} = 8$  Hz, *o*- $\text{C}_6\text{H}_4(\text{OC}_6\text{H}_5)$ ), 6.97 (d, 2H,  $^3J_{\text{HH}} = 9$  Hz, *m*- $\text{C}_6\text{H}_4(\text{OC}_6\text{H}_5)$ ), 2.44 (s, 3H,  $\text{CH}_3\text{C}_6\text{H}_4\text{SO}_2$ ), 2.17 (s, 3H,  $\text{N}=\text{C}(\text{CH}_3)$ ). HRMS (ESI):  $m/z$  381.1263 [ $\text{C}_{21}\text{H}_{20}\text{N}_2\text{O}_3\text{S} + \text{H}^+$ ] Calcd. 381.1267. Anal. Calcd. for  $\text{C}_{21}\text{H}_{20}\text{N}_2\text{O}_3\text{S}$ : C, 66.30; H, 5.30; N, 7.36; S, 8.43. Found: C, 65.55; H, 4.98; N, 6.89; S, 9.21%.

(*E*)-*N'*-(1-(4-fluorophenyl)ethylidene)-4-methylbenzenesulfonohydrazide (**10**).<sup>12</sup> Yields: 0.000 g, 0% (**1b**), 0.063 g, 25% (**2b**), 0.039 g, 15% (**3b**), 0.159 g, 62% (**4b**).

$^1\text{H}$  NMR ( $\text{CDCl}_3$ , 400 MHz, 25 °C):  $\delta$  ppm, 7.93 (d, 2H,  $^3J_{\text{HH}} = 8$  Hz, *o*- $\text{CH}_3\text{C}_6\text{H}_4\text{SO}_2$ ), 7.68–7.64 (m, 2H, *m*- $\text{CH}_3\text{C}_6\text{H}_4\text{SO}_2$ ), 7.35 (d, 2H,  $^3J_{\text{HH}} = 8$  Hz, *o*- $\text{C}_6\text{H}_4\text{F}$ ), 7.07–7.03 (m, 2H, *m*- $\text{C}_6\text{H}_4\text{F}$ ), 2.44 (s, 3H,  $\text{CH}_3\text{C}_6\text{H}_4\text{SO}_2$ ), 2.16 (s, 3H,  $\text{N}=\text{C}(\text{CH}_3)$ ). HRMS (ESI):  $m/z$  307.0915 [ $\text{C}_{15}\text{H}_{15}\text{N}_2\text{FO}_2\text{S} + \text{H}^+$ ] Calcd. 307.0911. Anal. Calcd. for  $\text{C}_{15}\text{H}_{15}\text{N}_2\text{FO}_2\text{S}$ : C, 58.81; H, 4.94; N, 9.14; S, 10.46. Found: C, 58.70; H, 5.30; N, 8.46; S, 11.04%.

(*E*)-Methyl 4-(1-(2-tosylhydrazono)ethyl)benzoate (**11**).<sup>12</sup> Yields: 0.000 g, 0% (**1b**), 0.089 g, 41% (**2b**), 0.040 g, 19% (**3b**), 0.143 g, 65% (**4b**).

$^1\text{H}$  NMR ( $\text{CDCl}_3$ , 400 MHz, 25 °C):  $\delta$  ppm, 8.03 (d, 2H,  $^3J_{\text{HH}} = 8$  Hz, *o*- $\text{CH}_3\text{C}_6\text{H}_4\text{SO}_2$ ), 7.94 (d, 2H,  $^3J_{\text{HH}} = 8$  Hz, *o*- $\text{C}_6\text{H}_4(\text{CO}_2\text{CH}_3)$ ), 7.73 (d, 2H,  $^3J_{\text{HH}} = 8$  Hz, *m*- $\text{CH}_3\text{C}_6\text{H}_4\text{SO}_2$ ), 7.35 (d, 2H,  $^3J_{\text{HH}} = 8$  Hz, *m*- $\text{C}_6\text{H}_4(\text{CO}_2\text{CH}_3)$ ), 3.94 (s, 3H,  $\text{CO}_2\text{CH}_3$ ), 2.44 (s, 3H,  $\text{CH}_3\text{C}_6\text{H}_4\text{SO}_2$ ), 2.19 (s, 3H,  $\text{N}=\text{C}(\text{CH}_3)$ ). HRMS (ESI):  $m/z$  347.1069 [ $\text{C}_{17}\text{H}_{18}\text{N}_2\text{O}_4\text{S} + \text{H}^+$ ] Calcd. 347.1060. Anal. Calcd. for  $\text{C}_{17}\text{H}_{18}\text{N}_2\text{O}_4\text{S}$ : C, 58.95; H, 5.24; N, 8.09; S, 9.26. Found: C, 58.73; H, 5.45; N, 9.04; S, 9.89%.

(*E*)-*N'*-(1-(4-bromophenyl)ethylidene)-4-methylbenzenesulfonohydrazide (**12**).<sup>12</sup> Yields: 0.000 g, 0% (**1b**), 0.110 g, 54% (**2b**), 0.025 g, 12% (**3b**), 0.122 g, 60% (**4b**).

$^1\text{H}$  NMR ( $\text{CDCl}_3$ , 400 MHz, 25 °C):  $\delta$  ppm, 7.92 (d, 2H,  $^3J_{\text{HH}} = 8$  Hz, *o*- $\text{CH}_3\text{C}_6\text{H}_4\text{SO}_2$ ), 7.75 (s, 1H,  $\text{NH}$ ), 7.54 (d, 2H,  $^3J_{\text{HH}} = 9$  Hz, *o*- $\text{C}_6\text{H}_4\text{Br}$ ), 7.49 (d, 2H,  $^3J_{\text{HH}} = 9$  Hz, *m*- $\text{C}_6\text{H}_4\text{Br}$ ), 7.34 (d, 2H,  $^3J_{\text{HH}} = 8$  Hz, *m*- $\text{CH}_3\text{C}_6\text{H}_4\text{SO}_2$ ), 2.44 (s, 3H,  $\text{CH}_3\text{C}_6\text{H}_4\text{SO}_2$ ), 2.15 (s, 3H,  $\text{N}=\text{C}(\text{CH}_3)$ ). HRMS (ESI):  $m/z$  367.0114 [ $\text{C}_{15}\text{H}_{15}\text{BrN}_2\text{O}_2\text{S} + \text{H}^+$ ] Calcd. 367.0110. Anal. Calcd. for  $\text{C}_{15}\text{H}_{15}\text{BrN}_2\text{O}_2\text{S}$ : C, 49.06; H, 4.12; N, 7.63; S, 8.73. Found: C, 48.83; H, 3.42; N, 7.41; S, 8.78%.

(*E*)-*N'*-(1-(4-chlorophenyl)ethylidene)-4-methylbenzenesulfonohydrazide (**13**).<sup>12</sup> Yields: 0.000 g, 0% (**1b**), 0.1451 g, 61% (**2b**), 0.022 g, 10% (**3b**), 0.125 g, 53% (**4b**).

$^1\text{H}$  NMR ( $\text{CDCl}_3$ , 400 MHz, 25 °C):  $\delta$  ppm, 7.90 (d, 2H,  $^3J_{\text{HH}} = 8$  Hz, *o*- $\text{CH}_3\text{C}_6\text{H}_4\text{SO}_2$ ), 7.81 (s, 1H,  $\text{NH}$ ), 7.58 (d, 2H,  $^3J_{\text{HH}} =$



8 Hz, *o*-C<sub>6</sub>H<sub>4</sub>Cl), 7.33 (d, 2H, <sup>3</sup>J<sub>HH</sub> = 8 Hz, *m*-C<sub>6</sub>H<sub>4</sub>Cl), 7.31 (d, 2H, <sup>3</sup>J<sub>HH</sub> = 8 Hz, *m*-CH<sub>3</sub>C<sub>6</sub>H<sub>4</sub>SO<sub>2</sub>), 2.42 (s, 3H, CH<sub>3</sub>C<sub>6</sub>H<sub>4</sub>SO<sub>2</sub>), 2.13 (s, 3H, N=C(CH<sub>3</sub>)). HRMS (ESI): *m/z* 323.0611 [C<sub>15</sub>H<sub>15</sub>ClN<sub>2</sub>O<sub>2</sub>S + H]<sup>+</sup> Calcd. 323.0616. Anal. Calcd. for C<sub>15</sub>H<sub>15</sub>ClN<sub>2</sub>O<sub>2</sub>S: C, 55.81; H, 4.68; N, 8.68; S, 9.93. Found: C, 55.30; H, 4.40; N, 8.23; S, 10.52%.

(*E*)-*N'*-(1-(2-Methoxyphenyl)ethylidene)-4-methylbenzenesulfonohydrazide (**14**)<sup>12</sup>. Yields: 0.000 g, 0% (**1b**), 0.049 g, 20% (**2b**), 0.020 g, 9% (**3b**), 0.061 g, 25% (**4b**).

<sup>1</sup>H NMR (CDCl<sub>3</sub>, 400 MHz, 25 °C): δ ppm, 7.83 (d, 2H, <sup>3</sup>J<sub>HH</sub> = 8 Hz, *o*-CH<sub>3</sub>C<sub>6</sub>H<sub>4</sub>SO<sub>2</sub>), 7.41 (t, 1H, <sup>3</sup>J<sub>HH</sub> = 8 Hz, *p*-C<sub>6</sub>H<sub>4</sub>(OCH<sub>3</sub>)), 7.35 (d, 2H, <sup>3</sup>J<sub>HH</sub> = 8 Hz, *m*-CH<sub>3</sub>C<sub>6</sub>H<sub>4</sub>SO<sub>2</sub>), 7.04 (t, 1H, <sup>3</sup>J<sub>HH</sub> = 8 Hz, *m*-C<sub>6</sub>H<sub>4</sub>(OCH<sub>3</sub>)), 6.99 (d, 1H, <sup>3</sup>J<sub>HH</sub> = 8 Hz, *o*-C<sub>6</sub>H<sub>4</sub>(OCH<sub>3</sub>)), 6.96 (d, 1H, <sup>3</sup>J<sub>HH</sub> = 8 Hz, *o*-C<sub>6</sub>H<sub>4</sub>(OCH<sub>3</sub>)), 3.70 (s, 3H, OCH<sub>3</sub>), 2.47 (s, 3H, CH<sub>3</sub>C<sub>6</sub>H<sub>4</sub>SO<sub>2</sub>), 2.19 (s, 3H, N=C(CH<sub>3</sub>)). HRMS (ESI): *m/z* 319.1115 [C<sub>16</sub>H<sub>18</sub>N<sub>2</sub>O<sub>3</sub>S + H]<sup>+</sup> Calcd. 319.1111. Anal. Calcd. for C<sub>16</sub>H<sub>18</sub>N<sub>2</sub>O<sub>3</sub>S: C, 60.36; H, 5.70; N, 8.80; S, 10.07. Found: C, 59.76; H, 5.18; N, 8.47; S, 9.10%.

**General Procedure for the Synthesis Acetylhydrazones Anticonvulsant Active Compounds.** A reaction mixture of the terminal alkyne (1.00 mmol), acetohydrazide (1.00 mmol), AgSbF<sub>6</sub> (0.01 mmol, 1 mol %), and **2b** (0.01 mmol, 1 mol %) in *ca.* 5 mL of CH<sub>3</sub>CN was refluxed at 95 °C for 6 h, after which it was cooled to room temperature. The volatiles were then removed *in vacuo*, and the residue was purified by column chromatography using neutral alumina as the stationary phase and a mixed medium of petroleum ether and EtOAc as the mobile phase to give the pure products **15**–**18** (Table 4) that was confirmed by <sup>1</sup>H NMR, mass spectrometry, and elemental analysis (Figures S172–S187).

- A reaction mixture of the terminal alkyne (1.00 mmol), acetohydrazide (1.00 mmol), AgSbF<sub>6</sub> (0.01 mmol, 1 mol %), and [1,3-bis(2,6-diisopropylphenyl)imidazol-2-ylidene]AuCl (0.01 mmol, 1 mol %) in *ca.* 5 mL of CH<sub>3</sub>CN was refluxed at 95 °C for 6 h, after which it was cooled to room temperature. The volatiles were then removed *in vacuo*, and the residue was purified by column chromatography using neutral alumina as the stationary phase and a mixed medium of petroleum ether and EtOAc as the mobile phase to give the pure products **15**–**18** (Table 4) that was confirmed by <sup>1</sup>H NMR, mass spectrometry, and elemental analysis (Figures S172–S187).
- A reaction mixture of the terminal alkyne (1.00 mmol), acetohydrazide (1.00 mmol), AgSbF<sub>6</sub> (0.01 mmol, 1 mol %), and [1,3-bis(mesityl)imidazol-2-ylidene]AuCl (0.01 mmol, 1 mol %) in *ca.* 5 mL of CH<sub>3</sub>CN was refluxed at 95 °C for 6 h, after which it was cooled to room temperature. The volatiles were then removed *in vacuo*, and the residue was purified by column chromatography using neutral alumina as the stationary phase and a mixed medium of petroleum ether and EtOAc as the mobile phase to give the pure products **15**–**18** (Table 4) that was confirmed by <sup>1</sup>H NMR, mass spectrometry, and elemental analysis (Figures S172–S187). The characterization data of compounds **15**–**18** are shown in Figures 20–23.

(*E*)-*N'*-(1-Phenylethylidene)acetohydrazide (**15**)<sup>55</sup>. Yields: 0.024 g, 16% (**2b**).

<sup>1</sup>H NMR (CDCl<sub>3</sub>, 400 MHz, 25 °C): δ ppm, 8.71 (s, 1H, NH), 7.78–7.76 (m, 2H, *o*-C<sub>6</sub>H<sub>5</sub>), 7.43–7.41 (m, 3H, C<sub>6</sub>H<sub>5</sub>), 2.42 (s, 3H, CH<sub>3</sub>CO), 2.24 (s, 3H, NCH<sub>3</sub>). HRMS (ESI): *m/z*

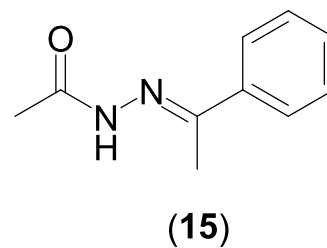


Figure 20. Characterization data of **15**

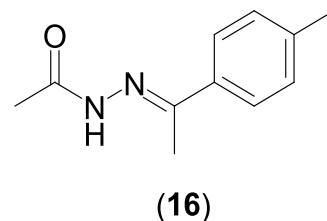


Figure 21. Characterization data of **16**

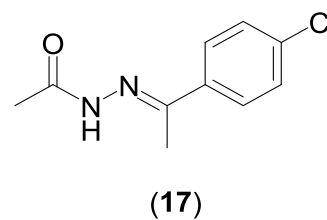


Figure 22. Characterization data of **17**.

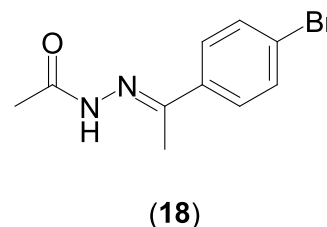


Figure 23. Characterization data of **18**.

199.0848 [C<sub>10</sub>H<sub>12</sub>N<sub>2</sub>O + Na]<sup>+</sup> Calcd. 199.0842. Anal. Calcd. for C<sub>10</sub>H<sub>12</sub>N<sub>2</sub>O: C, 68.16; H, 6.86; N, 15.90. Found: C, 67.74; H, 5.90; N, 15.33%.

(*E*)-*N'*-(1-(*p*-Tolyl)ethylidene)acetohydrazide (**16**)<sup>55</sup>. Yields: 0.039 g, 24% (**2b**).

<sup>1</sup>H NMR (CDCl<sub>3</sub>, 400 MHz, 25 °C): δ ppm, 8.67 (s, 1H, NH), 7.66 (d, 2H, <sup>3</sup>J<sub>HH</sub> = 8 Hz, *o*-C<sub>6</sub>H<sub>4</sub>CH<sub>3</sub>), 7.22 (d, 2H, <sup>3</sup>J<sub>HH</sub> = 8 Hz, *m*-C<sub>6</sub>H<sub>4</sub>CH<sub>3</sub>), 2.41 (s, 3H, CH<sub>3</sub>CO), 2.21 (s, 3H, NCH<sub>3</sub>). HRMS (ESI): *m/z* 213.0994 [C<sub>11</sub>H<sub>14</sub>N<sub>2</sub>O + Na]<sup>+</sup> Calcd. 213.0998. Anal. Calcd. for C<sub>11</sub>H<sub>14</sub>N<sub>2</sub>O: C, 69.45; H, 7.42; N, 14.73. Found: C, 68.98; H, 7.41; N, 14.38%.

(*E*)-*N'*-(1-(4-Chlorophenyl)ethylidene)acetohydrazide (**17**)<sup>55</sup>. Yields: 0.013 g, 9% (**2b**).

<sup>1</sup>H NMR (CDCl<sub>3</sub>, 400 MHz, 25 °C): δ ppm, 8.61 (s, 1H, NH), 7.70 (d, 2H, <sup>3</sup>J<sub>HH</sub> = 9 Hz, *o*-C<sub>6</sub>H<sub>4</sub>Cl), 7.38 (d, 2H, <sup>3</sup>J<sub>HH</sub> = 9 Hz, *m*-C<sub>6</sub>H<sub>4</sub>Cl), 2.41 (s, 3H, CH<sub>3</sub>CO), 2.21 (s, 3H, NCH<sub>3</sub>). HRMS (ESI): *m/z* 233.0452 [C<sub>10</sub>H<sub>11</sub>ClN<sub>2</sub>O + Na]<sup>+</sup> Calcd. 233.0452. Anal. Calcd. for C<sub>10</sub>H<sub>11</sub>ClN<sub>2</sub>O: C, 57.02; H, 5.26; N, 13.30. Found: C, 57.18; H, 5.29; N, 12.78%.

(*E*)-*N'*-(1-(4-Bromophenyl)ethylidene)acetohydrazide (**18**)<sup>55</sup>. Yields: 0.021 g, 15% (**2b**).

$^1\text{H}$  NMR ( $\text{CDCl}_3$ , 400 MHz, 25 °C):  $\delta$  ppm, 8.57 (s, 1H, NH), 7.63 (d, 2H,  $^3J_{\text{HH}} = 9$  Hz, *o*-C<sub>6</sub>H<sub>4</sub>Br), 7.54 (d, 2H,  $^3J_{\text{HH}} = 9$  Hz, *m*-C<sub>6</sub>H<sub>4</sub>Br), 2.41 (s, 3H, C<sub>6</sub>H<sub>5</sub>CO), 2.21 (s, 3H, NCH<sub>3</sub>). HRMS (ESI): *m/z* 276.9944 [C<sub>10</sub>H<sub>11</sub>BrN<sub>2</sub>O + Na]<sup>+</sup> Calcd. 276.9947. Anal. Calcd. for C<sub>10</sub>H<sub>11</sub>BrN<sub>2</sub>O: C, 47.08; H, 4.35; N, 10.98. Found: C, 46.43; H, 4.39; N, 10.68%.

## METHODOLOGY

In the present study, all DFT calculations are performed with the Gaussian 09 Revision D.01,<sup>57</sup> while for spectroscopic calculations ( $^{13}\text{C}$  NMR), Orca 4.2 version software<sup>68</sup> is used. For the optimization of the geometries, Grimme's dispersion-corrected B3LYP functional (B3LYP-D3) has been taken into consideration.<sup>60</sup> The optimization calculations and imaginary frequency calculations of all species such as precatalyst (1–4) **b**, **4b'**, reactant, intermediates, and transition states have been carried out with the basis set SDD<sup>58</sup> for gold(I) metal and 6-31G\* for C, H, N, O, Cl, and S atoms (Supporting Information Table S8–S37).<sup>59–61</sup> We have carried out frequency calculations to obtain the minima on the potential-energy surface (PES) and to get the free energy correction energy. The gas phase energy has been amended by taking the solvation energy with a higher level of theory (B3LYP-D3/def2-TZVP).<sup>64</sup> All the spin density values have been reported with a higher level of theory (B3LYP-D3/def2-TZVP) (Table S41). For getting the solvation energy, we have taken the polarizable continuum model (PCM) model into account,<sup>65</sup> along with the solvent acetonitrile (CH<sub>3</sub>CN). PCM model solvation-free energy is computed by calculating the electrostatic term, dispersion-repulsion term, and cavitation term. Here, solvent acetonitrile (CH<sub>3</sub>CN) has been used according to the reported experimental condition (Table 7). Two types of software have been used for visualization of optimized geometry, namely, Chemcraft 1.6<sup>81</sup> and Gaussview 6.0.<sup>82</sup> Natural bonding analysis (NBO)<sup>69</sup> and Wiberg bond index (WBI)<sup>70</sup> analysis also has been done in Gaussian 09 software by performing DFT methods. NBO analysis explains the details of the bonding orbitals present in the bond and also provides the natural charges (Figures S206–S212 and Table S40). WBI analysis gives the bond index value, which tells about the bond character, whether it is a single bond, double bond, or triple bond.

The steric map plot calculations have been carried out from the SambVca 2.0 (a web tool for analyzing catalytic pockets with topographic steric maps).<sup>75</sup> The XYZ coordinates in this online tool for computing steric map plots are taken from optimized geometries obtained using Gaussian 09.<sup>57</sup> In this SambVca 2.0 web tool, it gives the relationship between the steric effect and the percentage of buried volume (%  $V_{\text{Bur}}$ ). Going from redder to bluer color in the steric map plot shows a decrease in steric effect and vice versa. For plotting the steric map, we can manually change the default values such as atomic radii, sphere radius, and mesh spacing for numerical integration, based on our needs. For our study we have taken default values into the accounts. In our calculations, we have also included the hydrogen atoms in our input.

For the  $^{13}\text{C}$  NMR calculations in ORCA 4.2 software,<sup>68</sup> we have taken the hybrid generalized gradient approximation (GGA) B3LYP functional.<sup>60,61</sup> In our calculations, the resolution of identity (RIJK) approximation has been employed throughout.<sup>69</sup> This RI approximation has been found to be fast for small to medium molecules. The basis set combination used for  $^{13}\text{C}$  NMR is Sapporo-DKH3-DZP-2012 for gold(I) metal,<sup>70</sup> DKH-def2-TZVP(-f) for the Cl atom,<sup>83</sup> and IGLO-II for the

carbon atom,<sup>71</sup> and for the rest of the atoms, Si, O, N, and H, the DKH-def2-SVP<sup>64,72</sup> basis set has been taken into account. Optimized coordinates of Gaussian 09 software have been used for the  $^{13}\text{C}$  NMR calculations.

## ASSOCIATED CONTENT

### Supporting Information

The Supporting Information is available free of charge at <https://pubs.acs.org/doi/10.1021/acsomega.3c01925>.

$^1\text{H}$  NMR,  $^{13}\text{C}\{^1\text{H}\}$  NMR,  $^{19}\text{F}\{^1\text{H}\}$  NMR, IR, HRMS, and CHNS data of the AAOC ligand precursor (1–4) **a** as well as corresponding gold complexes (1–4) **b**, (1–4) **c**, and (1–4) **d**;  $^1\text{H}$  NMR, HRMS, and CHNS data of the catalysis products (5–14) and total synthesis products (15–18); steric map plot for precatalyst (1–4) **b**,  $^{13}\text{C}$  NMR calculations for (1–4) **b**, Chemdraw mechanism for hydrohydrogenation reaction of 4-ethynyltoluene (HC≡CPhMe) with *p*-toluenesulfonyl hydrazide (NH<sub>2</sub>NHSO<sub>2</sub>C<sub>6</sub>H<sub>4</sub>CH<sub>3</sub>); DFT method-optimized coordinates, natural charges, NBO plots, WBI value, spin density, and structural parameters of species (4b'), reactant species (A), transition states ((TS1), (TS1'), (TS2), (TS2'), (TS3), (TS4), (TS4'), (TS4''), (TS4'''), and (TS5)), and intermediates ((A), (B), (C), (D), (E), and (E')), energy profile diagram for both hydrazide and acetylene coordination pathway, exhibiting proton transfer via H<sub>2</sub>O-assisted pathway and another hydrazide group-assisted and direct proton transfer pathway (PDF)

X-ray crystallographic data for the AAOC ligand precursor CCDC-1936844 (for 1a) and CCDC-1949239 (for 3a) and for the gold complexes CCDC-1949238 (for 1b), CCDC-2071056 (for 1c), CCDC-2152819 (for 1d), CCDC-1974061 (for 2b), CCDC-1989852 (for 2c), CCDC-2102959 (for 2d), CCDC-1980626 (for 3b), CCDC-2071055 (for 3c), CCDC-2156345 (for 3d), CCDC-1974062 (for 4b), CCDC-1989853 (for 4c), and CCDC-2099515 (for 4d) (CIF)

## AUTHOR INFORMATION

### Corresponding Authors

Gopalan Rajaraman – Department of Chemistry, Indian Institute of Technology Bombay, Mumbai 400 076, India; [orcid.org/0000-0001-6133-3026](https://orcid.org/0000-0001-6133-3026); Email: [rajaraman@chem.iitb.ac.in](mailto:rajaraman@chem.iitb.ac.in)

Prasenjit Ghosh – Department of Chemistry, Indian Institute of Technology Bombay, Mumbai 400 076, India; [orcid.org/0000-0002-9479-8177](https://orcid.org/0000-0002-9479-8177); Email: [pghosh@chem.iitb.ac.in](mailto:pghosh@chem.iitb.ac.in); Fax: +91 22 2572 3480

### Authors

Jyoti Singh – Department of Chemistry, Indian Institute of Technology Bombay, Mumbai 400 076, India; [orcid.org/0000-0003-4693-3992](https://orcid.org/0000-0003-4693-3992)

Sunita Sharma – Department of Chemistry, Indian Institute of Technology Bombay, Mumbai 400 076, India

A. P. Prakasham – Department of Chemistry, Indian Institute of Technology Bombay, Mumbai 400 076, India; Present Address: Current Affiliation: Laboratory of Macromolecular and Organic Chemistry, Institute for Complex Molecular Systems, Department of Chemical Engineering and Chemistry, Eindhoven University of



Technology, Eindhoven, Netherlands; [orcid.org/0000-0001-7651-679X](https://orcid.org/0000-0001-7651-679X)

Complete contact information is available at:  
<https://pubs.acs.org/10.1021/acsomega.3c01925>

## Author Contributions

<sup>†</sup>J.S. and S.S. contributed equally to this work.

## Notes

The authors declare no competing financial interest.

## ACKNOWLEDGMENTS

We thank the Department of Science and Technology and Science and Engineering Research Board (grant No.: CRG/2019/000029, CRG/2022/001697 and SB/SJF/2019-20/12), New Delhi, India, and Council of Scientific & Industrial Research (CSIR) {01(2880)/17/EMR-II} New Delhi, India, for financial support of this research. We gratefully acknowledge the Single Crystal X-ray Diffraction Facility, Department of Chemistry, IIT Bombay, Mumbai, India, for the crystallographic characterization data. We gratefully acknowledge the HPC Facility, IIT Bombay, Mumbai, India, for the computational calculation data. J.S. thanks the DST-INSPIRE, New Delhi, India, and S.S. thanks the UGC, New Delhi, India for the research fellowship.

## REFERENCES

- (1) Beauchemin, A. M. Recent developments in Cope-type hydroamination reactions of hydroxylamine and hydrazine derivatives. *Org. Biomol. Chem.* **2013**, *11*, 7039–7050.
- (2) Guisado-Barrios, G.; Soleilhavoup, M.; Bertrand, G. 1H-1,2,3-Triazol-5-ylidenes: Readily Available Mesoionic Carbenes. *Acc. Chem. Res.* **2018**, *51*, 3236–3244.
- (3) Tashrif, Z.; Mohammadi Khanaposhtani, M.; Biglar, M.; Larijani, B.; Mahdavi, M. Recent Advances in Alkyne Hydroamination as a Powerful Tool for the Construction of C-N Bonds. *Asian J. Org. Chem.* **2020**, *9*, 969–991.
- (4) (a) Pradhan, S. K.; Kedia, V.; Kour, P. Review on different materials and their characterization as rocket propellant. *Mater. Today: Proc.* **2020**, *33*, 5269–5272. (b) Elder, D. P.; Snodin, D.; Teasdale, A. Control and analysis of hydrazine, hydrazides and hydrazones—Genotoxic impurities in active pharmaceutical ingredients (APIs) and drug products. *J. Pharm. Biomed. Anal.* **2011**, *54*, 900–910. (c) Serov, A.; Kwak, C. Direct hydrazine fuel cells: A review. *Appl. Catal., B* **2010**, *98*, 1–9. (d) Narang, R.; Narasimhan, B.; Sharma, S. A review on biological activities and chemical synthesis of hydrazide derivatives. *Curr. Med. Chem.* **2012**, *19*, 569–612. (e) Yan, L.; Zhang, S.; Xie, Y.; Mu, X.; Zhu, J. Recent Progress in the Development of Fluorescent Probes for the Detection of Hydrazine (N<sub>2</sub>H<sub>4</sub>). *Crit. Rev. Anal. Chem.* **2022**, *52*, 210–229. (f) Cheng, Y.; Wu, X.; Xu, H. Catalytic decomposition of hydrous hydrazine for hydrogen production. *Sustainable Energy Fuels* **2019**, *3*, 343–365. (g) Nguyen, K. H.; Hao, Y.; Chen, W.; Zhang, Y.; Xu, M.; Yang, M.; Liu, Y.-N. Recent progress in the development of fluorescent probes for hydrazine. *Luminescence* **2018**, *33*, 816–836.
- (5) Manzano, R.; Wurm, T.; Rominger, F.; Hashmi, A. S. K. Room-temperature hydroamination of terminal alkynes catalyzed by saturated abnormal N-heterocyclic carbene-gold(I) complexes. *Chem. – Eur. J.* **2014**, *20*, 6844–6848.
- (6) Niemeier, J. K.; Kjell, D. P. Hydrazine and Aqueous Hydrazine Solutions: Evaluating Safety in Chemical Processes. *Org. Process Res. Dev.* **2013**, *17*, 1580–1590.
- (7) He, H.-Y.; Niikura, H.; Du, Y.-L.; Ryan, K. S. Synthetic and biosynthetic routes to nitrogen-nitrogen bonds. *Chem. Soc. Rev.* **2022**, *51*, 2991–3046.
- (8) Heaton, B. T.; Jacob, C.; Page, P. Transition metal complexes containing hydrazine and substituted hydrazines. *Coord. Chem. Rev.* **1996**, *154*, 193–229.
- (9) (a) Mueller, T. E.; Hultsch, K. C.; Yus, M.; Foubelo, F.; Tada, M. Hydroamination: Direct Addition of Amines to Alkenes and Alkynes. *Chem. Rev.* **2008**, *108*, 3795–3892. (b) Severin, R.; Doye, S. The catalytic hydroamination of alkynes. *Chem. Soc. Rev.* **2007**, *36*, 1407–1420.
- (10) Cebrowski, P. H.; Roveda, J.-G.; Moran, J.; Gorelsky, S. I.; Beauchemin, A. M. Intermolecular Cope-type hydroamination of alkynes using hydrazines. *Chem. Commun.* **2008**, *4*, 492–493.
- (11) Alex, K.; Tillack, A.; Schwarz, N.; Beller, M. Zinc-promoted hydroamination of terminal alkynes: an efficient domino synthesis of indoles. *Angew. Chem., Int. Ed.* **2008**, *47*, 2304–2307.
- (12) Morozov, O. S.; Gribanov, P. S.; Asachenko, A. F.; Dorovatovskii, P. V.; Khrustalev, V. N.; Rybakov, V. B.; Nechaev, M. S. Hydroamination of Arylalkynes Catalyzed by an Expanded Ring N-Heterocyclic Carbene (er-NHC) Gold Complex Under Solvent-Free Conditions. *Adv. Synth. Catal.* **2016**, *358*, 1463–1468.
- (13) Zimin, D. P.; Dar'in, D. V.; Rassadin, V. A.; Kukushkin, V. Y. Gold-Catalyzed Hydroamination of Terminal Alkynes. *Org. Lett.* **2018**, *20*, 4880–4884.
- (14) (a) Roveda, J.-G.; Clavette, C.; Hunt, A. D.; Gorelsky, S. I.; Whipp, C. J.; Beauchemin, A. M. Hydrazides as Tunable Reagents for Alkene Hydroamination and Aminocarbonylation. *J. Am. Chem. Soc.* **2009**, *131*, 8740–8741. (b) Loiseau, F.; Clavette, C.; Raymond, M.; Roveda, J.-G.; Burrell, A.; Beauchemin, A. M. Improved Cope-type hydroamination reactivity of hydrazine derivatives. *Chem. Commun.* **2011**, *47*, 562–564.
- (15) Kinjo, R.; Donnadieu, B.; Bertrand, G. Gold-catalyzed hydroamination of alkynes and allenes with parent hydrazine. *Angew. Chem., Int. Ed.* **2011**, *50*, 5560–5563.
- (16) López-Gómez, M. J.; Martin, D.; Bertrand, G. Anti-Bredt N-heterocyclic carbene: an efficient ligand for the gold(I)-catalyzed hydroamination of terminal alkynes with parent hydrazine. *Chem. Commun.* **2013**, *49*, 4483–4485.
- (17) (a) Yazdani, S.; Junor, G. P.; Peltier, J. L.; Gembicky, M.; Jazzar, R.; Grotjahn, D. B.; Bertrand, G. Influence of Carbene and Phosphine Ligands on the Catalytic Activity of Gold Complexes in the Hydroamination and Hydroamination of Alkynes. *ACS Catal.* **2020**, *10*, 5190–5201. (b) Rotta-Loria, N. L.; Chisholm, A. J.; MacQueen, P. M.; McDonald, R.; Ferguson, M. J.; Stradiotto, M. Exploring the influence of phosphine ligation on the gold-catalyzed hydroamination of terminal alkynes at room temperature. *Organometallics* **2017**, *36*, 2470–2475.
- (18) Arduengo, A. J.; Harlow, R. L.; Kline, M. A stable crystalline carbene. *J. Am. Chem. Soc.* **1991**, *113*, 361–363.
- (19) (a) Hopkinson, M. N.; Richter, C.; Schedler, M.; Glorius, F. An overview of N-heterocyclic carbenes. *Nature* **2014**, *510*, 485–496. (b) Vignolle, J.; Cattoen, X.; Bourissou, D. Stable N-heterocyclic Singlet Carbenes. *Chem. Rev.* **2009**, *109*, 3333–3384. (c) Bourissou, D.; Guerret, O.; Gabbai, F. P.; Bertrand, G. Stable Carbenes. *Chem. Rev.* **2000**, *100*, 39–92. (d) Melaimi, M.; Soleilhavoup, M.; Bertrand, G. Stable Cyclic Carbenes and Related Species beyond Diaminocarbenes. *Angew. Chem., Int. Ed.* **2010**, *49*, 8810–8849.
- (20) (a) Kinzhalov, M. A.; Luzyanin, K. V. Synthesis and Contemporary Applications of Platinum Group Metals Complexes with Acyclic Diaminocarbene Ligands (Review). *Russ. J. Inorg. Chem.* **2022**, *67*, 48–90. (b) Kinzhalov, M. A.; Grachova, E. V.; Luzyanin, K. V. Tuning the luminescence of transition metal complexes with acyclic diaminocarbene ligands. *Inorg. Chem. Front.* **2022**, *9*, 417–439. (c) Kinzhalov, M. A.; Luzyanin, K. V. Reactivity of acyclic diaminocarbene ligands. *Coord. Chem. Rev.* **2019**, *399*, No. 213014.
- (21) Martin, D.; Lassauque, N.; Donnadieu, B.; Bertrand, G. A Cyclic Diaminocarbene with a Pyramidalized Nitrogen Atom: A Stable N-Heterocyclic Carbene with Enhanced Electrophilicity. *Angew. Chem., Int. Ed.* **2012**, *51*, 6172–6175.
- (22) (a) Frey, G. D.; Dewhurst, R. D.; Kousar, S.; Donnadieu, B.; Bertrand, G. Cyclic (alkyl)(amino)carbene gold(I) complexes: A

- synthetic and structural investigation. *J. Organomet. Chem.* **2008**, *693*, 1674–1682. (b) Lavallo, V.; Canac, Y.; DeHope, A.; Donnadiou, B.; Bertrand, G. A Rigid Cyclic (Alkyl)(amino)carbene Ligand Leads to Isolation of Low-Coordinate Transition-Metal Complexes. *Angew. Chem., Int. Ed.* **2005**, *44*, 7236–7239. (c) Lavallo, V.; Canac, Y.; Präsang, C.; Donnadiou, B.; Bertrand, G. Stable Cyclic (Alkyl)-(Amino)Carbenes as Rigid or Flexible, Bulky, Electron-Rich Ligands for Transition-Metal Catalysts: A Quaternary Carbon Atom Makes the Difference. *Angew. Chem., Int. Ed.* **2005**, *44*, 5705–5709. (d) Jazzar, R.; Dewhurst, R. D.; Bourg, J.-B.; Donnadiou, B.; Canac, Y.; Bertrand, G. Intramolecular “hydroiminiumation” of alkenes: application to the synthesis of conjugate acids of cyclic alkyl amino carbenes (CAACs). *Angew. Chem., Int. Ed.* **2007**, *46*, 2899–2902. (e) Lavallo, V.; Frey, G. D.; Kousar, S.; Donnadiou, B.; Bertrand, G. Allene formation by gold catalyzed cross-coupling of masked carbenes and vinylidenes. *Proc. Natl. Acad. Sci.* **2007**, *104*, 13569–13573. (f) Lavallo, V.; Frey, G. D.; Donnadiou, B.; Soleilhavoup, M.; Bertrand, G. Homogeneous Catalytic Hydroamination of Alkynes and Allenes with Ammonia. *Angew. Chem., Int. Ed.* **2008**, *47*, 5224–5228. (g) Zeng, X.; Frey, G. D.; Kinjo, R.; Donnadiou, B.; Bertrand, G. Synthesis of a Simplified Version of Stable Bulky and Rigid Cyclic (Alkyl)(amino)carbenes, and Catalytic Activity of the Ensuing Gold(I) Complex in the Three-Component Preparation of 1,2-Dihydroquinoline Derivatives. *J. Am. Chem. Soc.* **2009**, *131*, 8690–8696. (h) Zeng, X.; Soleilhavoup, M.; Bertrand, G. Gold-Catalyzed Intermolecular Markovnikov Hydroamination of Allenes with Secondary Amines. *Org. Lett.* **2009**, *11*, 3166–3169.
- (23) Jazzar, R.; Bourg, J.-B.; Dewhurst, R. D.; Donnadiou, B.; Bertrand, G. Intramolecular “Hydroiminiumation and -amidiniumation” of Alkenes: A Convenient, Flexible, and Scalable Route to Cyclic Iminium and Imidazolium Salts. *J. Org. Chem.* **2007**, *72*, 3492–3499.
- (24) Slaughter, L. M. Acyclic Aminocarbenes in Catalysis. *ACS Catal.* **2012**, *2*, 1802–1816.
- (25) (a) Manzano, R.; Rominger, F.; Hashmi, A. S. K. Saturated Abnormal NHC–Gold(I) Complexes: Synthesis and Catalytic Activity. *Organometallics* **2013**, *32*, 2199–2203. (b) Hashmi, A. S. K.; Riedel, D.; Rudolph, M.; Rominger, F.; Oesser, T. Regioselective Formation of Saturated Abnormal NHC–Gold(I) Complexes by [3+2] Cycloaddition of Azomethine Ylides and Isonitrile Gold(I) Complexes. *Chem. – Eur. J.* **2012**, *18*, 3827–3830.
- (26) (a) Rao, M. N.; Manne, R.; Tanski, J. M.; Butcher, R.; Ghosh, P. One pot synthesis of propargylamines by three component amine-aldehyde-acetylene (A3) coupling catalyzed by neutral Ag(I) and Au(I) and cationic Pd(II) and Ni(II) complexes of a pincer N-heterocyclic carbene. *Mol. Catal.* **2022**, *529*, No. 112515. (b) Prakasham, A. P.; Ta, S.; Dey, S.; Ghosh, P. One pot tandem dual C–C and C–O bond reductions in the  $\beta$ -alkylation of secondary alcohols with primary alcohols by ruthenium complexes of amido and picolyl functionalized N-heterocyclic carbenes. *Dalton Trans.* **2021**, *50*, 15640–15654. (c) Singh, C.; Prakasham, A. P.; Gangwar, M. K.; Butcher, R. J.; Ghosh, P. One-Pot Tandem Hiyama Alkynylation/Cyclizations by Palladium(II) Acyclic Diaminocarbene (ADC) Complexes Yielding Biologically Relevant Benzofuran Scaffolds. *ACS Omega* **2018**, *3*, 1740–1756. (d) Kumar, R.; Katari, M.; Choudhary, A.; Rajaraman, G.; Ghosh, P. Computational Insight Into the Hydroamination of an Activated Olefin, As Catalyzed by a 1,2,4-Triazole-Derived Nickel(II) N-Heterocyclic Carbene Complex. *Inorg. Chem.* **2017**, *56*, 14859–14869. (e) Kumar, A.; Gangwar, M. K.; Prakasham, A. P.; Mhatre, D.; Kalita, A. C.; Ghosh, P. Accessing a Biologically Relevant Benzofuran Skeleton by a One-Pot Tandem Heck Alkynylation/Cyclization Reaction Using Well-Defined Palladium N-Heterocyclic Carbene Complexes. *Inorg. Chem.* **2016**, *55*, 2882–2893. (f) Modak, S.; Gangwar, M. K.; Nageswar Rao, M.; Madasu, M.; Kalita, A. C.; Dorcet, V.; Shejale, M. A.; Butcher, R. J.; Ghosh, P. Fluoride-free Hiyama coupling by palladium abnormal N-heterocyclic carbene complexes. *Dalton Trans.* **2015**, *44*, 17617–17628. (g) Ramasamy, B.; Ghosh, P. The Developing Concept of Bifunctional Catalysis with Transition Metal N-Heterocyclic Carbene Complexes. *Eur. J. Inorg. Chem.* **2016**, *2016*, 1448–1465. (h) Prakasham, A. P.; Ghosh, P. Nickel N-heterocyclic carbene complexes and their utility in homogeneous catalysis. *Inorg. Chim. Acta* **2015**, *431*, 61–100.
- (27) (a) Kumar, A.; Naaz, A.; Prakasham, A. P.; Gangwar, M. K.; Butcher, R. J.; Panda, D.; Ghosh, P. Potent Anticancer Activity with High Selectivity of a Chiral Palladium N-Heterocyclic Carbene Complex. *ACS Omega* **2017**, *2*, 4632–4646. (b) Ray, S.; Mohan, R.; Singh, J. K.; Samantaray, M. K.; Shaikh, M. M.; Panda, D.; Ghosh, P. Anticancer and antimicrobial metallopharmaceutical agents based on palladium, gold, and silver N-heterocyclic carbene complexes. *J. Am. Chem. Soc.* **2007**, *129*, 15042–15053.
- (28) (a) Katari, M.; Rao, M. N.; Rajaraman, G.; Ghosh, P. Computational Insight into a Gold(I) N-Heterocyclic Carbene Mediated Alkyne Hydroamination Reaction. *Inorg. Chem.* **2012**, *51*, 5593–5604. (b) Dash, C.; Shaikh, M. M.; Butcher, R. J.; Ghosh, P. Highly Convenient Regioselective Intermolecular Hydroamination of Alkynes Yielding Ketimines Catalyzed by Gold(I) Complexes of 1,2,4-triazole Based N-heterocyclic Carbenes. *Inorg. Chem.* **2010**, *49*, 4972–4983. (c) Samantaray, M. K.; Pang, K.; Shaikh, M. M.; Ghosh, P. Unprecedented long-range 1,7-bromination in gold complexes of N-(aryl) imino functionalized N-heterocyclic carbenes. *Dalton Trans.* **2008**, *36*, 4893–4902. (d) Samantaray, M. K.; Pang, K.; Shaikh, M. M.; Ghosh, P. From large 12-membered macrometallacycles to ionic (NHC)(2)M+Cl- type complexes of gold and silver by modulation of the N-substituent of amido-functionalized N-heterocyclic carbene (NHC) Ligands. *Inorg. Chem.* **2008**, *47*, 4153–4165. (e) Ray, L.; Katiyar, V.; Barman, S.; Raihan, M. J.; Nanavati, H.; Shaikh, M. M.; Ghosh, P. Gold(I) N-heterocyclic carbene based initiators for bulk ring-opening polymerization of L-lactide. *J. Organomet. Chem.* **2007**, *692*, 4259–4269. (f) Ray, L.; Katiyar, V.; Raihan, M. J.; Nanavati, H.; Shaikh, M. M.; Ghosh, P. First Example of a Gold(I) N-Heterocyclic-Carbene-Based Initiator for the Bulk Ring-Opening Polymerization of L-Lactide. *Eur. J. Inorg. Chem.* **2006**, *2006*, 3724–3730.
- (29) Samantaray, M. K.; Dash, C.; Shaikh, M. M.; Pang, K.; Butcher, R. J.; Ghosh, P. Gold(III) N-Heterocyclic Carbene Complexes Mediated Synthesis of beta-Enaminones From 1,3-Dicarbonyl Compounds and Aliphatic Amines. *Inorg. Chem.* **2011**, *50*, 1840–1848.
- (30) (a) Casalnuovo, A. L.; Calabrese, J. C.; Milstein, D. Nitrogen-hydrogen activation. 1. Oxidative addition of ammonia to iridium(I). Isolation, structural characterization and reactivity of amidoiridium hydrides. *Inorg. Chem.* **1987**, *26*, 971–973. (b) Koelliker, R.; Milstein, D. Evidence for an unprecedented Ir(H)(NH3).dblarw. Ir(H2)(NH2) equilibrium and hydrogen exchange between NH and CH bonds. *J. Am. Chem. Soc.* **1991**, *113*, 8524–8525. (c) Khaskin, E.; Iron, M. A.; Shimon, L. J. W.; Zhang, J.; Milstein, D. N–H Activation of Amines and Ammonia by Ru via Metal–Ligand Cooperation. *J. Am. Chem. Soc.* **2010**, *132*, 8542–8543. (d) Kuhn, N.; Bohnen, H.; Kreutzberg, J.; Bläser, D.; Boese, R. 1, 3, 4, 5-Tetramethyl-2-methyleneimidazoline— an ylidic olefin. *J. Chem. Soc., Chem. Commun.* **1993**, 1136–1137. (e) Koelliker, R.; Milstein, D. Facile NH Cleavage of Ammonia. *Angew. Chem., Int. Ed.* **1991**, *30*, 707–709.
- (31) Alder, R. W.; Butts, C. P.; Orpen, A. G. Stable Aminoxy- and Aminothiocarbenes. *J. Am. Chem. Soc.* **1998**, *120*, 11526–11527.
- (32) Cordero, B.; Gomez, V.; Platero-Prats, A. E.; Reves, M.; Echeverria, J.; Cremades, E.; Barragan, F.; Alvarez, S. Covalent radii revisited. *Dalton Trans.* **2008**, *21*, 2832–2838.
- (33) Seo, H.; Snead, D. R.; Abboud, K. A.; Hong, S. Bulky Acyclic Aminoxy-carbene Ligands. *Organometallics* **2011**, *30*, 5725–5730.
- (34) Banditelli, G.; Bonati, F.; Calogero, S.; Valle, G.; Wagner, F. E.; Wordel, R. A gold-197 Moessbauer study of a series of isocyanide, carbene, or methanide derivatives of gold. The crystal structure of trans,trans- and cis,cis-[(carbene)2Au]ClO4 and of cis,trans-(carbene)AuCl (carbene = p-MeC6H4NHCOEt). *Organometallics* **1986**, *5*, 1346–1352.
- (35) Minghetti, G.; Baratto, L.; Bonati, F. Carbene complexes from the reaction of ionic isocyanide complexes of gold(I) with alcohols and amines. *J. Organomet. Chem.* **1975**, *102*, 397–406.
- (36) Lemke, J.; Pinto, A.; Niehoff, P.; Vasylyeva, V.; Metzler-Nolte, N. Synthesis, structural characterisation and anti-proliferative activity of



NHC gold amino acid and peptide conjugates. *Dalton Trans.* **2009**, *35*, 7063–7070.

(37) Ibrahim, N.; Vilhelmsen, M. H.; Pernpointner, M.; Rominger, F.; Hashmi, A. S. K. Gold Phenolate Complexes: Synthesis, Structure, and Reactivity. *Organometallics* **2013**, *32*, 2576–2583.

(38) Visbal, R.; Herrera, R. P.; Gimeno, M. C. Thiolate Bridged Gold(I)-NHC Catalysts: New Approach for Catalyst Design and its Application to Trapping Catalytic Intermediates. *Chem. – Eur. J.* **2019**, *25*, 15837–15845.

(39) Mui, Y. F.; Fernández-Gallardo, J.; Elie, B. T.; Gubran, A.; Maluenda, I.; Sanaú, M.; Navarro, O.; Contel, M. A. Titanocene–Gold Complexes Containing N-Heterocyclic Carbene Ligands Inhibit Growth of Prostate, Renal, and Colon Cancers in Vitro. *Organometallics* **2016**, *35*, 1218–1227.

(40) Dada, O.; Curran, D.; O’Beirne, C.; Muller-Bunz, H.; Zhu, X.; Tacke, M. Synthesis and cytotoxicity studies of novel NHC–Gold(I) pseudohalides and thiolates. *J. Organomet. Chem.* **2017**, *840*, 30–37.

(41) Hirtenlehner, C.; Krims, C.; Hölbling, J.; List, M.; Zabel, M.; Fleck, M.; Berger, R. J. F.; Schoefberger, W.; Monkowius, U. Syntheses, crystal structures, reactivity, and photochemistry of gold(III) bromides bearing N-heterocyclic carbenes. *Dalton Trans.* **2011**, *40*, 9899–9910.

(42) Curado, N.; Giménez, N.; Miachin, K.; Aliaga-Lavrijsen, M.; Cornejo, M. A.; Jarzecki, A. A.; Contel, M. Preparation of Titanocene–Gold Compounds Based on Highly Active Gold(I)-N-Heterocyclic Carbene Anticancer Agents: Preliminary in vitro Studies in Renal and Prostate Cancer Cell Lines. *ChemMedChem* **2019**, *14*, 1086–1095.

(43) Rubbiani, R.; Schuh, E.; Meyer, A.; Lemke, J.; Wimberg, J.; Metzler-Nolte, N.; Meyer, F.; Mohr, F.; Ott, I. TrxR inhibition and antiproliferative activities of structurally diverse gold N-heterocyclic carbene complexes. *MedChemComm* **2013**, *4*, 942–948.

(44) Romanov, A. S.; Becker, C. R.; James, C. E.; Di, D.; Credgington, D.; Linnolahti, M.; Bochmann, M. Copper and Gold Cyclic (Alkyl)(amino)carbene Complexes with Sub-Microsecond Photoemissions: Structure and Substituent Effects on Redox and Luminescent Properties. *Chem. – Eur. J.* **2017**, *23*, 4625–4637.

(45) (a) Hashmi, A. S. K. Gold-Catalyzed Organic Reactions. *Chem. Rev.* **2007**, *107*, 3180–3211. (b) Corma, A.; Leyva-Pérez, A.; Sabater, M. J. Gold-Catalyzed Carbon–Heteroatom Bond-Forming Reactions. *Chem. Rev.* **2011**, *111*, 1657–1712. (c) Xie, J.; Pan, C.; Abdulkader, A.; Zhu, C. Gold-catalyzed C(sp<sup>3</sup>)–H bond functionalization. *Chem. Soc. Rev.* **2014**, *43*, 5245–5256. (d) Harris, R. J.; Widenhoefer, R. A. Gold carbenes, gold-stabilized carbocations, and cationic intermediates relevant to gold-catalyzed enyne cycloaddition. *Chem. Soc. Rev.* **2016**, *45*, 4533–4551. (e) Asiri, A. M.; Hashmi, A. S. K. Gold-catalyzed reactions of diynes. *Chem. Soc. Rev.* **2016**, *45*, 4471–4503.

(46) (a) Hashmi, A. S. K.; Schwarz, L.; Choi, J.-H.; Frost, T. M. A New Gold-Catalyzed C–C Bond Formation. *Angew. Chem., Int. Ed.* **2000**, *39*, 2285–2288. (b) Hashmi, A. S. K.; Frost, T. M.; Bats, J. W. Highly Selective Gold-Catalyzed Arene Synthesis. *J. Am. Chem. Soc.* **2000**, *122*, 11553–11554.

(47) (a) Yadav, S.; Ray, S.; Singh, A.; Mobin, S. M.; Roy, T. K.; Dash, C. Dinuclear gold(I)-N-heterocyclic carbene complexes: Synthesis, characterization, and catalytic application for hydrohydrazidation of terminal alkynes. *Appl. Organomet. Chem.* **2020**, *34*, No. e5942. (b) Flores-Jarillo, M.; Mendoza-Espinosa, D.; Salazar-Pereda, V.; González-Montiel, S. Synthesis and Catalytic Benefits of Tetranuclear Gold(I) Complexes with a C<sub>4</sub>-Symmetric Tetratriazol-5-ylidene. *Organometallics* **2017**, *36*, 4305–4312. (c) Mendoza-Espinosa, D.; Rendón-Nava, D.; Alvarez-Hernández, A.; Angeles-Beltrán, D.; Negrón-Silva, G. E.; Suárez-Castillo, O. R. Visible-Light-Promoted AuI to AuIII Oxidation in Triazol-5-ylidene Complexes. *Chem. – Asian J.* **2017**, *12*, 203–207.

(48) Zhu, S.; Liang, R.; Chen, L.; Wang, C.; Ren, Y.; Jiang, H. A direct and practical approach for the synthesis of Au(I)-NHC complexes from commercially available imidazolium salts and Au(III) salts. *Tetrahedron Lett.* **2012**, *53*, 815–818.

(49) (a) Hashmi, A. S. K. Homogeneous Gold Catalysis Beyond Assumptions and Proposals—Characterized Intermediates. *Angew. Chem., Int. Ed.* **2010**, *49*, 5232–5241. (b) Lauterbach, T.; Asiri, A. M.;

Hashmi, A. S. K. Chapter Five - Organometallic Intermediates of Gold Catalysis. In *Advances in Organometallic Chemistry*, Pérez, P. J. Ed.; Vol. 62; Academic Press, 2014; pp. 261–297.

(50) (a) Pernpointner, M.; Hashmi, A. S. K. Fully Relativistic, Comparative Investigation of Gold and Platinum Alkyne Complexes of Relevance for the Catalysis of Nucleophilic Additions to Alkynes. *J. Chem. Theory Comput.* **2009**, *5*, 2717–2725. (b) Lein, M.; Rudolph, M.; Hashmi, S. K.; Schwerdtfeger, P. Homogeneous Gold Catalysis: Mechanism and Relativistic Effects of the Addition of Water to Propyne. *Organometallics* **2010**, *29*, 2206–2210.

(51) (a) Krauter, C. M.; Hashmi, A. S. K.; Pernpointner, M. A New Insight into Gold(I)-Catalyzed Hydration of Alkynes: Proton Transfer. *ChemCatChem* **2010**, *2*, 1226–1230. (b) Nunes dos Santos Comprido, L.; Klein, J. E. M. N.; Knizia, G.; Kästner, J.; Hashmi, A. S. K. On the Accessible Reaction Channels of Vinyl Gold(I) Species:  $\pi$ - and  $\sigma$ -Pathways. *Chem. – Eur. J.* **2017**, *23*, 10901–10905.

(52) Bew, S. P.; Hiatt-Gipson, G. D.; Lovell, J. A.; Poullain, C. Mild Reaction Conditions for the Terminal Deuteration of Alkynes. *Org. Lett.* **2012**, *14*, 456–459.

(53) Shahkhatuni, A. A.; Shahkhatuni, A. G.; Ananikov, V. P.; Harutyunyan, A. S. NMR-monitoring of H/D exchange reaction of ketones in solutions of imidazolium ionic liquids. *J. Mol. Liq.* **2022**, *362*, No. 119746.

(54) Dimmock, J. R.; Sidhu, K. K.; Tumber, S. D.; Basran, S. K.; Chen, M.; Quail, J. W.; Yang, J.; Rozas, I.; Weaver, D. F. Some aryl semicarbazones possessing anticonvulsant activities. *Eur. J. Med. Chem.* **1995**, *30*, 287–301.

(55) Dimmock, J. R.; Vashishtha, S. C.; Stables, J. P. Anticonvulsant properties of various acetylhydrazones, oxamoylhydrazones and semicarbazones derived from aromatic and unsaturated carbonyl compounds. *Eur. J. Med. Chem.* **2000**, *35*, 241–248.

(56) Rollas, S.; Küçükgül, S. Biological Activities of Hydrazone Derivatives. *Molecules* **2007**, *12*, 1910–1939.

(57) Frisch, M. J.; Trucks, G. W.; Schlegel, H. B.; Scuseria, G. E.; Robb, M. A.; Cheeseman, J. R.; Scalmani, G.; Barone, V.; Mennucci, B.; Petersson, G. *Gaussian 09*, Revision D. 01, Gaussian, Inc.: Wallingford CT 2009. See also: URL: <http://www.gaussian.com>.

(58) Roy, L. E.; Hay, P. J.; Martin, R. L. Revised Basis Sets for the LANL Effective Core Potentials. *J. Chem. Theory Comput.* **2008**, *4*, 1029–1031.

(59) Mitin, A. V.; Baker, J.; Pulay, P. An improved 6-31 G\* basis set for first-row transition metals. *J. Chem. Phys.* **2003**, *118*, 7775–7782.

(60) (a) Becke, A. D. Density-functional thermochemistry. V. Systematic optimization of exchange-correlation functionals. *J. Chem. Phys.* **1997**, *107*, 8554–8560. (b) Antony, J.; Grimme, S. Density functional theory including dispersion corrections for intermolecular interactions in a large benchmark set of biologically relevant molecules. *Phys. Chem. Chem. Phys.* **2006**, *8*, 5287–5293.

(61) Becke, A. D. Density-functional exchange-energy approximation with correct asymptotic behavior. *Phys. Rev. A* **1988**, *38*, 3098–3100.

(62) (a) Sen, A.; Vyas, N.; Pandey, B.; Rajaraman, G. Deciphering the mechanism of oxygen atom transfer by non-heme Mn IV–oxo species: an ab initio and DFT exploration. *Dalton Trans.* **2020**, *49*, 10380–10393. (b) Ansari, A.; Kaushik, A.; Rajaraman, G. Mechanistic Insights on the ortho-Hydroxylation of Aromatic Compounds by Non-heme Iron Complex: A Computational Case Study on the Comparative Oxidative Ability of Ferric-Hydroperoxo and High-Valent FeIV=O and FeV=O Intermediates. *J. Am. Chem. Soc.* **2013**, *135*, 4235–4249.

(63) (a) Cantú Reinhard, F. G.; Faponle, A. S.; de Visser, S. P. Substrate Sulfoxidation by an Iron(IV)-Oxo Complex: Benchmarking Computationally Calculated Barrier Heights to Experiment. *J. Phys. Chem. A* **2016**, *120*, 9805–9814. (b) Lundberg, M.; Siegbahn, P. E. M. Agreement between experiment and hybrid DFT calculations for O–H bond dissociation enthalpies in manganese complexes. *J. Comput. Chem.* **2005**, *26*, 661–667.

(64) Weigend, F.; Ahlrichs, R. Balanced basis sets of split valence, triple zeta valence and quadruple zeta valence quality for H to Rn: Design and assessment of accuracy. *Phys. Chem. Chem. Phys.* **2005**, *7*, 3297–3305.

- (65) Tomasi, J.; Mennucci, B.; Cammi, R. Quantum Mechanical Continuum Solvation Models. *Chem. Rev.* **2005**, *105*, 2999–3094.
- (66) Glendening, E. D.; Landis, C. R.; Weinhold, F. NBO 6.0: Natural bond orbital analysis program. *J. Comput. Chem.* **2013**, *34*, 1429–1437.
- (67) Mayer, I. Bond orders and valences in the SCF theory: a comment. *Theor. Chim. Acta* **1985**, *67*, 315–322.
- (68) Neese, F.; Wennmohs, F.; Becker, U.; Riplinger, C. The ORCA quantum chemistry program package. *J. Chem. Phys.* **2020**, *152*, 224108.
- (69) Altun, A.; Izsák, R.; Bistoni, G. Local energy decomposition of coupled-cluster interaction energies: Interpretation, benchmarks, and comparison with symmetry-adapted perturbation theory. *Int. J. Quantum Chem.* **2021**, *121*, No. e26339.
- (70) de Almeida, C. A.; Pinto, L. P. N. M.; Dos Santos, H. F.; Paschoal, D. F. S. Vibrational frequencies and intramolecular force constants for cisplatin: assessing the role of the platinum basis set and relativistic effects. *J. Mol. Model.* **2021**, *27*, 322.
- (71) (a) Kaupp, M.; Malkin, O. L.; Malkin, V. G. Interpretation of <sup>13</sup>C NMR chemical shifts in halomethyl cations. On the importance of spin-orbit coupling and electron correlation. *Chem. Phys. Lett.* **1997**, *265*, 55–59. (b) Krivdin, L. B. Computational protocols for calculating <sup>13</sup>C NMR chemical shifts. *Prog. Nucl. Magn. Reson. Spectrosc.* **2019**, *112*, 103–156.
- (72) (a) Fraser, H. W. L.; Payne, E. H.; Sarkar, A.; Wilson, L. R. B.; Mitcov, D.; Nichol, G. S.; Rajaraman, G.; Piligkos, S.; Brechin, E. K. [(V IV O) 2 M II5](M= Ni, Co) Anderson wheels. *Dalton Trans.* **2021**, *50*, 12495–12501. (b) Pantazis, D. A.; Neese, F. All-Electron Scalar Relativistic Basis Sets for the Actinides. *J. Chem. Theory Comput.* **2011**, *7*, 677–684.
- (73) (a) Kondrashova, S. A.; Polyancev, F. M.; Ganushevich, Y. S.; Latypov, S. K. DFT Approach for Predicting <sup>13</sup>C NMR Shifts of Atoms Directly Coordinated to Nickel. *Organometallics* **2021**, *40*, 1614–1625. (b) Gu, B.-B.; Wu, W.; Jiao, F.-R.; Jiao, W.-H.; Li, L.; Sun, F.; Wang, S.-P.; Yang, F.; Lin, H.-W. Asperflotone, an 8(14→15)-abeo-Ergostane from the Sponge-Derived Fungus *Aspergillus flocculosus* 16D-1. *J. Org. Chem.* **2019**, *84*, 300–306. (c) Beytur, M.; Avinca, I. Molecular, Electronic, Nonlinear Optical and Spectroscopic Analysis of Heterocyclic 3-Substituted-4-(3-methyl-2-thienylmethyleneamino)-4,5-dihydro-1H-1,2,4-triazol-5-ones: Experiment and DFT Calculations. **2021**, *27* (1), 1–16, DOI: 10.1515/hc-2020-0118.
- (74) Kaupp, M. Interpretation of NMR Chemical Shifts. *Calc. NMR EPR Parameters* **2004**, 293–306.
- (75) Falivene, L.; Credendino, R.; Poater, A.; Petta, A.; Serra, L.; Oliva, R.; Scarano, V.; Cavallo, L. SambVca 2.A Web Tool for Analyzing Catalytic Pockets with Topographic Steric Maps. *Organometallics* **2016**, *35*, 2286–2293.
- (76) Teles, J. H.; Brode, S.; Chabanas, M. Cationic gold (I) complexes: highly efficient catalysts for the addition of alcohols to alkynes. *Angew. Chem., Int. Ed.* **1998**, *37*, 1415–1418.
- (77) Hashmi, A. S. K.; Weyrauch, J. P.; Frey, W.; Bats, J. W. Gold Catalysis: Mild Conditions for the Synthesis of Oxazoles from N-Propargylcarboxamides and Mechanistic Aspects. *Org. Lett.* **2004**, *6*, 4391–4394.
- (78) Becerra-Figueroa, L.; Ojeda-Porras, A.; Gamba-Sánchez, D. Transamidation of Carboxamides Catalyzed by Fe(III) and Water. *J. Org. Chem.* **2014**, *79*, 4544–4552.
- (79) Brandys, M.-C.; Jennings, M. C.; Puddephatt, R. J. Luminescent gold(I) macrocycles with diphosphine and 4,4'-bipyridyl ligands. *J. Chem. Soc., Dalton Trans.* **2000**, *24*, 4601–4606.
- (80) Sheldrick, G. M. A short history of SHELX. *Acta Crystallogr., Sect. A: Found. Crystallogr.* **2008**, *64*, 112–122.
- (81) Zhurko, G. A. *ChemCraft software*, version 1.6. 2014.
- (82) Dennington, R.; Keith, T.; Millam, J. *GaussView*; Semichem Inc: Shawnee Mission, KS 2009.
- (83) Petrov, A. I. Quantum chemical modeling of the thermodynamics of the formation of Au(III), Pd(II), and Pt(II) chloride complexes. *J. Mol. Model.* **2022**, *28*, 391.